

Modelling Double-Skin Facades

Allan Dickson (B.Eng)

A thesis submitted for the Degree:
MSc Energy Systems & the Environment

Department of Mechanical Engineering
University of Strathclyde, Glasgow UK

1	ABSTRACT	4
2	INTRODUCTION	6
2.1	HISTORY OF THE DOUBLE-SKIN FACADE	6
2.2	DEFINITION OF THE MODERN DOUBLE-SKIN FACADE	8
2.3	USEFUL CLASSIFICATION OF FACADE CONFIGURATIONS - BELGIAN BUILDING RESEARCH INSTITUTE STUDY	9
2.3.1	<i>Choosing appropriate classifications to model – investigation strategy</i>	12
3	MODELLING DOUBLE-SKIN FACADES	13
3.1	ENERGY FLOWPATHS	13
3.2	ESP-R (BUILDING SIMULATION SOFTWARE)	14
3.3	AIRFLOW MODELLING (NODAL NETWORK & CFD).....	15
3.4	CONVECTION IN THE DOUBLE-SKIN FACADE.....	16
3.4.1	<i>Enclosed cavity (free-convection)</i>	17
3.4.2	<i>Ventilated open cavities</i>	19
3.4.3	<i>Closing Remarks on Convection in Double-skin Facades</i>	20
3.4.4	<i>The role of CFD</i>	21
4	MODELLING APPROACH	23
4.1	INTRODUCTION	23
4.2	OVERVIEW OF MODELS USED IN INVESTIGATION	23
4.2.1	<i>General modelling considerations</i>	25
5	AIR-FLOW WINDOW (DOUBLE-SKIN FACADE WITH NO CAVITY BLIND)	26
5.1	CAVITY CLOSED.....	27
5.2	EXTERNAL FACADE OPEN.....	31
5.3	INTERNAL & EXTERNAL FACADE OPEN	37
5.4	CONTROLLING ALL THREE OPERATIONAL CONDITIONS:.....	38
5.5	PERFORMANCE OF AIRFLOW-WINDOW.....	41
6	DOUBLE-SKIN FACADES WITH ROLLER-BLIND SHADING	44
6.1	PILOT MODEL - STRATEGY.....	44
6.2	INSTABILITY ISSUES WITH THE PILOT MODEL	45
6.2.1	<i>Time-step control relaxation</i>	46

6.2.2	<i>A simplified airflow model</i>	47
6.3	BLIND POSITION ABSTRACTION	48
6.4	CAVITY TEMPERATURES.....	53
6.5	BLIND PHYSICAL PROPERTIES & FACADE PERFORMANCE	54
6.5.1	<i>Solar absorptivity & emissivity</i>	55
6.6	MULTI-STOREY FACADES - DISCRETISATION OF CAVITY.....	57
6.6.1	<i>The effect of fictitious surfaces</i>	60
6.7	AIR-FLOW NETWORK – DISCHARGE CO-EFFICIENT SENSITIVITY	62
6.8	CONTROL OF DOUBLE-SKIN FACADE WITH ROLLER BLIND	63
6.8.1	<i>The effect of large fictitious divisions</i>	63
6.8.2	<i>Conclusions on fictitious surface utilisation</i>	67
6.8.3	<i>Example of shading control operation</i>	68
7	DOUBLE-SKIN FACADES WITH VENETIAN BLINDS.....	72
7.1	SOLAR MODEL ISSUES	72
7.1.1	<i>ESP-r solar model</i>	73
7.2	METHODS OF MODELLING VENETIAN SLATS	74
7.3	SAW-TOOTH VENETIAN MODEL INVESTIGATION	75
7.3.1	<i>Testing the model (insolation)</i>	77
7.3.2	<i>Further testing in complete simulations</i>	81
7.3.3	<i>Significance of saw-tooth insolation results</i>	82
7.3.4	<i>Long-wave radiation exchange in Sawtooth model</i>	84
7.3.5	<i>Convection in Sawtooth model</i>	87
7.4	CONCLUSIONS FROM SAW-TOOTH MODEL.....	88
7.5	VENETIAN MODELLING - THE IDEAL SIMULATION PROGRAM	90
8	CONCLUSIONS & RECOMMENDATIONS	92
8.1	INITIAL GEOMETRICAL CONSIDERATIONS.....	92
8.2	MODELLING PRE-REQUISITES	93
8.2.1	<i>Insolation distribution</i>	93
8.2.2	<i>Longwave radiation</i>	93
8.3	AIRFLOW-WINDOW MODELLING (DOUBLE-FACADES WITHOUT SHADING)	93
8.4	DOUBLE-SKIN FACADES WITH ROLLER BLINDS.....	96
8.4.1	<i>Ventilation</i>	96

8.4.2	<i>Convection</i>	98
8.4.3	<i>Vertical division of cavity in multi-storey type facades</i>	99
8.4.4	<i>Control of operation mode</i>	99
8.5	DOUBLE-SKIN FACADES WITH VENETIAN BLINDS	101
9	REFERENCES	104
	Appendix A – Climatic analysis of periods used in simulations	106
	Appendix B – Nodal network air-flow calculation check.....	109
	Appendix C– Insolation results when “misur” =6&10 for Venetian saw-tooth model with 6 divisions in outer façade	111
	Appendix D- Insolation results when “misur” =6&10 for Venetian saw-tooth model with 12 divisions in outer facade	112
	Appendix E - Erroneous insolation results sample (for 15th March) when MISUR=46.....	113
	Appendix F – Source code fix in “Convect2.F”, convection correlations	114
	Appendix G – Source code fix to display multi-page Surface Convection menu	115

1 Abstract

The double facade - a highly dynamic system reacting to the climate through a co-ordinated use of shading, ventilation & construction components – deserves a calculation method offering a similarly dynamic resolution of the building physics involved. Dynamic building energy software is the natural choice to facilitate this.

Examples of double facade modelling are however very rare and modelling guidelines are virtually non-existent. A major issue with building energy software also concerns building physics simplifications becoming problematic in the new double-facade domain. Where as previously building skins provided fairly strict physical boundaries to the outside, double facades have a much closer and complicated interaction with external environment – so the level of resolution initially provided may now not be sufficient. In this study an examination of the potential limits of building energy software (ESP-r) is undertaken in conjunction with an extensive sensitivity analysis of double facade configurations to help answer this question. The study also aims to provide helpful modelling guidelines in doing so.

It is apparent in the study that modelling double-skin facades is a complex task involving the adaptive control of major energy flowpaths during the facades changing operation modes, such as convection, ventilation and insolation distribution. Indeed a wide range of operation regimes is evident. The characteristics of double-skin cavity itself significantly impact on the environment behind the internal facade and results are highly sensitive to the way it is modelled. To obtain an accurate prediction of the facade performance, it is very important to ensure appropriate treatment of: solar insolation, cavity convection regimes, surface view-factors, blind spatial position, airflow resistances, vertical temperature gradient and cavity divisions with fictitious divisions.

A complete representation of airflow windows is attainable via a separate zone representing the window cavity, controllable across all modes of operation. Double-skin facades utilising roller blind shading are modelled with two-zones representing the cavity. Complete control of this type of facade is attainable via property substitution and the use of fictitious constructions. Although these fictitious surfaces introduce errors they are tolerable in the main – particularly in a design situation where the ability to represent significantly different operation modes is important. Facades spanning significant heights can be further divided vertically with the use of fictitious surfaces in order to expose significant

1 Abstract

vertical temperature gradients. Double-skin facades utilising Venetian blinds are modelled with two zones again but with a dividing surface constructed in a saw-tooth pattern. Such a depiction is found to offer the best representation for the complex processes associate with the Venetian blind system in ESP-r.

2 Introduction

The double-skin facade is rapidly becoming a common design feature in European architecture, driven by the following main factors (Poirazis, 2004):

- the aesthetic desire for an all glass-facade that leads to increased transparency, closer link to the outside and the creation of a certain corporate image.
- the reduction in energy use during the occupation stage of the building.
- the practical need for a more natural indoor environment and lesser reliance on artificial plant.
- acoustic benefits for buildings in noise polluted areas.

The need to predict a double facade's performance is therefore necessary, for issues of energy consumption and the potential for environmental damage.

2.1 History of the Double-skin facade

The double-skin facade is by no means a new concept as with many low energy techniques we see regaining favour today. Many years ago the benefits of using an unheated buffer space were recognised in relation to creating an improved thermal environment for human occupation. Many old houses in central Europe utilise box-type windows, where a casement of glass is positioned in front of the internal window along with shutters to increase thermal insulation. The unit is opened in summer to promote a free-flow of air to the inside and shutters can additionally be drawn to block solar gain. Oesterle (2000) quotes these units to have a Uvalue of $2.5\text{W/m}^2\text{K}$. Elsewhere Saelens, (2002) mentions that:

“in 1849, Jean-Baptiste Jobard at that time director of the Industrial Museum in Brussels, described an early version of a mechanically ventilated multiple skin facade. He mentions how in winter hot air should be circulated between two glazings, while in summer it should be cold air”.

Moving to the modern day, advances in architecture in the 20th century meant that the size and number of windows were no longer limited by structural considerations of the past. It was now

2 Introduction

possible to create glazed walls but architectural freedom was still limited by the constraints of building physics and thermal comfort. In fully glazed buildings increased heat losses and problematic condensation and summer overheating meant that it was necessary to resort to mechanical plant to compensate for shortfalls in the operation of the building skin. The available technology and the lack of environmental awareness at the time often created buildings with high energy consumption and correspondingly great emissions of pollutants. Additionally, acoustical performance was very poor and weather tightness was below acceptable limits. Advances in glass architecture centred on the development of new insulating units to improve the performance of fully glazed buildings.

Insulating double glazing was developed with a smaller gap than box-type windows such that the two panes open at once. Louvred blinds were also often inserted between panes as a means of sun-shading. The oil crises in 1973 & 1979 boosted the rate of development in insulating glazing further as greater awareness on energy consumption became apparent. Innovative improvements such as the addition of low-emissivity coatings and inert gas filled cavities were made. In the same years awareness grew in the field of solar architecture in relation to good external shading, thermal mass and the role played by variable ventilation. In the 1990's a further breakthrough regarding glazing was achieved with the development of spectrally selective glazing allowing high visible spectrum transmission whilst blocking other wavelengths of incident solar radiation. Such materials offer a solution where high quality adjustable shading devices cannot be installed. Other technologies such as electro-chromic and photo-chromic glazing are also now available which can change their properties depending on environmental conditions. All these developments are promising but it will be a long time before any will be available in large enough quantities to make them economic to use.

In contrast, double skin facades achieve flexible operation through a combined system of components which are both known and used already - allowing the regulation of heat, cold, light & noise in such a way that comfort is achieved with low energy consumption. Further they also provide an extra level of acoustic insulation and allow natural window ventilation via an intake of air into the cavity between the two layers of the facade - a set-up that can offer the appropriate level security required for night purging in some situations. Reduced solar gain and free ventilation is an obvious way of saving energy if it allows plant operation to be alleviated for at least part of the time. Awareness too is increasingly growing to adopt natural ventilation in response to badly designed air conditioning systems, which are frequently named as one of the causes of the infamous SBS.

2.2 Definition of the modern double-skin facade

In the author's opinion, the Belgian Building Research Institute [BBRI], (2002) provides a reliable definition of a double-skin facade in its source book:

"A facade covering one or several storeys constructed with multiple glazed skins. The skins can be air tight or not. In this kind of facade, the air cavity situated between the skins is naturally or mechanically ventilated. The air cavity ventilation strategy may vary with time. Devices and systems are generally integrated in order to improve the indoor climate with active or passive techniques. Most of the time such systems are managed in semi automatic way via control systems."

The layers of the facade are described below:

- Exterior Glazing: Usually it is a hardened single glazing. This exterior facade can be fully glazed.
- Interior glazing: Insulating double glazing unit (clear, low E coating, solar control glazing, etc can be used). Almost always this layer is not completely glazed.
- The air cavity between the two panes. It can be totally natural, fan supported or mechanically ventilated. The width of the cavity can vary as a function of the applied concept between 200 mm to more than 2m. This width influences the way that the facade is maintained.
- The interior window can be opened by the user. This may allow natural ventilation of the offices.
- Automatically controlled solar shading is integrated inside the air cavity.
- As a function of the facade concept and of the glazing type, heating radiators can be installed next to the facade.

2.3 Useful classification of facade configurations - Belgian Building Research Institute Study

The stated aim of the BBRI study (2002) is to investigate the potential of active facades, the related problems and risks in order to devise guidance in standardisation and technical approvals. To facilitate this they have developed a classification system to describe different double-skin facade configurations based on a database of case-studies. This will be useful for model development in this study.

Facades are classified according to:

- The ventilation type

This relates to the ventilation in the air cavity situated between the two glazed facades which can consist of:

1. *Natural ventilation*
2. *Mechanical ventilation*

- Partitioning of the air cavity

The partitioning of the air cavity refers to the physical division of the air cavity. Distinction is firstly made to separate windows from facades.

1. *Air-flow Windows*
2. *Double-Skin Facades:-*

2 Introduction

One storey height facade modules	The air cavity is divided horizontally and vertically at the level of each facade module. Naturally ventilated double facades with one storey-height facade modules are also known as a 'Box window' type. They note that most of the mechanically ventilated facades in Belgium have a one-storey-height facade module partitioning type.
Corridor facade	Corridor facades are characterised by a wide air cavity partitioned at the level of each storey. Essentially this is a one storey module that forms a corridor which can cover either a whole storey or several adjacent zones.
Multiple storey facade	Multiple storey facades are not partitioned vertically or horizontally. The air cavity extends a large height with metallic maintenance grids at the level of each storey allowing circulation. In extreme cases, the air cavity can envelop the whole of the building without any partitioning.
Shaft-box facade	Shaft box facades are very similar in nature to the one-storey height module. However the modules are linked with building high vertical shafts by means of a bypass opening. The stack effect draws the air from the box windows into the vertical shafts and from there up to the top, where it is emitted.

Table 1 – Double-skin facade configurations, from Belgian Building Research Institute Study (BBRI, 2002)

- Ventilation mode

This area of the classification relates to the origin and the destination of the air circulating in the cavity. Five ventilation modes are distinguished:

1. *Outdoor air curtain,*
2. *Indoor air curtain,*
3. *Air supply,*
4. *Air exhaust,*
5. *Air buffer,*

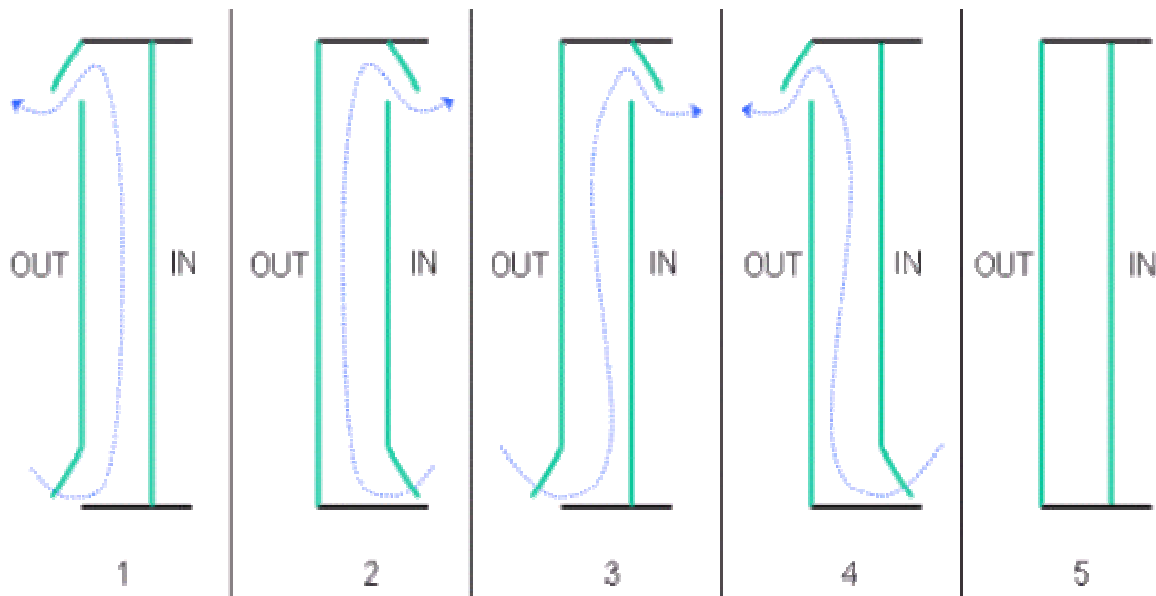


Figure 1 BBRI ventilation classification diagram

(<http://www.bbri.be/activefacades/images/schema/ventilation-modes-ADE-001.jpg>)

Further design characteristics that focus the classifications are noted:

- Naturally ventilated facades change operational mode depending on conditions.
- Mechanically ventilated facades are generally not equipped with inlets and are most of the time characterized by only one ventilation mode (ventilation modes 2,4 & 5)
- Double ventilated facades are composed by two glazed skins, generally one single glazing and one insulating glazing. Facades ventilated with indoor air tend to have the insulated glazing placed at the outside layer where as those ventilated with outside air have it placed at the inside.

Wider classification

The authors of the study recognize that the above classification method can produce large number of permutations and of course not all of these are actually employed in practice. As such they have also proposed a wider classification in order to characterize the different double ventilated facades commonly found in operation. These are:

- Climate facade - Ventilation is mechanical and air flows from inside to outside
- **Double skin facade** – Ventilation is natural and air flows from exterior to exterior (ventilation mode 1 - Figure 1)
- Interactive facade – Ventilation is natural/mechanical assisted and from either interior/exterior to interior/exterior

2.3.1 Choosing appropriate classifications to model – investigation strategy

Like the BBRI study, it is appropriate to widen the classification of facades so that an exhaustive modeling study of every permutation isn't undertaken, rather the main double-skin facade features in different configurations are considered in this study. Modeling minor variations in different configurations would be a trivial task anyhow once methods are set. The crux of the problem is really related to modeling double-skin facade features correctly. Most uncertainty in this area pertains to:

- Naturally ventilated cavities (convection modes, ventilation openings)
- Blind representation (positional sense)
- Cavity sub-divisions (stratification in multi-storey facades)
- Combined convection, shading & ventilation control
- Venetian blind representation

Modeling a mechanically ventilated facade involves a straightforward modification on a naturally ventilated one - simply a case of specifying an air-flow rate (and airflow origin) in the cavity. On the other hand, blind representation is a feature that is important in nearly all common double-skin facades.

Determining what needs to be appropriately accounted for in different configurations is important. By starting with the most simple cases of double-skin facades (eg. Airflow-window) and progressively adding in more detail (eg. shading), a picture of how to best model the different configurations is built up along with the limitations faced. From the foregoing discussion, the wider BBRI classification of the double-skin facade is most suited to this approach and many similarities with its characteristics can be found permeating through the models. Further details on specific models through this approach can be found in section 4.

3 Modelling Double-Skin Facades

3.1 Energy flowpaths

As mentioned, double-skin facades range from multi-storey types to single airflow windows, they can also utilise differing types of components such as roller blinds or Venetian blinds, as well as having key topography differences such as cavity depth. All of these factors can significantly affect the thermo-fluid processes occurring in double-skin facades.

To accurately predict the thermal energy performance in the many possible different typologies requires a simulation program capable of an appropriate resolution. Furthermore, thermo-fluid processes in double facade systems are highly dynamic in nature and closely coupled in the heat and mass transfer domains.

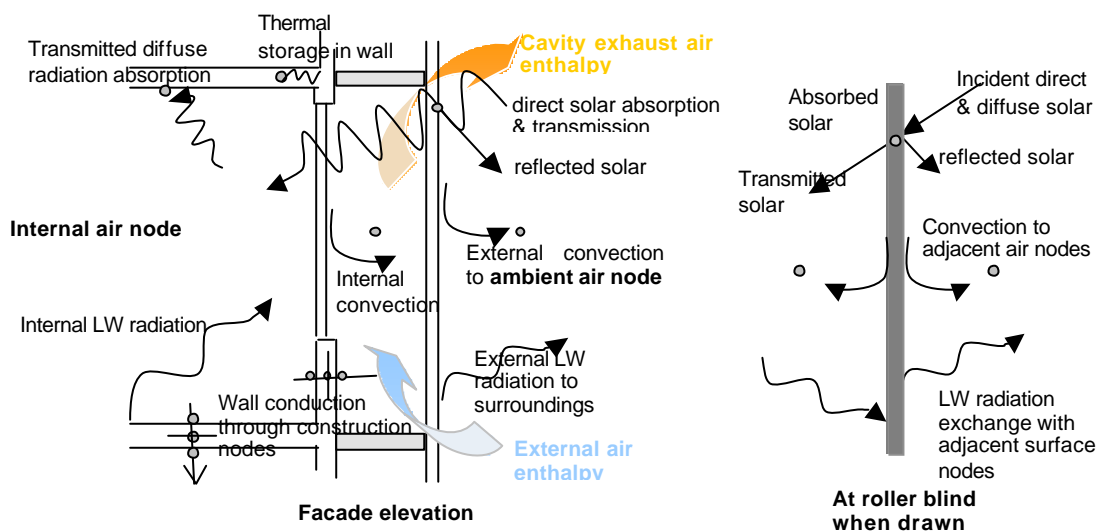


Figure 2 - Flowpath diagram for dynamic thermal processes in a double-skin facade

As a pre-requisite therefore a simulation tool should be capable of describing and solving dynamic energy and mass-flow equations for multi-zone. Programs such as ESP-r, EnergyPlus and TRNSYS are prime candidates in the multi-zone category, capable of performing the necessary “whole-building” assessments. Though these advanced simulation programs are by no means ideal and all face similar obstacles regarding the level of resolution necessary to model some major thermodynamic flowpaths in double-facades.

3 Modelling Double-Skin Facades

In particular, the author believes that ESP-r offers an excellent opportunity for progression towards the ideal state due to its open-source code and versatility arising from its traditional research based roots. To this effect, ESP-r will be the program of choice for the remaining study into modelling double facades. This study will inevitably take ESP-r to its limits in the challenge to best model double facades; it shall define areas of weakness and propose remedial action where appropriate.

3.2 ESP-r (Building Simulation Software)

The ESP-r building simulation software has been in constant development since its first prototype was developed (Clarke, 1979). It has evolved in the direction of a fully integrated solver - in the pursuit to better represent the interactions of physical processes occurring in buildings. It integrates heat transfer processes, inter-zone airflow, intra-zone air flow, electrical power flow, HVAC plant, moisture flows & natural lighting.

ESP-r's "Project Manager" provides a central interface from which model creation, simulation and results analysis is controlled:

- database maintenance
- geometry generation & construction attribution
- pre-thermal simulation tasks such as solar insolation prediction & view factor calculation
- heat, air, moisture flow domains
- control law generation & attribution
- simulation control & initiation
- visual results analysis

ESP-r's building thermal model is founded upon a finite-volume heat balance discretisation method. Construction components, surfaces and zones are represented by nodes (see Figure 2), for which an energy balance is performed on each. Conduction, convection and radiation exchanges are described relative to other system nodes to generate a series of equations describing energy transfer over space & time. Solar insolation is included in these equations by way of a direct solar-tracking processor, which is combined with the diffuse distribution. This equation set is then solved simultaneously to provide the thermal state at each node and the energy exchange between them.

3 Modelling Double-Skin Facades

ESP-r also employs a partitioned solution approach such that a separate solver treats other solution domains (e.g. network air flow, CFD). Interactions between physical processes in different domains are accounted for by passing information between solvers on a time-step basis; known as a coupled solution evolution. Furthermore this enables an optimized treatment of each domains equation sets which can be very sparse. The co-operative solver approach in ESP-r is thoroughly documented elsewhere [Clarke & Tang] as is ESP-r's treatment of physical processes (ESRU). The remainder of this section will focus on the main choices to be made concerning modelling double-skin facades in ESP-r.

3.3 Airflow modelling (Nodal network & CFD)

In recent times, two dynamic solution methods have been successfully incorporated into ESP-r

- Nodal network method
- Computational fluid dynamics (CFD)

In the network method, a network of nodes represents the pressures and temperatures in rooms, parts of rooms and system components. Inter-nodal connections represent air-paths associated with cracks, specific openings, doors, ducts, fans etc. It is assumed that for each type of connection there exists an unambiguous relationship between the flow through the component and the pressure difference across it. Conservation of mass at each node produces a set of simultaneous, non-linear equations, which can be solved by a process of iteration to determine flow results.

In CFD the conservation equations for mass, momentum and thermal energy are solved for all nodes of a cellular grid that is placed within the domain. In theory, the CFD approach is applicable to any thermo-fluid phenomenon. However, in practice, and in the building physics domain in particular, there are several problematic issues relating to computational power and the nature of flow-fields (especially at surfaces).

Significant progress in ESP-r's CFD application has been made recently [Negrao (1995), Beausoleil-Morrison(2000)]; notable features are:

- K-e turbulence model & laminar model

3 Modelling Double-Skin Facades

- Ability to account for natural buoyant flow boundaries with appropriate near wall functions (Yuan, 1993)
- Ability to be coupled with building thermal domain
- Ability to provide CFD determined convection co-efficients to the building simulator
- Ability to distinguish between natural, forced & mixed flow regimes and select appropriate near wall treatment.
- Ability to check when conditions are such that CFD is likely to be incapable of providing accurate results (e.g. weak turbulence conditions) and switch to use traditional correlations for heat transfer.
- Ability to connect with the air-flow network (only two-connections presently)

A trade-off exists between the two methods. The network method can be connected over the entire building and is much faster since it employs far fewer nodes but will only provide information about bulk flows. On the other hand, CFD can provide details about the nature of the flow field. The nodal network shall be the primary tool in this study, supported by CFD.

It is important to note that there is a considerable lack of data in relation to airflow components in buildings. As such, justified approximations will need to be made in these instances. It is outwith the scope of this study to provide new data for components.

3.4 Convection in the Double-Skin Facade

This is arguably one of the most ambiguous flow-paths found in building energy simulation and so deserves consideration. Lots of work has been undertaken recently to incorporate the most relevant and up-to-date correlations for building simulation into ESP-r [Beausoleil-Morrison, (2000)]. A review of the most appropriate relationships for double facades is equally required.

Different convection regimes manifest themselves in a double-skin facade depending on its particular operation. For example in the wide BBRI classification of a double-skin facade – the cavity can be sealed and have only internal circulation or it can be open with air flowing through the cavity from outside.

3 Modelling Double-Skin Facades

3.4.1 Enclosed cavity (free-convection)

A rectangular cavity is created when the double-skin facade is closed and if we assume that the cavity is air-tight then only free-convection occurs. This is a particular convection problem that has been widely studied in the past [Ostrach(1972), Catton (1978)] and is typically defined by the dimensionless cavity aspect ratio and the Rayleigh number (evaluated with the cavity depth as characteristic depth). Furthermore, flow & convection regimes in narrow and wide cavities are distinguished over a range of Rayleigh numbers.

Narrow cavities:

When the cavity aspect ratio (in the vertical & horizontal sense) is much greater than 1 and the Rayleigh number is less than the critical value $Ra_{L,c}=1708$, buoyancy forces cannot overcome the resistance imposed by viscous forces. Heat transfer by advection is constrained and so conduction governs. As such, the convection co-efficient tends towards $h=k/L$ ($Nu_L=1$). This situation however, will likely only happen in double-glazing systems whose aspect ratios are above 50. In double-skin facades these ratios are much lower, typically between 5 and 40, even in a narrow air-flow window.

Wide Cavities:

In wider cavities and when $Ra_{L,c}>1708$, convection governs. For aspect ratios in the range $2<(H/L)<10$ the correlation below has been suggested by Catton (1979).

$$Nu_L = 0.22 \left[\frac{Pr}{0.2 + Pr} \cdot Ra_L \right]^{0.28} \left[\frac{H}{L} \right]^{\frac{1}{4}} \quad \text{Valid for } Pr < 10^5 \text{ \& } 10^3 < Ra_L < 10^{10}$$

Equation 1

Similar correlations exist for other Prandtl, Rayleigh & aspect ratio ranges. However these equations are not best suited to building energy simulation because:

- the correlations are not widely applicable to larger cavity aspect ratios, especially for the Prandtl numbers ranges found with buildings (e.g. $Pr \sim 0.72$).
- the equations are based upon convection between two parallel surface temperatures where as building simulation software forms energy balances at each surface based upon the adjacent air temperature.

3 Modelling Double-Skin Facades

From another perspective, considering that boundary layers in wider cavities do not merge and remain moderately isolated, they essentially become room like zones. Therefore wall convection correlations for rectangular zones may give reasonable results. In this case, correlations for a vertical wall with no heating or cooling can be used [Alamdari and Hammond (1983)].

$$h_{c,i} = \left[\left(1.5 \left(\frac{\Delta q}{H} \right)^{0.25} \right)^6 + (1.23(\Delta q)^{0.33})^6 \right]^{\frac{1}{6}}$$

Equation 2

where $\Delta\theta$ is the temperature difference between the wall and the zone air temperature and H is the wall height (m). This correlation is particularly suited to building simulation being in a convenient dimensional and continuous form. Other Alamdari and Hammond correlations for buoyancy driven flow from horizontal floor and ceiling surfaces are more appropriate for those building surfaces. They encompass laminar, transitional, and turbulent flow regimes, and claim to cover the full range of temperatures and dimensions relevant to building applications. Further reference is made to [Beausoleil-Morrison (2000)] where the worth of such correlations has been studied and made available in the ESP-r system via automatic attribution.

3.4.2 Ventilated open cavities

Stack-driven natural flow

When the external skin of the double-skin facade is opened and buoyant forces drive air, this regime is described by free-convection correlations in parallel plate channels.

Again distinction is made in the literature between narrow and wide cavities. In narrow channels a fully-developed, Hagen-Poiseuille velocity profile is created as the boundary layers merge. In wider & shorter channels, boundary layer interference is small and heat transfer can be described better by that for flow along an isolated vertical plate.

Bar-Cohen & Rohsenow (1984) developed correlations for a complete range of cavity aspects based on relationships for the fully-developed regime and those for isolated plates. For symmetric isothermal vertical plates the following correlation is given:

$$Nu_L = \left[\frac{576}{(Ra_L \cdot L/H)^2} + \frac{2.87}{(Ra_L \cdot L/H)^{\frac{1}{2}}} \right]^{\frac{1}{2}}$$

Equation 3

The fully developed limit corresponds to $Ra_L(L/H) < 10$.

The isolated plate limit corresponds to $Ra_L(L/H) > 100$.

For the aspect ratios found in double-skin facades with air around 300K, operation is again most likely to relate to the wide limit – that of the isolated plate. In this case, general correlations from Alamdari and Hammond (1983) for walls, floors and ceilings can also be used. The fully developed limit only really corresponds to flow beginning around double-glazing aspect ratios.

Wind-driven flow

Flow caused by wind pressure is by definition forced convection and may interfere with buoyancy driven natural ventilation. In a large multi-storey facade where significant wind pressure differences

3 Modelling Double-Skin Facades

occur over the widely spaced facade inlet and outlets, both will typically occur. This then becomes a mixed convection regime.

Incropera and De Witt (1981) give the following limits for natural, mixed and forced convection regimes:

$$\begin{aligned} Gr_H \gg Re_H^2 & \quad \text{natural convection} \\ Gr_H \approx Re_H^2 & \quad \text{mixed convection} \\ Gr_H \ll Re_H^2 & \quad \text{forced convection} \end{aligned}$$

Equation 4

For the forced convection case, different correlations have traditionally existed for flow/convection regimes for entrance region flow and that for fully-developed flow in the cavity. Bejan (1984) however combines both to give an average Nusselt number valid for the entire length of a cavity, covering laminar and turbulent flow.

$$Nu_H = 0.664 Pr^{1/3} \cdot Re_{x,tr}^{1/2} + 0.0296 Pr^{1/3} (Re_H^{4/5} - Re_{x,tr}^{4/5}) \quad Pr > 0.5$$

Equation 5

$Re_{x, tr}$ is the Reynolds number at the length before which transition to fully developed flow. The following relation for transition in a turbulent regime can be used to estimate distance:

$$X_{tr} / D_h = 10$$

Equation 6

Where D_h = hydraulic diameter of the cavity cross-section.

3.4.3 Closing Remarks on Convection in Double-skin Facades

Different convection regimes exist depending on the operation of the double-facade; closed/open, forced/natural flow. Controlling the deployment of the appropriate correlation in simulation is therefore

necessary in a detailed model. Much work has been carried out in this area - the automatic and adaptive control of relevant convection correlations in ESP-r [Beausoleil-Morrison (2000)].

From a performance prediction perspective there nevertheless exists the problem of stochastic climate data and how convection varies with different conditions. One particular example is the multi-storey facade where wind effects can cause significant forced flow that may augment or diminish buoyant flow. However, much uncertainty can be removed by considering what is important in the simulation. For example if the focus was on overheating, the warmest days typically occur when conditions are still and the stack effect is relied upon. Buoyancy-induced flow could therefore be seen as a worst-case scenario. In this study, flow will therefore be restricted to buoyancy induced.

3.4.4 The role of CFD

CFD applications applied in the building setting have traditionally offered the user the ability to determine detailed flow & temperature fields in a domain – after having supplied appropriate boundary conditions. This attribution can be erroneous though, since the ability to predict the convective heat transfer at a surface is governed by the CFD program's ability to predict the surface boundary layer temperature & velocity profiles. Because excessive grid refinement and the use of complex near wall turbulence models is restricted by computational resources, near-wall functions are adopted. The reliability of these functions is questionable in the building domain however – they are not suited to predicting weakly turbulent forces and those governed by buoyancy forces (Beausoleil-Morrison, 2000). For this reason, only a general indication of flow in buildings can be gained at most. Trying to predict surface convection co-efficients would be highly dangerous. Furthermore these CFD applications work in stand-alone mode and so from a building simulation perspective supplying suitable boundary conditions was difficult. They only practically offer a snapshot of the flow field at one instance in time.

Recently however, significant progress in the field of coupled CFD/building simulation has been made (Beausoleil-Morrison,2000). In ESP-r, appropriate wall-functions describing buoyant boundary layers (Yuan et al, 1993) have been added and the CFD simulation can be coupled with the building simulation to swap appropriate boundary conditions. Furthermore the software has the capability to check the flow regimes on each surface, based upon Equation 4, and select/reject near-wall functions. On this basis, CFD provides a much better platform from which to assess convection co-efficients

3 Modelling Double-Skin Facades

when no experimental back-up is available. It is still recommended that the latter be used first and foremost though. Coupled CFD simulations require great computational resource and will take considerably longer than employing an experimentally determined correlation in the building simulator.

4 Modelling Approach

4.1 Introduction

Although building simulation software is advanced in its treatment of real-life energy processes, modelling complex environments and systems typically involves a level of simplification or abstraction for practical reasons. For example, representing a room air zone as a bulk temperature that then pertains to all regions within it or say changing a transparent constructions optical property to represent the closing of blinds.

This level of abstraction/simplification can also have much to do with the purpose of the simulation (i.e. determining annual energy consumption as opposed to ensuring comfortable local air flow patterns) all whilst ensuring prohibitive computational effort is avoided - both in model creation & simulation CPU effort.

Double facade modelling is an area that encompasses many such issues and how best to approach them is a theme which is addressed by this thesis. The method adopted is founded on an well-defined pilot model – allowing us to explore the sensitivities surrounding double-skin facades simulation - then progresses to more complex configurations.

4.2 Overview of models used in investigation

Table 2 overleaf outlines the progression of models used in the investigation.

4 Modelling Approach

Model	Purpose
Airflow-window	<p>To provide the simplest representation of a double facade typology (a simple air-flow type window) and a full-control regime.</p> <p>To investigate the use of different convection correlations in the facade cavity</p>
CFD model of closed cavity	To investigate how the airflow patterns vary with cavity aspect ratio (closed cavity) and if it is appropriate to use general room convection regimes.
Base Pilot Model	<p>To provide the most reliable representation of a typical double facade configuration currently possible according to BBRI study. The roller blind shading model.</p> <p>Serves as a pathfinder to explore model sensitivities (i.e. blind position, blind properties, air-flow network & control issues)</p>
Multi-storey model	Based on base pilot model. To specifically investigate the effects of thermal gradient in the double facade.
Roller-blind control model	To investigate the holistic control of roller-blind shading, via optical & thermo-physical property substitution. Integrated control of day-lighting, cavity air-flow, cavity convection and internal temperature.
Venetian Saw-tooth model	To investigate the significance of Venetian blind geometry on major thermodynamic flowpaths. To serve as a guideline for providing the most accurate representation currently possible and to explore limitations in modelling this subject.
Venetian Float model	To provide further resolution to the above problem, particularly in terms of long wave radiation modelling.

Table 2 – Outline of Models used throughout the study

4.2.1 General modelling considerations

When the layout of the building is very regular we can reduce the problem from the whole width or depth of the building to a representative repeating section in combination with dynamically similar boundary conditions. In a double-skinned building the perimeter zones adjacent to the facade should be included along with the double-skin facade itself. Where the double facade spans multi-stories and where thermal breaks are not significant, the stack effect requires the model to include the full height of the facade. The simulation period needs to cover at least a full day preceded by several simulation start-up days in order to account for thermal storage effects of the construction.

To provide controlled conditions in each of the models, wind effects are not considered until later when the performance of common configurations is investigated. The stack-effect therefore provides the sole driving force for natural ventilation through the system. It is a particularly relevant scenario nevertheless since still conditions tend to coincide with worst case overheating cases when the stack-effect is relied upon.

5 Air-flow window (Double-skin facade with no cavity blind)

5 Air-flow window (Double-skin facade with no cavity blind)

The air-flow window is a basic form of the double-skin facade. It shall be used as a root case to begin our investigation into modelling the operation of double-skin facades (i.e. the double skin facade without cavity blind).

The airflow-window model is made to be the full floor-to-ceiling height, with typical double-skin facades in mind. A diagram of the model is shown in Figure 3:

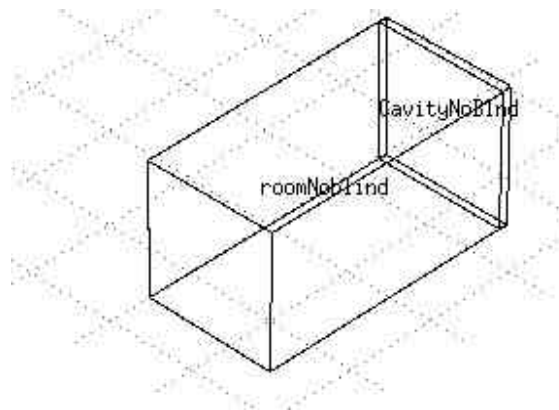


Figure 3 – Diagram of airflow-window model

- The airflow window cavity is 0.2m wide, representing typical window depths found in practice.
- The window is east facing due to the lack of shading.
- Solar insolation is determined by the ray-tracing method in ESP-r.
- The external glass layer is a single pane of float glass ($U=5.38 \text{ W/m}^2\text{K}$) and the internal layer is a double-glazing construction ($U=2.75\text{W/m}^2\text{K}$)
- Dynamically similar conditions are assumed for all boundaries other than the east facing window which is external.
- View factors are determined by the ray-tracing method in ESP-r.
- Initially, the internal zone is heated to a 20°C set-point (ideal control) from 9h00 to 24h00hrs.
- Initially, simulations are carried out for the 15th March at 1 minute time steps (climatic details can be found in Appendix A).

5 Air-flow window (Double-skin facade with no cavity blind)

The modelling strategy is to simulate the airflow -window in three different operation modes:

- Cavity closed
- External facade opened (internal cavity flow)
- Internal & external facade opened (full airflow)

and then combine all in a suitable control scheme.

5.1 Cavity Closed

The cavity is assumed to be air-tight and so the convection regime shall therefore be commensurate with that of a rectangular zone (Equation 2 type correlations) in the isolated plate limit. As discussed these correlations are said to encompass laminar, transitional, and turbulent flow regimes, and cover the full range of temperatures and dimensions relevant to building applications. Still since the walls are particularly close in this case and boundary layers may interact, a CFD domain is employed in the cavity to provide some level of convection validation.

Details of CFD model:

- CFD domain included in cavity only – conflated with building solver (level5)
- K-e turbulence model solver employed with Yuan wall functions when buoyancy governed flow is apparent.
- Rectangular gridding of 30 cells x 30 cells x 5cells (width x height x depth)
- Velocity & temperature solved
- Initial cell temperature of 20°C.
- Initial x, y & z velocities of 0.001m/s.
- Initial turbulence model values: $k=0.005$, $\epsilon=0.005$.
- Boussinesq approximation for buoyancy (Reference temperature of 20°C)
- Convergence criteria set to maximum of 500 iterations and maximum sum of residuals = $1e-5$
- 15th March simulation - 5 time steps per hour and 1 start-up day owing to the long CFD simulation time at each time step

A comparison of the results using the Alamdari & Hammond correlations, with the CFD results is shown below.

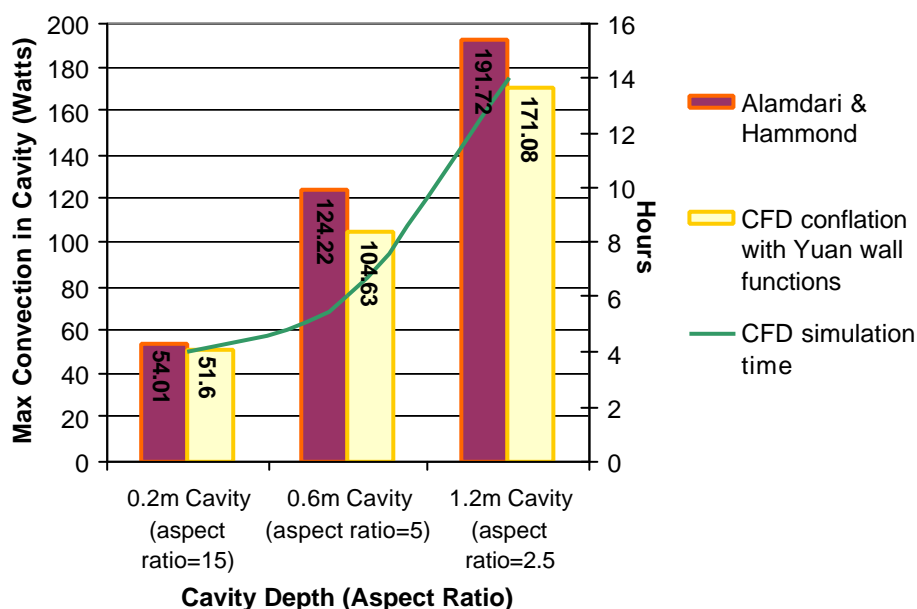
5 Air-flow window (Double-skin facade with no cavity blind)

Model convection regime	Maximum Total convection in cavity	Minimum Total convection in cavity	Heating in internal perimeter zone (kWhrs)	Number of heating hours required
Alamdari & Hammond correlations (ESP-r Defaults)	54.01	17.00	2.07	15
CFD results (k-e turbulence model with Yuan wall functions)	53.29	15.91	2.17	15.2

Table 3 – Comparison of convection in closed cavity using Alamdari correlations and using CFD (no blind)

It is apparent that the maximum convection values are very similar (within 2% of each other). However this close similarity is not evident over the entire day as the minimum convection values illustrate. The overall effect this variation has is around a 5% difference in the energy required to maintain the zone at 20°C. In line with typical double-skin facades, CFD simulations for deeper cavities were also investigated. A comparison of the maximum heat transfer by convection predicted by these and using CFD with Yuan wall functions is illustrated in Graph 1 below.

Maximum Cavity Convection (CFD Vs Alamdari & Hammond correlations)



Graph 1 – Comparison of calculated convection heat transfer, CFD Vs Alamdari & Hammond correlations (isolated plate limit)

5 Air-flow window (Double-skin facade with no cavity blind)

It is clear that differences in the convection flowpath are significant over a range of cavity aspect ratios (differences of between 5 & 15% noted). For this reason it is highly recommended that experimental validation of the convection results be undertaken before commencing a detailed modelling study. Unfortunately, experimental data to help validate the above situation is not available and it is outwith the scope of this study to generate it. Relying entirely on CFD to gauge heat transfer co-efficients is traditionally difficult. It was emphasised previously however, that the CFD solver in ESP-r is very robust compared to general stand-alone CFD solvers. This is mainly because:

- It incorporates experimentally validated Yuan wall functions specific to buoyancy driven flows.
- It will check whether the convection regime is forced, buoyant or mixed in nature and attribute the appropriate near wall treatment. (Beausoleil-Morrison, 2000)
- It will check for weak turbulence conditions where the standard $k\epsilon$ model with log-law wall function is likely to make significant errors and revert to the most suitable experimental correlations in such a case.

In terms of judging what heat transfer prediction is best, the author's opinion is more likely to favour the CFD prediction mainly because the Alamdari & Hammond correlations aren't 100% suited to narrow cavities where boundary layers can interact. The ESP-r CFD simulation accounts for such interactions by increasing the air-domain resolution and employing validated functions for surface boundary interactions. Of course it was noted that the CFD calculated convection co-efficients were indeed being used by the building simulator. Figure 4 shows the flow fields predicted by the CFD simulations in the different cavities.

In light of the lack of experimental evidence, overall it is perhaps most sensible at present to opt for a worst-case situation; that being with the Alamdari & Hammond correlations when surface convection in the cavity is greatest. Consequently the heat loss from the internal perimeter zone is greater, which impinges adversely on plant requirements/ internal conditions. Progress in the other modelling areas would also be hindered due to the long simulation time. Graph 1 also gives an idea of the increasing simulation time with cavity size (more cells) requiring as much as 14 hrs for a one-day simulation. On the other hand, simulations with bulk-air representations take under 2 minutes.

Still, in the strictest sense of modelling double facades, the actual ability to specify an appropriate convection regime is the most important factor. Indeed ESP-r allows for this, as and when appropriate experimental data/relationships are made available. Furthermore, the software is written in such a

5 Air-flow window (Double-skin facade with no cavity blind)

fashion that allows for adaptive control of convection regimes i.e. the regime can be switched depending on whether the cavity is closed or open.

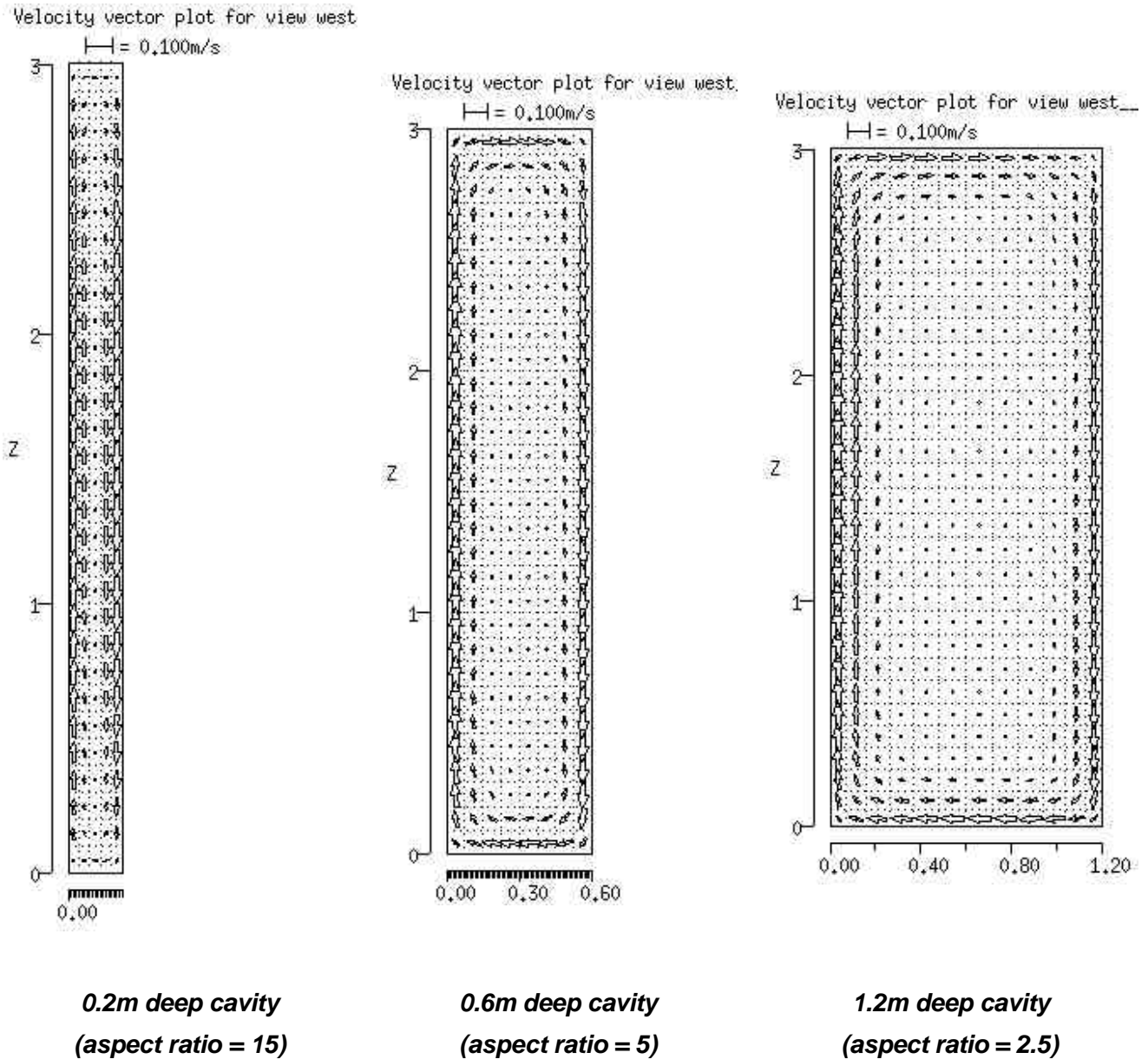


Figure 4 – CFD predicted flow field (velocity vectors) for different cavity aspect ratios

5 Air-flow window (Double-skin facade with no cavity blind)

5.2 External facade Open

When the external facade is opened, airflow is permitted in the cavity space. Buoyancy driven flow is considered by incorporating an airflow network.

The airflow network consists of:

- 1 external node representing the outside
- 1 internal node representing the air in the cavity.
- Inlet component modelled as an orifice (3m wide by 0.1 deep, discharge-coefficient =0.65)
- Outlet component identical to inlet component.
- Two connections between the nodes via inlet and outlet components

The resistance to airflow in the cavity is assumed to be negligible compared to that presented by the inlet and outlets. The roughness of float glass is especially low [$<2\text{nm}$ (Abrisa, 2004) compared to commercial steel say, $50\mu\text{m}$ (Incropera & De-Witt, 1996)] - considering general flow in ducts this would result in a very small pressure drop over the 3m long cavity. This assumption is therefore valid. It is also reasonable to neglect wind effects since any static wind pressure differences around a building, measured across the height of an air-flow window will be small. The convection regime will therefore be similar to that of buoyancy forced free-convection between parallel plates.

Previously in the discussion concerning this convection regime, it was hypothesised that Alamdari & Hammond correlations utilised in ESP-r will give good predictions with the specific Bar-Cohen & Rohsenow correlation (Equation 3). This was of course in the isolated plate limit when boundary layers do not interfere. Though we commented that in the aspect ratios associated with double-skin facades, the isolated plate limit, $Ra_L(L/H) > 100$, should always be satisfied. For example for only a 0.1°C difference between surface and cavity inlet temperatures ($T_s - T_8$) the limit is calculated below:

5 Air-flow window (Double-skin facade with no cavity blind)

$$Ra_L = g\beta(T_s - T_8)L^3/\alpha\nu = 75182.71$$

Air@300K

And,

$$\alpha = 2.219E-05 \text{ (m}^2\text{/s)}$$

$$\nu = 1.568E-05 \text{ (m}^2\text{/s)}$$

$$Ra_L(L/H) = (75182.71 \times 15) \gg 100$$

$$\beta = 1/300 \text{ (1/K)}$$

In actual fact, the depth of the cavity would have to be nearer 1cm (like double glazing) for fully developed Hagen-Poiseuille flow to occur.

Regarding the simulations, the model is assigned the latter differing correlations to gauge similarities. In addition a correlation developed specifically for the SOLVENT air-flow window is included in the comparison [Molina & Maestre(2002)]:

$$Hc = 3(T_s - T_8)^{1/3}$$

Equation 7

This provides us with a level of validation, felt more robust than in the CFD case before because it is based on actual experimental data.

It is typically the case that the external face of the airflow-window/double-facade will be opened in mild conditions to offset climate. In light of this a spring day (1st of May) is selected in the simulation period and the internal zone is made free-floating. Table 4 below highlights the significant results of the simulations employing the different convection regimes.

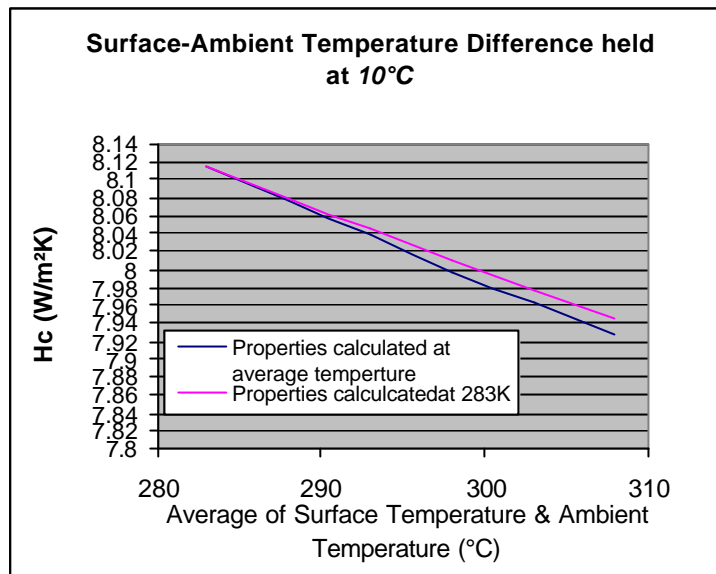
5 Air-flow window (Double-skin facade with no cavity blind)

Convection correlation	Max. Cavity Temperature (°C)	Max. Cavity Mass-flow rate (kg/s)	Max. Internal room Temperature [free-float] (°C)
Alamdari & Hammond correlations (ESP-r Defaults)	10.69	0.14	22.08
Bar-Cohen & Rohsenow (Equation 3) general correlation for flow in vertical channels (<i>air-properties at 283K</i>)	11.36	0.15	21.39
Molina & Maestre (Equation 7) SOLVENT air-flow window	11.54	0.15	21.23

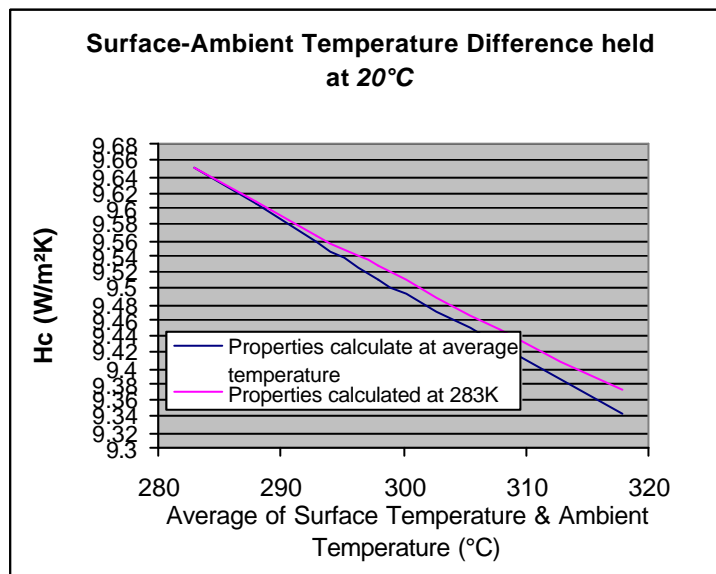
Table 4 – Comparison of different convection regimes for flow through airflow window cavity (i.e. double skin facade with no shading) - 1May

Nb. The air-properties required in the Bar-Cohen & Rohsenow correlation are to be evaluated at the average of the surface temperature and the incoming air temperature (ambient). This was based upon the value calculated (283K) in the Alamdari & Hammond case to give a good initial estimation. However the error in assuming this is very small indeed and we can actually apply the correlation over a wide range of operational temperature with negligible discrepancies. We can illustrate this by calculating the convection co-efficient based on 10°C & 20°C surf-air-temperature differences, once with air properties calculated at the average value and once at a selected constant value (283K):

5 Air-flow window (Double-skin facade with no cavity blind)



Graph 2 – Error in Bar-Cohen & Rohsenow correlation by assuming air properties at constant value (10°C temperature difference between surfaces and air)

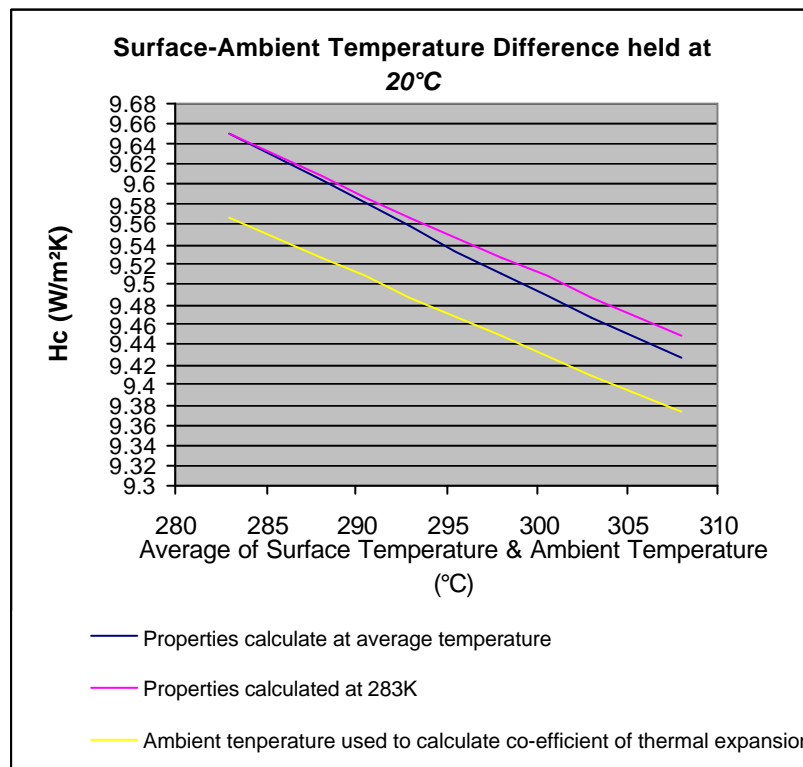


Graph 3– Error in Bar-Cohen & Rohsenow correlation by assuming air properties at constant value (20°C temperature difference between surfaces and air)

Nb. Air-properties are based on values from Rogers & Mayhew (2000) and linear interpolation is assumed for calculating properties in-between given data.

5 Air-flow window (Double-skin facade with no cavity blind)

These results show that errors ranging from zero to only $0.03\text{W/m}^2\text{K}$ are apparent and that the biggest errors result for the biggest temperature differences. Therefore we can confidently implement the Bar-Cohen & Rohsenow correlation within the ESP-r code without the need for a property database and the results will be applicable. Furthermore if we choose a better property temperature estimate of say 300K , then errors when the temperature is above and below this value will cancel out. However what is still important is that we calculate the co-efficient of thermal expansion ($1/T$) with the varying temperature value since this governs the Nusselt number equation. Still, we can simplify the code by estimating this temperature to vary according to the ambient temperature and good results will be achieved (only **small $0.1\text{W/m}^2\text{K}$** differences in H_c). Graph 3 is reproduced below with this simplification super-imposed:



Graph 4 - Graph 3 reproduced with ambient temperature simplification super-imposed:

The small error resulting using the incoming ambient temperature to calculate the co-efficient of thermal expansion means that it is an acceptable simplification. Also it is in a simple format for incorporation into ESP-r. The code representing this is shown in Appendix F.

5 Air-flow window (Double-skin facade with no cavity blind)

Concerning the results in Table 4, it is clear that the general Bar-Cohen & Rohsenow correlation for flow between vertical plates gives good results when compared with the experimentally derived correlation specifically for the SOLVENT airflow-window. The Alamdari & Hammond results would therefore appear to underestimate the heat transfer to the air, subsequently causing less of buoyant force to drive air through the channel. As a result the mass-flow is around 12.5% lower and more heat is able to dissipate towards the internal zone. Under free-float conditions, the internal zone is estimated to be one degree warmer, which can have a significant effect if cooling is employed. For example by controlling the zone to 20C (ideal control) with 100W plant capacity for illustrative purposes the cooling differences are significant:

Convection Correlation	Cooling Energy in Internal zone (Whrs)	Hours of cooling required
Alamdari & Hammond Correlations (ESP-r defaults)	310	5.7
Bar-Cohen & Rohsenow correlation (Equation 3)	200	2.1

Table 5 – Choice of convection correlation & its effect on internal energy requirements

Based on the foregoing considerations, the Bar-Cohen & Rohsenow correlation is selected as being suitable to define convection in a double-skin facade cavity.

5 Air-flow window (Double-skin facade with no cavity blind)

5.3 Internal & External facade Open

When the internal and external facade is opened, air can pass directly into the room as in a normal openable window. In this case, the air flowing into the room will be at ambient temperature. This can easily be represented by further air-flow connections which can be controlled to open at a desired internal set-point.

Since we are considering the ventilation to be one-sided we must either:

- incorporate two airflow connections to represent flow in at the bottom of the window and flow out at the top of the window.
- employ a bi-directional flow component to represent single-sided ventilation.

In an airflow-window the internal window is often bottom hung or side-hung (opening inwards) or is capable of both. For each different opening characteristic, windows exhibit very different airflow resistances (Heiselberg et al, 1999) and getting appropriate data can be difficult. This creates a multitude of further permutations in the characteristic of a double-skin facade. Although this is not a trivial matter, it is a design issue and requires the simulation user to supply the appropriate mathematical description at the time. No attempt is made in this study to calibrate the airflow to a specific window design. Furthermore window opening is stochastic in nature being dependent on user habits and so estimation will be relied upon anyway.

5 Air-flow window (Double-skin facade with no cavity blind)

5.4 Controlling all three operational conditions:

The control of the three different operational regimes:

- facade closed
- outer facade open (ventilated cavity)
- inner & outer façade open (full-ventilation)

can be achieved through the astute use of current ESP-r options.

The desired system control characteristics chosen are show in Figure 5 below:

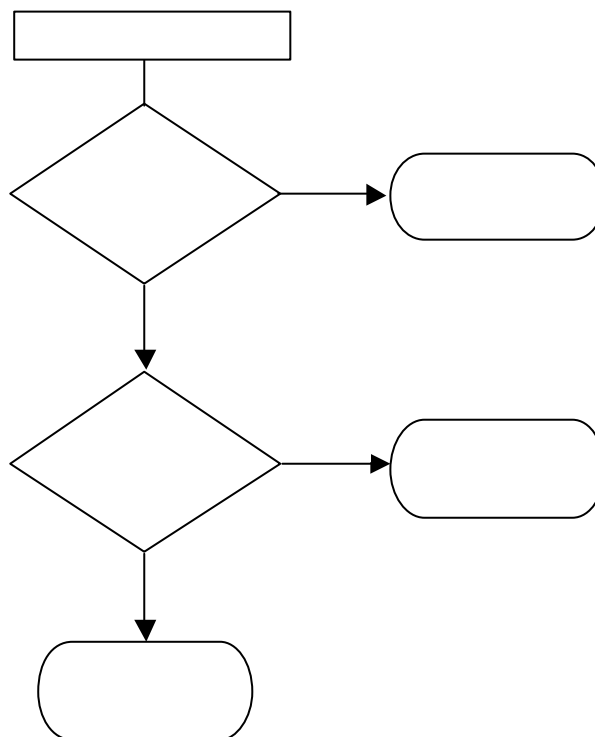


Figure 5 – Airflow -window desired control characteristics

To achieve this requires control of three different domains: internal temperature, convection & airflow.

5 Air-flow window (Double-skin facade with no cavity blind)

Temperature control (internal zone sensor setpoint =19°C)

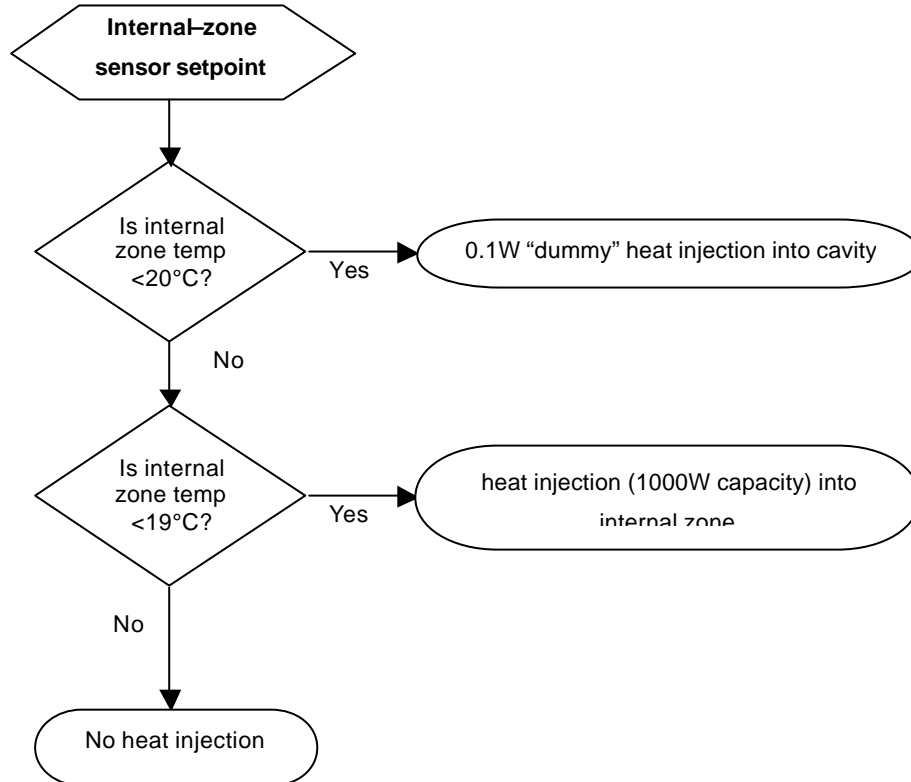


Figure 6 – Airflow window temperature control diagram

Nb. the 0.1W “dummy” heat injection into the cavity is needed for adaptive convection control and is of course small enough not to distort the results. This is because convection control is presently based upon the sensed condition of whether or not zone heating/cooling is in operation.

5 Air-flow window (Double-skin facade with no cavity blind)

Convection Control

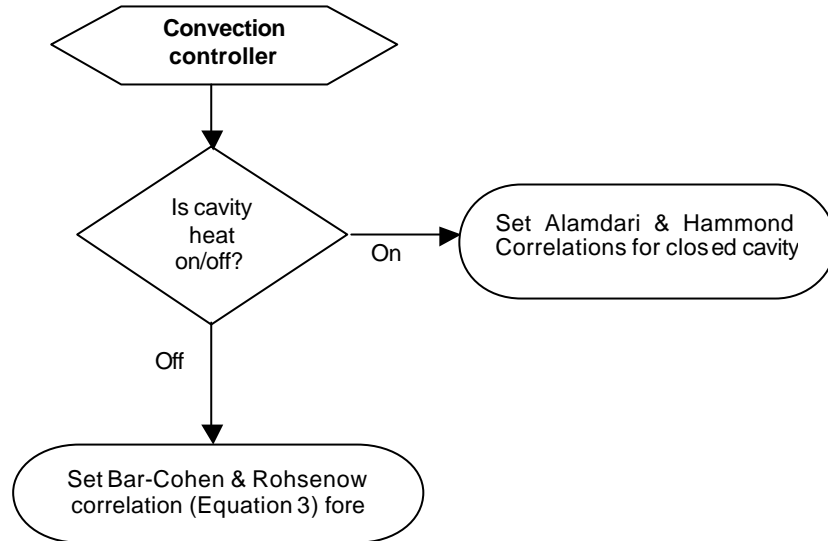


Figure 7 – Airflow-window convection control diagram

Airflow network control

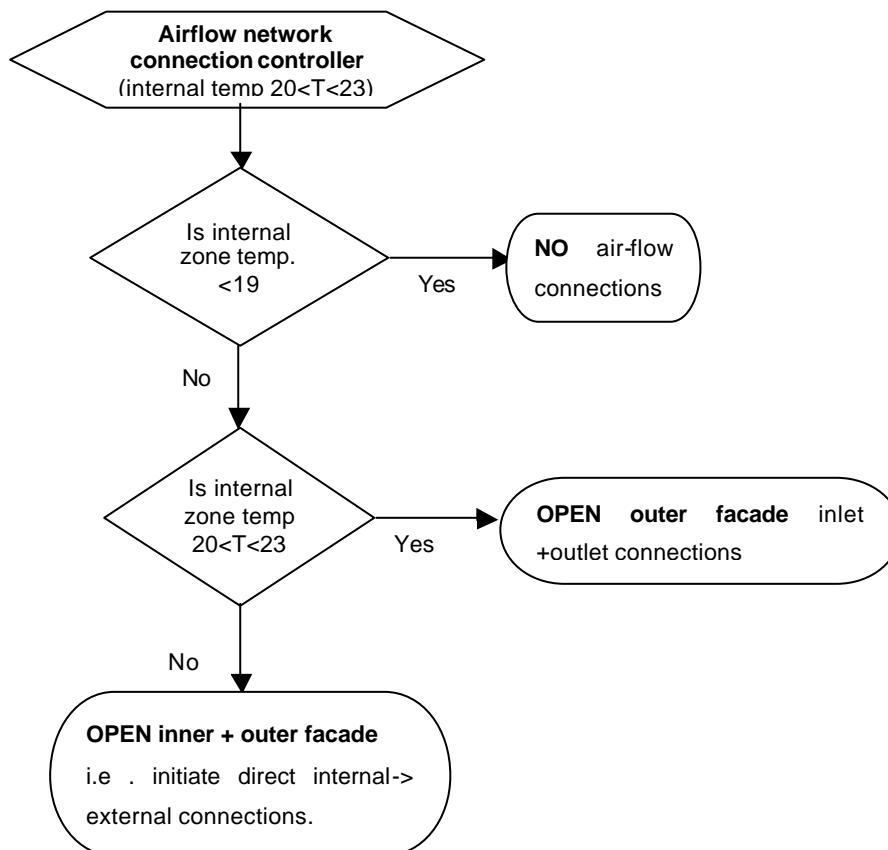


Figure 8 – Control diagram for airflow network connections

5 Air-flow window (Double-skin facade with no cavity blind)

5.5 Performance of Airflow-Window

For the purposes of this investigation, a bi-directional flow component is chosen to represent a window 2m in height with a discharge co-efficient of 0.65. The width of the bi-directional component is estimated to be the maximum opening depth of a bottom-hung casement open at 20°. The choice is made to keep the previous cavity connections, as airflow here will still occur keeping the temperatures in the cavity close to ambient. The airflow network as used in each operation mode is illustrated below

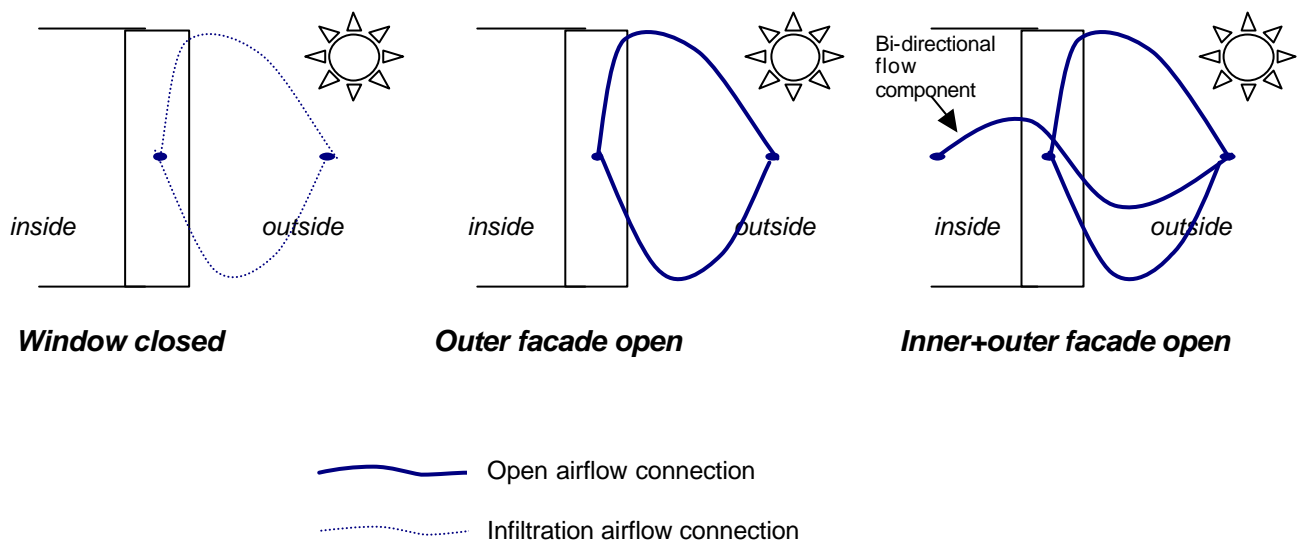


Figure 9 – Airflow networks used to represent different operation modes of airflow-window cavity

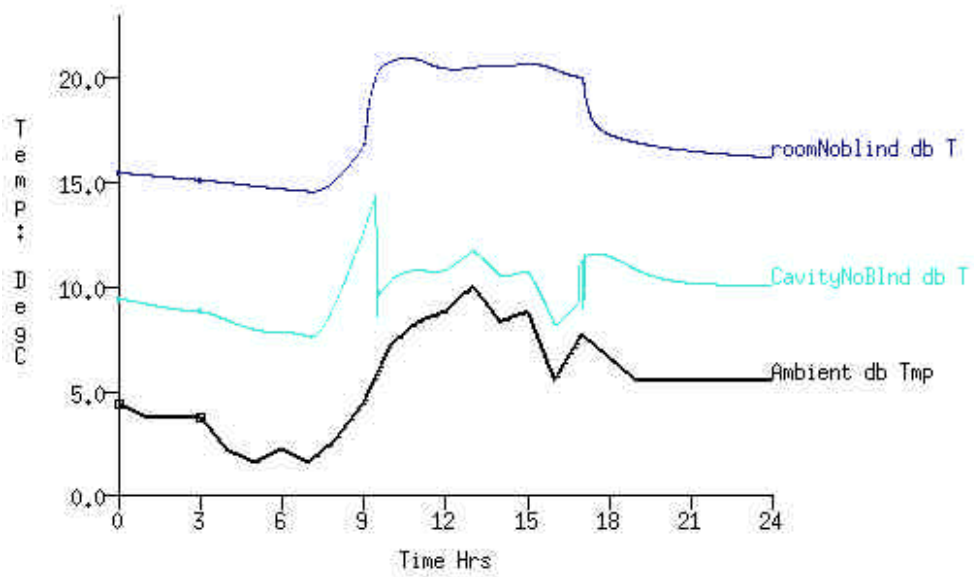
To make the simulation more realistic, internal gains are added (20W/m² for equipment & 1person/10m² between 09h00-17h00) and the inner layer is made to be single glazing. Two simulation days are chosen to highlight the control and effects of the different operating regimes:

- 1March – highlights opening of outer facade and cavity airflow
- 17April – highlights complete opening of the window and its effects

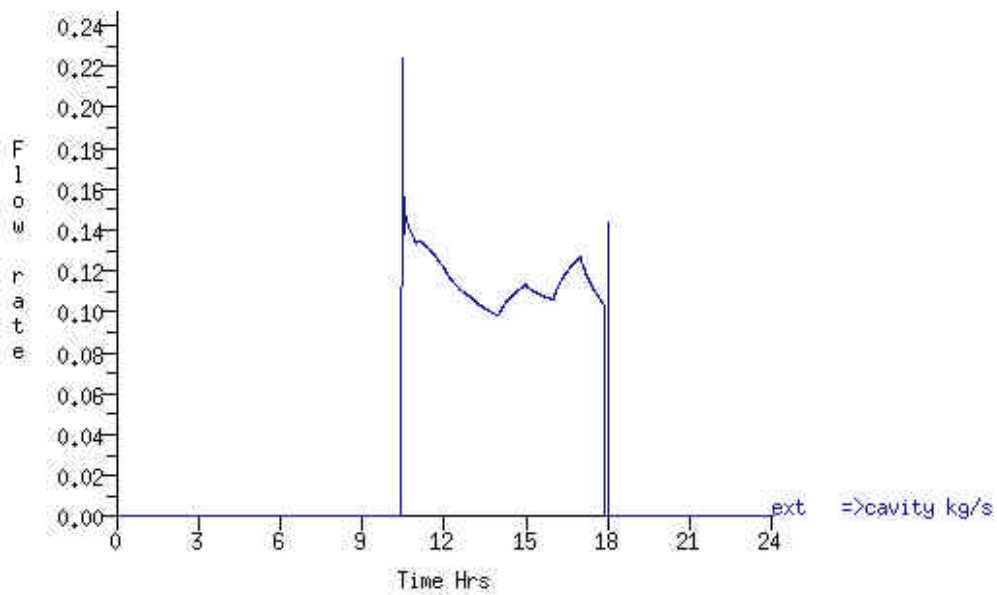
1March

As the internal room temperature rises above 20°C (Graph 5), the outer facade is opened and cavity airflow occurs (Graph 6) producing a noticeable temperature reduction in the cavity (Graph 5). This quickly quells the temperature in the internal zone without the need for cooling. Graph 7 illustrates the significant increase in conduction via the airflow window that provides this effect.

5 Air-flow window (Double-skin facade with no cavity blind)

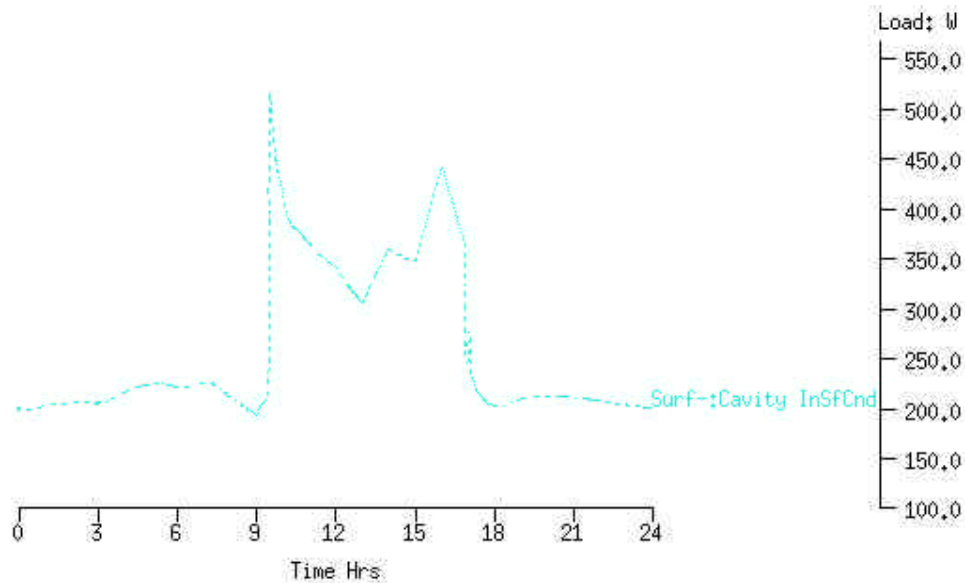


Graph 5 – Temperatures in airflow-window model(1March)



Graph 6 – Mass flow in airflow -window (1March)

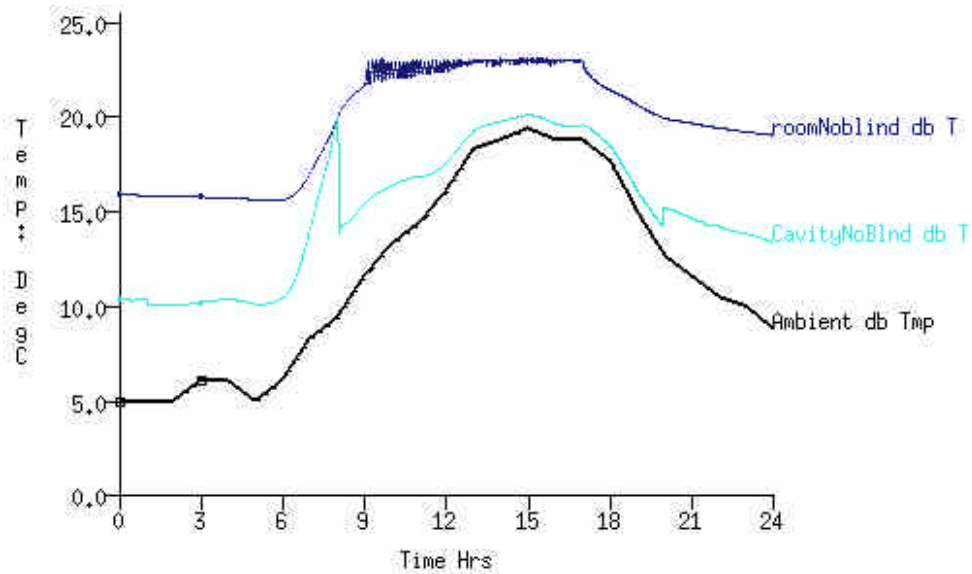
5 Air-flow window (Double-skin facade with no cavity blind)



Graph 7 – Conduction from internal zone to cavity (1March)

17 April

As the external climate warms, the complete opening of the window becomes apparent – control of the internal zone to 23°C setpoint (Graph 8). The outer facade opens slightly before this. The internal zone temperature is rapidly fluctuating because of the strict airflow setpoint. In reality, users would adjust windows to a suitable position to maintain steady conditions. The external ventilation in this case (between 4-10AC/h) means that no cooling energy is required.



Graph 8 – Temperatures in airflow-window model (17March)

6 Double-Skin Facades with Roller-Blind Shading

6.1 Pilot Model - Strategy

A pilot model (Figure 10) is proposed as the most reliable way of currently representing a double-skin facade and roller-blind shading device in order to obtain its energy performance. The model consists of a single-storey, box-type facade with roller blind, inlet and outlet orifices and an internal perimeter zone bounded by dynamically similar conditions. A nodal network is employed to represent bulk airflow in the cavity and connected to the outside as shown in Figure 10 below. It consists of a series of nodes representing air pressures and temperatures, four distributed over the cavity.

The cavity itself is discretised into 2 vertical zones. Such a discretisation allows for an account of different conditions in front of and behind the roller blind and to assign different airflow resistances either side of the blind. Nodes 2 and 5 in the air flow network represent an inlet and outlet region in the facade cavity respectively and are necessary where the facade is halved vertically by a roller blind, since a portion of air will flow via the blind gap spaces and provide additional resistance to flow. These nodes are not associated with any zone as such - node 2 is assigned the same temperature as the adjacent external air and node 5 the same as the top of the outer cavity.

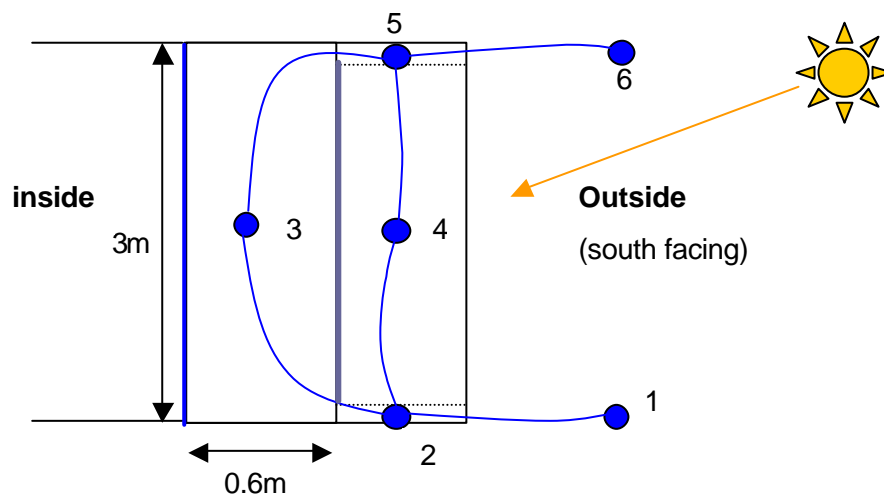


Figure 10 – Elevation of pilot model (roller blind)

6 Double-Skin Facades with Roller-Blind Shading

- The cavity is a 3m wide x 1.2m deep x 3m high. This cavity depth is towards the upper range of those commonly found double-skin facades.
- The internal zone is 5.8m deep, chosen bearing in mind a maximum room depth of 2.5 times the clear room height for adequate natural ventilation (single sided)[Oesterle, 2001]. In addition a minimum ventilation opening area of 2% of the floor area is required.
- The Bar-Cohen & Rohsenow correlation for convection between parallel plates is employed in the cavity zones (when air-flow is apparent) whereas Alamdari & Hammond correlations are assigned to the internal room.
- All boundaries apart from the external are considered dynamically similar.
- The air-flow network inlet & outlet dimensions are 3m x 0.1m (l x h) and their flow characteristics are based upon an orifice component with a discharge co-efficient of 0.65.
- The resistance to airflow through the cavity is assumed to be negligible compared to the air inlet & outlets. The resistance to airflow through the gap at the top and bottom of the blind (connections 2->3 & 3->5 in Figure 10) is assumed to be the same as for the main inlet & outlets. Ideal connections of little resistance are used to represent flow connections 2->4 & 4->5 in Figure 10.
- The outer facade consists of single glazing (6mm plate glass) and the inner facade consists of double-glazing (2x6mm plate glass). The fabric roller-blind is assumed opaque (0.2mm thick), having the following properties initially:

	Absorptivity	Emissivity	Density (kg/m ³)	Conductivity (W/m ² K)	Specific Heat (J/kgK)
Roller-blind material	0.6 (both faces)	0.9 (both faces)	186	0.06	1360

Table 6 – Default blind material properties

6.2 Instability issues with the pilot model

It is observed that results for pilot model simulations can be severely affected by instabilities. Particularly, rapid oscillations are apparent in the cavity airflow and temperature results.

6 Double-Skin Facades with Roller-Blind Shading

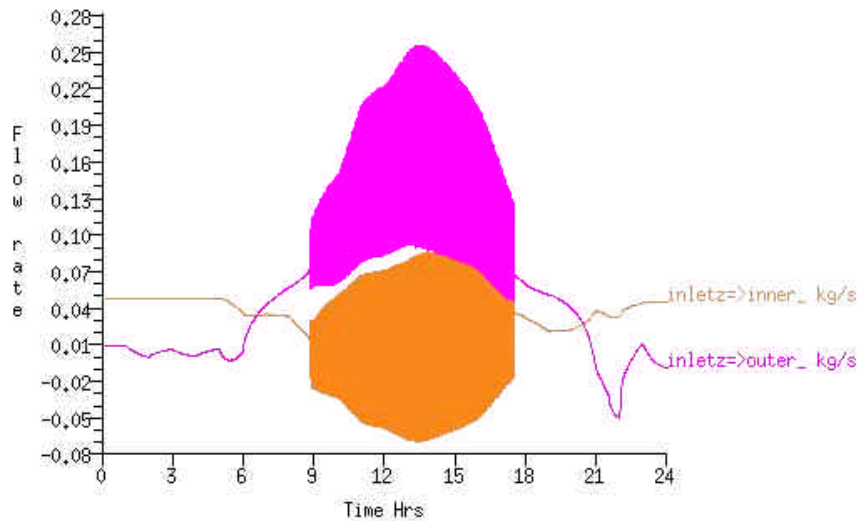


Figure 11 – Example of oscillations in cavity mass flow

It would appear that the closely-coupled nature of the heat & mass transfer in the cavity, as documented in previous nodal network simulations (Hensen), would be the cause. In particular, the splitting of the cavity and the inclusion of inlet and outlet region nodes give rise to nodes with very similar temperatures and flow-connections that have very little pressure drops across them (weak connections). These small differences are thought to be the reason for rapid swings in the calculation results.

6.2.1 Time-step control relaxation

It is found that reducing the simulation time-step to 1 minute can alleviate much of these instabilities. However, in certain climate conditions even that doesn't calm the oscillations. In these circumstances we can employ iteration control and a relaxation parameter (source code option), which often helps calm the oscillations.

This relaxation parameter is a value between 0 & 1, which affects the coupled iterations going on between the future building side energy results and the mass-flow results from the previous time-step. It essentially provides a weighted average of future and previous time-steps and can be thought of as a way of stopping the calculation jumping too far in front of itself. Large stepped changes are exactly what we don't want when we are dealing with very small differences. It was found that values of between 0.2 & 0.5 were most successful in quelling oscillations.

6 Double-Skin Facades with Roller-Blind Shading

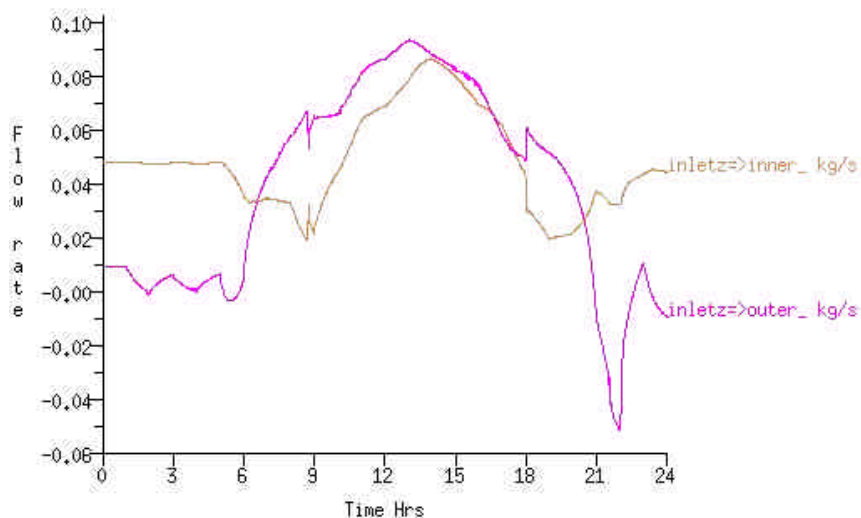


Figure 12 – Example of calmed results utilising relaxation parameter

In light of the unexpected instability error, a manual check on the air-flow calculation procedure due to the stack effect was carried out in order to fully appreciate the method and help spot any problems. This check confirmed the accuracy of the calculation and can be found in Appendix B.

6.2.2 A simplified airflow model

Another approach to remove the instabilities is to remove the so-called weak connections. The following simplification to the airflow model can be made and maintain the accuracy in the flow prediction. Inner and outer airflow paths in the simplified model are unlinked and completely separate.

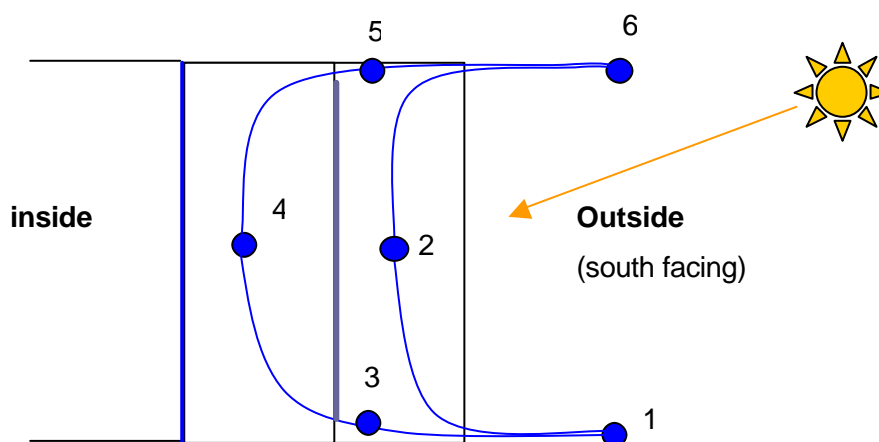
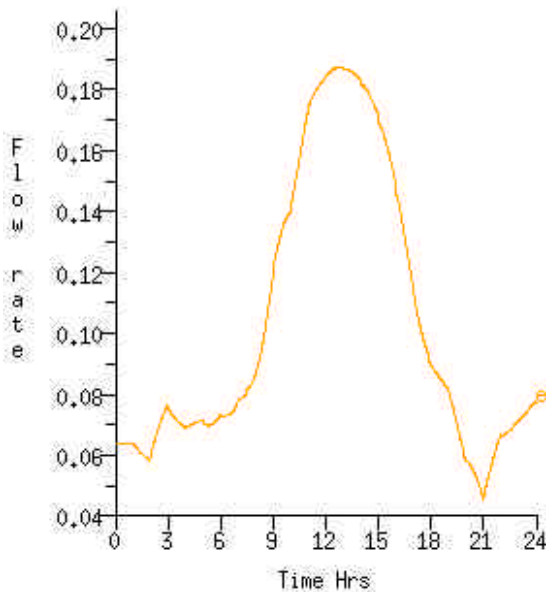


Figure 13 – Façade Elevation: Pilot model with simplified airflow network

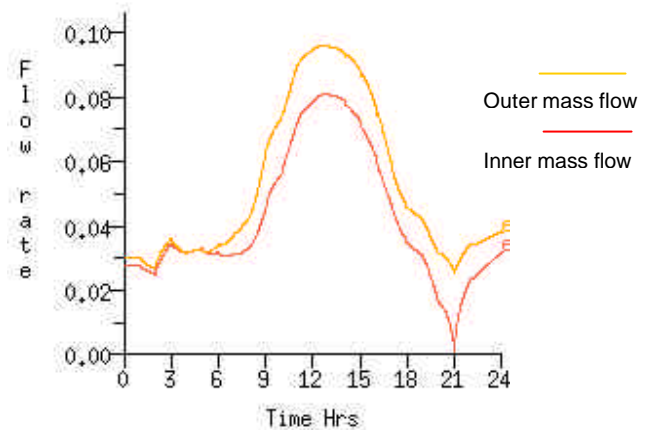
6 Double-Skin Facades with Roller-Blind Shading

Two inlet and outlet components are required in the simplified model and utilising a component with half the area of the inlet/outlet in the original pilot model maintains good results. Node 3 is set at the external air temperature, whilst node 5 at the same temperature as the inner cavity. A comparison of the mass flow results between the original pilot model & the simplified model, for the 10th July, is shown in graph below:

Original Pilot Model



Simplified Pilot Model



The separate inner & outer cavity mass flows sum to give an accurate estimation of the combined mass flow in the pilot model.

Graph 9 – Comparison of original & simplified network airflow models in pilot model

The peak mass flow in the cavity differs by only 5%. Though bulk-flow between the inner and outer cavities cannot occur in the simplified case. The inlet & outlet region nodes in the original model allowed for back flow to occur if one cavity was warmer than another.

6.3 Blind position abstraction

Firstly, to examine the sensitivity of the double facade system to modelling abstraction, the position of the cavity blinds in a basic model was considered. It might actually be the case that blinds are attached to the inner and outer facades, though it is not normally recommended (Oesterle,2001).

6 Double-Skin Facades with Roller-Blind Shading

Three approaches to modelling such a system with an essentially air-tight roller blind are likely to be:

- Case 1 - Attributing the blind optical & thermophysical properties to the cavity facing side of the outer facade's construction.
- Case 2 - Attributing the blind optical & thermophysical properties to the cavity facing side of the inner facade construction.
- Case 3 - Splitting the cavity zone into two by means of a partition made of the blind material, positioned exactly.

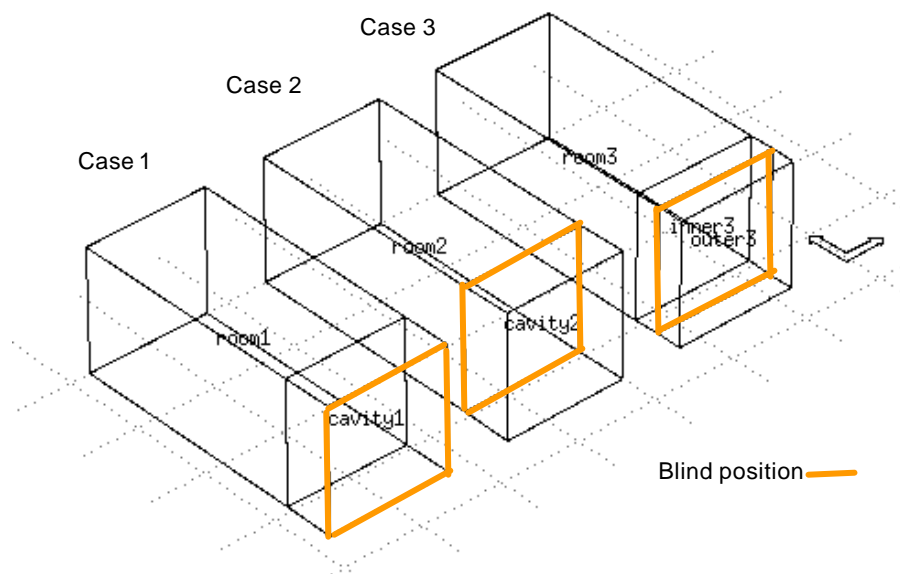
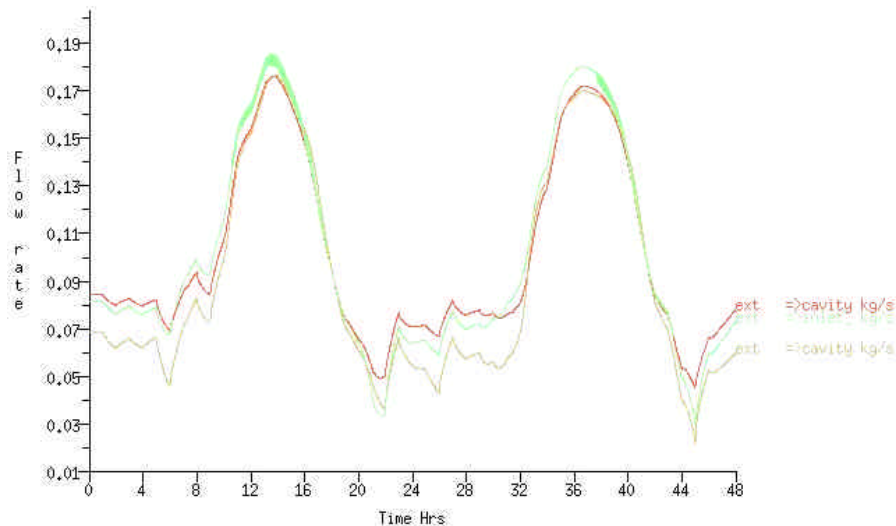


Figure 14 - Blind position sensitivity. From left to right are case 1, case 2 & case 3

An important modelling feature is noted here, regarding the way ESP-r treats solar properties. The outer facade in case 1 consists of an external layer of glass with an internal layer of blind material, which is opaque. However, attributing it as opaque in ESP-r will make the program take its absorptivity as that of the first layer (i.e. glass) and so most solar is reflected or quickly liberated on the external surface to the outside, which is obviously not representative of a double facade's operation. To get around this problem, the outer facade should be specified as transparent but with an overall transmissivity of zero. At first this may seem counterproductive, but by doing so we can force the simulation program to account for solar radiation passing through the first glass layer and being absorbed by the inside blind layer.

6 Double-Skin Facades with Roller-Blind Shading

Comparing the mass flows we can see that all three representations give similar results; where solar radiation is trapped in the cavity, absorbed by internal surfaces and partially convected to the internal air.



Graph 10 Mass-flows through double facade cavity for case 1,2&3

In case 3, the exact positioning of the roller blind results in

- the convection flowpath from the blind being further heightened since this time absorbed solar on the blind surface cannot be conducted away elsewhere, only stored.
- cavity air temperatures and stack induced flowrates increasing consequently
- an increased portion of solar radiation shared by the blind compared to case 2 due to its closer proximity to the outer facade; this abstraction will be more severe in deep cavities.
- approximately two/three times as much heat being convected to the outer cavity as to the inner cavity, which could impinge upon internal zone cooling requirements.
- an ability to represent higher airflow resistances in the inner cavity than the outer cavity (due to blind gap), causing higher temperatures there.

Nevertheless, the differences in peak mass flows are very small as are differences between cavity temperatures. This is an extremely good approximation for modelling the cavity but the differing flowpath characteristics causing the mass flow in case 3 can be more critical to the overall design of such a facade. For example the purpose of the double facade in summer should be to block solar gain

6 Double-Skin Facades with Roller-Blind Shading

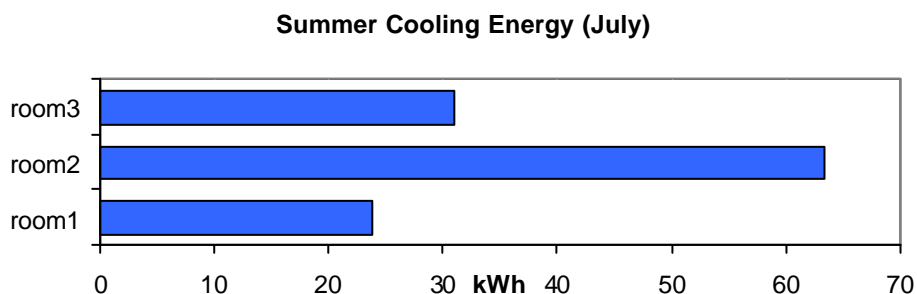
and channel heat away from the internal zones. A surface energy balance at the inner facade in each case highlights the real impact that these modelling abstractions have.

	case 1		case 2		case 3	
	Gain(kWh)	Loss(kWh)	Gain(kWh)	Loss(kWh)	Gain(kWh)	Loss(kWh)
Conductive flux	345	3300	427	5338	221	3579
Convective flux	45	387	0	2676	60	270
Long-wave internal radiation flux	3609	290	29	1547	3759	168
Shortwave radiation flux	0	0	9107	0	0	0

Table 7 – Comparison of surface energy balance at inner facade (excluding heat storage)

It is clear that the heat transfer to the internal perimeter zone by conduction differs greatly between cases. Especially in case 2, where the absorbed solar at this surface manifests itself more in direct conduction to the inside. Cases 1 & 3 are much more similar though, principally because the latter “direct” solar path is removed. In both these cases the energy absorbed must first be convected to the cavity air. Overall the differences noted are a result of where the solar is absorbed in the system. In case 2 the solar is directly absorbed into a perimeter zone surface where as in cases 1 & 3 the solar energy is first transferred to the cavity air.

By cooling the internal zone to 20°C we can determine the significance of blind position in an energy consumption analysis. Infiltration of 1AC/h is assumed via constant flow rate components in the airflow network.

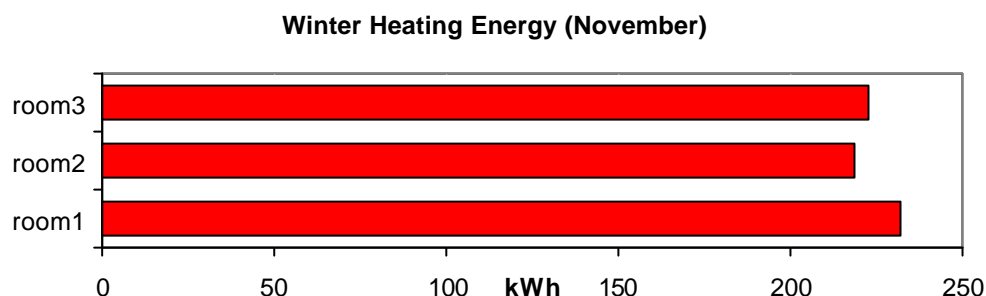


Graph 11 – Relative cooling energy comparison for July (no internal gains, infil=1AC/h)

6 Double-Skin Facades with Roller-Blind Shading

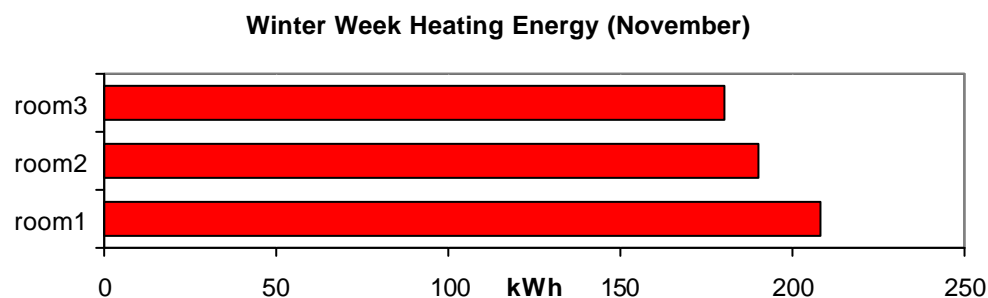
In summary, the spatial position of blind is important and by attributing it to the inner facade will result in over-estimation of cooling internally (by over 100%) - though a fairly reasonable estimation of airflow through the cavity is maintained. Attributing the blind to the outer facade provides a more accurate result (an underestimate of 20%) and again the mass flow prediction is good.

In winter, the effect of solar is much less dominant and predictions are much more similar (see Graph 12). With case 2, however, the blind will act as an insulation blanket on the internal double-glazing and hence underestimate heating requirements. If the blind should have large thermal resistance, this effect can be significantly exacerbated.



Graph 12 - Relative heating energy comparison for November (no internal gains, infil=1Ac/h)

In winter, it is more likely that the facade's airflow louvers will be shut to form a buffer space and so air change rates will be greatly reduced to infiltration levels. It is appropriate therefore to compare results again under these conditions. Also convection patterns will now shift from that of free-flow between vertical plates, towards that found in a general rectangular room. Alamdari & Hammond correlations are utilised for this purpose although not entirely suitable for high aspect-ratio cavities as previously shown. To represent closed louvers, the airflow network has been assigned with crack openings of 1mm around the louvers perimeter. Results are shown in Graph 13 below.



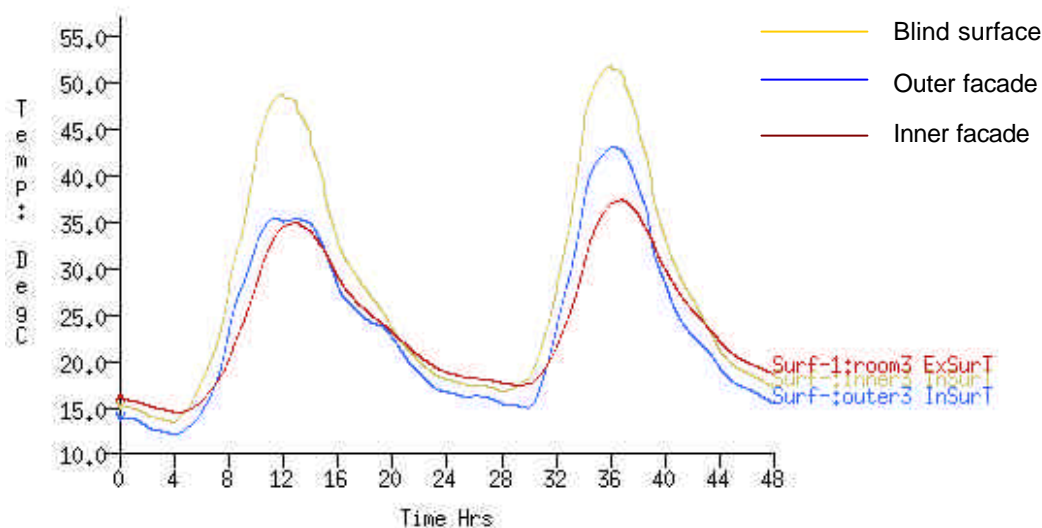
Graph 13 - Relative heating energy comparison (buffer space) for November (no internal gains, infil=1Ac/h)

6 Double-Skin Facades with Roller-Blind Shading

In conclusion, the spatial position of the blind significantly impacts on the internal energy predictions in different double-skin facade operation modes but less so in terms of cavity mass-flows. Incorporating the blinds at the outer facade gives best overall summer cooling energy estimation compared with blinds positioned in the middle of the cavity.

6.4 Cavity Temperatures

Predictions of cavity surface temperatures during the summer highlight that significant differences are obtained. Graph 14 shows that the blind surface heats up most, peaking at temperatures as high as 50C during the period of the 10th-11th July.



Graph 14 – Cavity surface temperatures (10-11July)

In light of such high temperature differences, it is important that we accurately predict surface view factors accurately. The use of the ray tracing method in ESP-r is highly recommended in place of the default area weighting calculation. In a high aspect ratio cavity, the area weighting method will produce poor results.

6 Double-Skin Facades with Roller-Blind Shading

6.5 Blind physical properties & facade performance

The physical properties of the roller blind can significantly influence the behaviour of the double-skin facade system. Firstly the blind thickness is considered, which directly influences its thermal mass.

Thickness & thermal mass

The pilot model with a centrally positioned blind is attributed with a 0.2mm and 5mm roller blind construction. Considering summer operation (shading drawn), with illustrative cooling to 20°C, the effect on three key performance variables (internal cooling energy, cavity mass flow, peak cavity temperature) is highlighted in Table 8 below:

Performance variables	5mm blind	0.2mm blind
Internal cooling energy (kWhrs)	5.57	7.01
Peak cavity mass flow (kg/s)	0.23	0.22
Peak cavity temperature (°C)	36.52	36.86

Table 8 – July 8th-15th illustrative summer cooling week with blind thermal mass varied

The internal cooling energy required differs by 20%, although this is an extreme case where thickness differs by a factor of 25 and no casual gains are present in the model. The reason is due to the low thermal capacity of the 0.2mm blind which heats up to much higher temperatures. Hence the longwave radiation transfer to the inside is significantly increased resulting a larger cooling required. Table 8 (surface energy balance) highlights that the longwave gain is over 10% greater and overall the heat conducted to the inside is around 9% greater.

	5mm blind	0.2mm blind
Max blind Temperature (°C)	41.3	44.5
LW gain at internal facade surface	2958	3357
Convection to cavity air at internal facade surface	194.35	97.67
Overall heat transfer to the inside (via conduction)	3104	3374

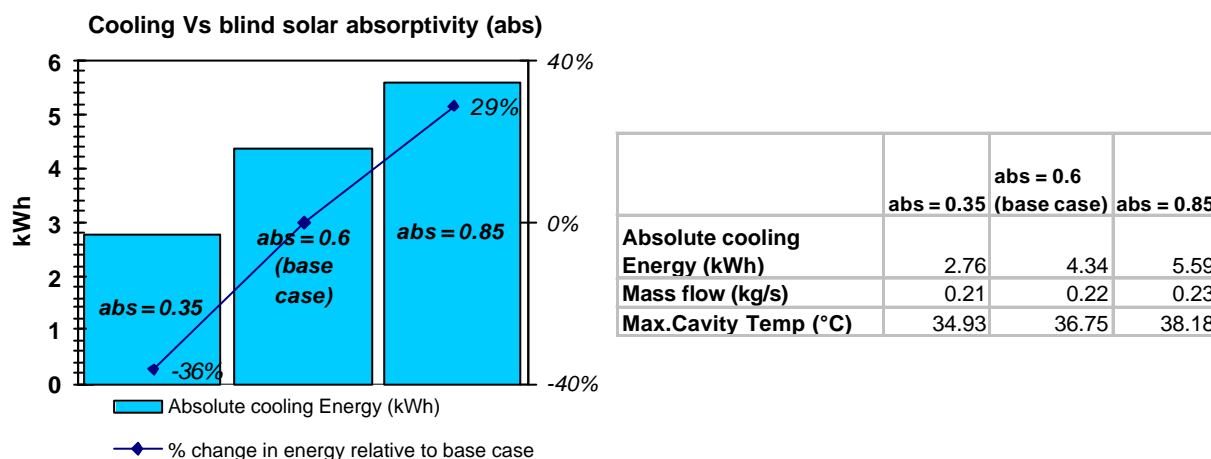
Table 9 – Internal facade surface energy balance (10th July)

6 Double-Skin Facades with Roller-Blind Shading

In reality, we are only likely to observe such high thermal mass with wooden type blinds. For example, in the situation with completely drawn wooden Venetian blinds. Roller blinds are more commonly to be found at thicknesses near 0.2mm, exhibiting low thermal mass.

6.5.1 Solar absorptivity & emissivity

The choice of fabric for the roller blind is very important in terms of a double-skin facade's function also. The variation of internal cooling load with the solar absorptivity of the opaque roller blind material is striking.



Graph 15 – Variation of internal cooling load with solar absorptivity of the roller blind material

Additional absorbed solar manifests itself in higher surface and cavity temperatures via convection and longwave radiation flowpaths. Consequently, cavity flow rates increase (5%) due to greater buoyancy forces helping dissipate heat. Even so, the system that directly reflects more solar provides the greatest protection against overheating.

The emissivity of the roller blind material has similarly significant effects in terms of the internal cooling energy required. By holding the blind material's absorptivity at 0.6, the effect of the variation in surface emissivity is determined – the results are highlighted in Table 10.

6 Double-Skin Facades with Roller-Blind Shading

	Internal Cooling Energy (kWh)
$\varepsilon_i=0.9 / \varepsilon_o=0.9$	4.34
$\varepsilon_i=0.6 / \varepsilon_o=0.6$	3.68
$\varepsilon_i=0.3 / \varepsilon_o=0.3$	2.39
$\varepsilon_i=0.9 / \varepsilon_o=0.6$	4.65
$\varepsilon_i=0.9 / \varepsilon_o=0.3$	5.11
$\varepsilon_i=0.6 / \varepsilon_o=0.9$	3.39
$\varepsilon_i=0.3 / \varepsilon_o=0.9$	1.81

ε_i = internal surface emissivity

ε_o = internal surface emissivity

Table 10 – The effect of blind surface emissivity on internal cooling energy

It is clear that a reduction in surface emissivity at the inside facing surface of the blind most positively affects the cooling requirements (over a 50% reduction in fact). This highlights the significance of the longwave flowpath from the warm blind to the inside. Reducing the emissivity of the outside facing surface on the other hand increases the cooling requirements, since longwave radiation is less readily rejected to the cooler outside. This does not have such a significant effect as the latter however.

6.6 Multi-storey facades - discretisation of cavity

Double facades such as the multi-storey type (Figure 15) can be modelled as a series of discrete smaller zones by perceptive use of the airflow network and fictitious surfaces (Figure 16).

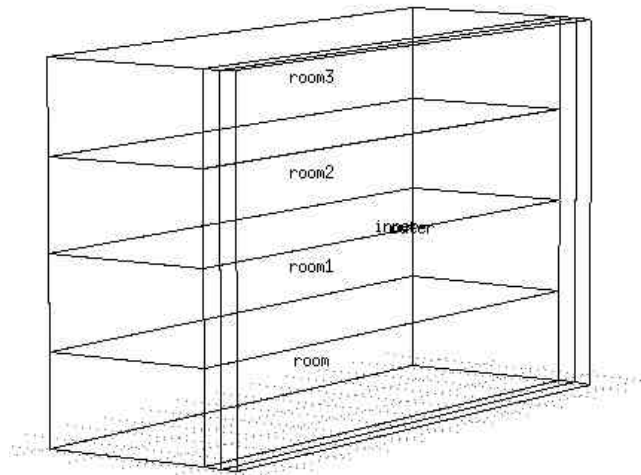


Figure 15 - Double facade multi-storey type

The sensitivity of various resolutions of discretisation is examined here in terms of three critical variables – internal zone cooling energy, cavity temperature and mass flow.

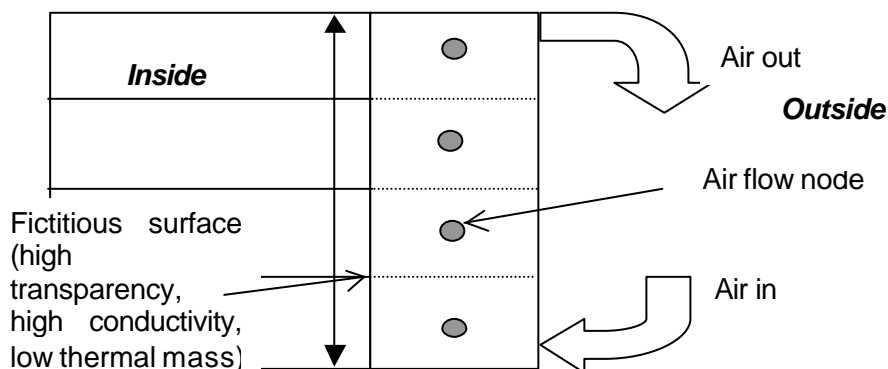
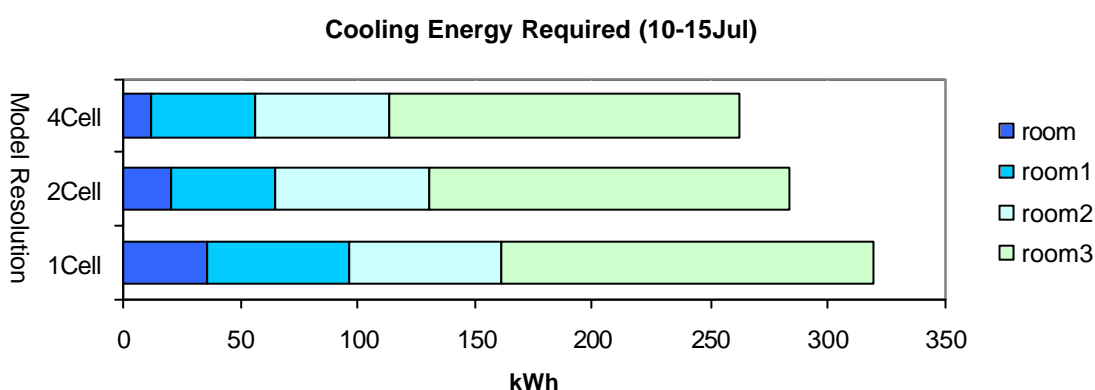


Figure 16 - 4cell discretisation of double facade

6 Double-Skin Facades with Roller-Blind Shading

The double facade model examined consists of a 4-story facade and internal perimeter zone, each storey being 3 metres high (Figure 15). Model attributes are as before in the case 3 model examining blind position previously. The network air-flow model connections between discretised zones are modelled as specific air-flow openings (discharge co-efficient, $C_d = 0.65$ by default) and they will offer negligible resistance to the flow of air in comparison to the 0.1m high inlet and outlet orifices ($C_d=0.65$) stretching the length of the outer facade. Only one external airflow node is considered in this analysis, which means that the stack-effect is the only driving force.

The sensitivity is gauged by splitting the outer cavity from a standard 1-cell representation through to a 4-cell representation so that there is one adjacent cell per floor. The results are shown below for an illustrative summer week (July 10th-15th). Significantly, the cooling requirements are affected by the choice of modelling resolution - overall the internal perimeter zone cooling is over-estimated by 20% when using a single-cell representation over a four-cell model.



Graph 16 – Cooling energy requirement in internal perimeter zones for different modelling resolutions

It is also interesting to note that cooling requirements for the top-zone are essentially the same in each case because the maximum temperatures (Table 11) calculated for each modelling resolution are very similar. Similarly, the temperature in the bottom half of the 2-cell double facade model (cell1) is very near that of the temperature of cell 2 in the 4-cell model, so cooling for room 2 is comparable. Thus by increasing the double facade discretisation we do not significantly affect the maximum temperature within the cavity but highlight the existence of lower temperatures due to thermal stratification. In terms of modelling worst case scenarios inside the building therefore, one-cell double facade representation would suffice, but for energy calculations such cellurisation is recommended to produce better results. The model also illustrates that the height of multi-storey facades should be limited due to excessive

6 Double-Skin Facades with Roller-Blind Shading

peak temperatures at the top (the ambient temperature peaks at 26°C in this case). It is apparent that is very necessary to keep the internal facade closed due to high cavity temperatures when the shading is drawn.

Double facade resolution			
	1Cell	2Cell	4Cell
Max Temp, Cell1	38.46°C	33.92°C	28.94°C
Max Temp, Cell2	-	38.9°C	32.64°C
Max Temp, Cell3	-	-	35.86°C
Max Temp, Cell4	-	-	38.14°C

Table 11 – Max cell temperatures in double facade models

Regarding mass flow within the double facade cavity, Table 12 shows that lower resolutions over-estimate the mass flows through the cavity, caused by the fact that a higher air temperature is averaged over it. A difference of around 20% is apparent in the mass flows calculated for the single cell double facade model as compared to the 4-cell model.

Double facade resolution			
	1Cell	2Cell	4Cell
Peak Mass flow	3.19kg/s	2.95kg/s	2.7kg/s

Table 12 – Peak mass flows within double facade models

It is therefore recommended to use floor-by-floor adjacent cells made with fictitious surfaces to gain sufficient resolution. Increasing the resolution further to having an adjacent cell per half floor would give slightly better results again but usually air-flow connections to the internal perimeter desired at each floor level would hinder it use.

6.6.1 The effect of fictitious surfaces

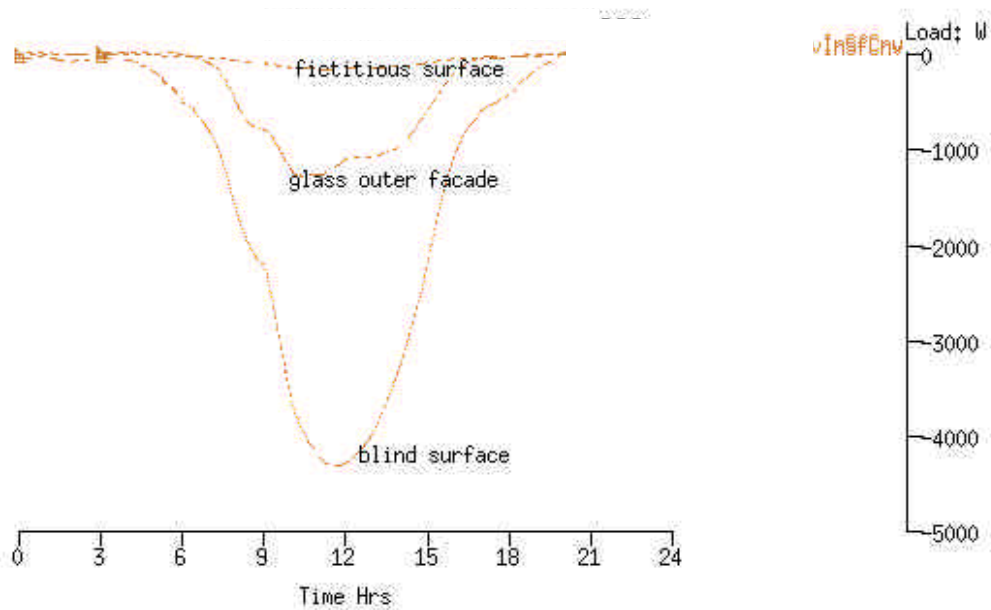
So-called fictitious surfaces are in essence dividing regions that attempt to offer a means of greater resolution by partitioning large zones with widely differing thermodynamic properties into appropriate sub-regions. They attempt to act as surfaces that do not influence heat flow paths, within the realm of the standard inter-zonal calculation method. A careful use of a material's physical characteristics allows this. As noted, fictitious materials are made of a material having a

- very low thermal mass
- very low solar absorptivity
- very high emissivity

This means that solar radiation will pass through the surface largely unhindered in magnitude (though directional attributes are lost). Furthermore, longwave radiation will be absorbed & transmitted readily owing to the high emissivity, low thermal mass combination. Indeed this was the concept incorporated in the dividing surfaces used in the multi-storey facade.

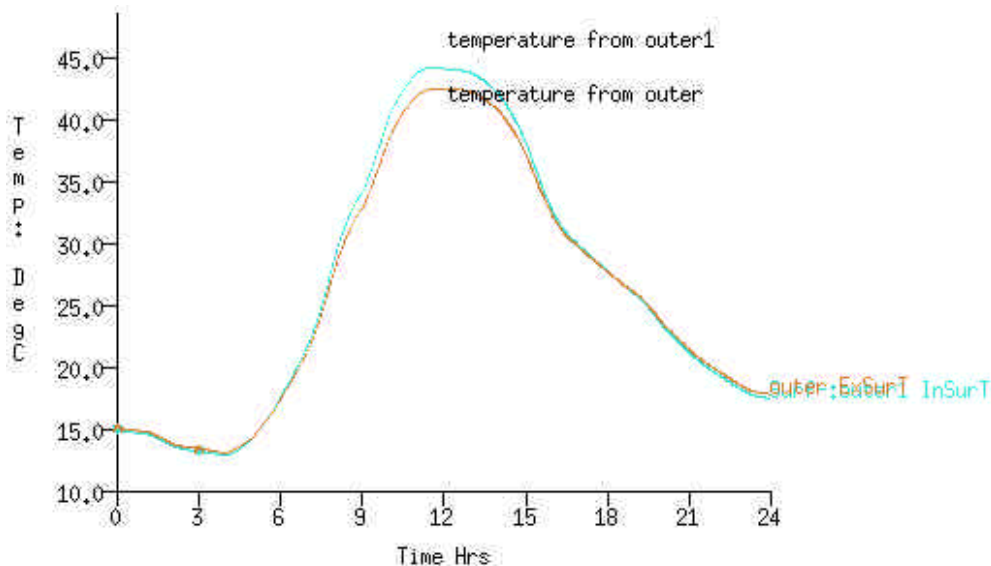
One further characteristic that was desired of the dividing surface was to have a very weak convection flowpath. That however was found to be affecting the solution results, which will be elaborated further. Firstly though, it is shown that this additional characteristic has small effect in the multi-storey facade previously. The principle reasons for the low fictitious surface convection are that the dividing surfaces make up a small portion of the total cavity surface area and exist at a considerably smaller temperature than that of the blind (negligible solar absorption). If we consider the outer bottom cell of previous 4-cell discretisation, this is clear:

6 Double-Skin Facades with Roller-Blind Shading



Graph 17 – Surface convection in multi-storey zone discretised with fictitious surfaces

However, trying to deliberately remove this convection flowpath (by setting the convection co-efficient to a very small value, $0.001\text{W/m}^2\text{K}$) results in a prediction error relating to the surface temperature predictions. The temperature prediction for the same surface looking from adjacent zones is different (Graph 18).



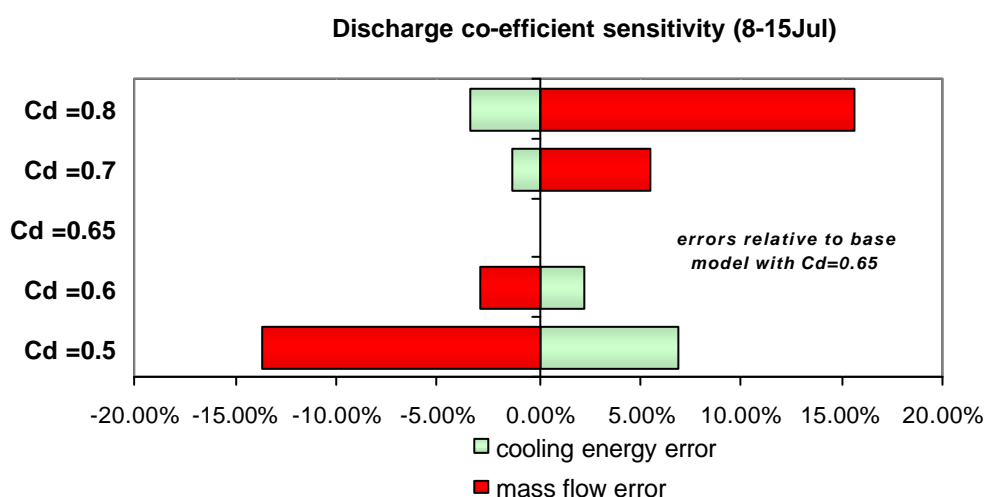
Graph 18 – Temperature results for the same surface, considered from opposing stacked zones.

6 Double-Skin Facades with Roller-Blind Shading

6.7 Air-flow network – discharge co-efficient sensitivity

Discharge co-efficients are a very important factor in air-flow openings, describing pressure loss characteristics. However, little guidance can be found regarding their selection, except for manufacturers data on the rare occasion. Also the information currently available exists for components that have been experimented on under forced flow conditions, not natural buoyancy flows and so may differ. Furthermore, many commercial airflow simulation programs have a built in discharge co-efficient of 0.65 for orifice type openings that cannot be modified. ESP-r however can accommodate different values and will allow the sensitivity of the discharge co-efficient, relating to different shaped openings, to be examined.

Utilising the multi-storey model previously for this study, the inlet and outlet discharge co-efficients are varied about the standard value of 0.65, from 0.5 to 0.8. Results of the study show that mass flow through the cavity is most significantly affected by a change in discharge co-efficient. Graph 19 below shows the errors in mass flow in combination with those for internal cooling energy relating to the choice of different discharge co-efficient. It highlights that a lower co-efficient will result in lower mass flows (by over 15% lower) because of the increased flow resistance, and vice-versa. However the cooling energy required by the internal zones is much less sensitive to the mass flow and it can be argued that this is the most important function of the double facade anyway, so the standard discharge co-efficient of 0.65 may be tolerated.



Graph 19 – Discharge co-efficient sensitivity (cooling & mass flow errors)

6 Double-Skin Facades with Roller-Blind Shading

The sensitivity of double facade cavity temperatures (Table 13) to mass flows due to the different discharge co-efficients is very small.

Cavity mass flow	2.33kg/s	2.62kg/s	2.7kg/s (Cd=0.65)	2.85kg/s	3.12kg/s
Max Temp, Cell1	30.8	30.15	28.94	28.79	28.58
Max Temp, Cell2	35.53	34.49	32.64	32.3	31.79
Max Temp, Cell3	39.09	37.98	35.86	35.44	34.74
Max Temp, Cell4	41.25	39.97	38.14	37.7	36.94

Table 13 – Maximum cavity temperatures sensitivity to discharge co-efficient

6.8 Control of double-skin facade with roller blind

It has been evident that representing the spatial position of the blind is very important, which cavity partitioning facilitates. However in a control scheme this surface has to be replaced when the blind is pulled up. A suitably benign surface is required to replace the blind. Previously it was found that fictitious surfaces (low absorptivity, low thermal mass, high conductivity & high emissivity) provided a solution for vertical dividing a multi-storey facade. Such a construction attribution meant that incident longwave radiation would be readily absorbed from one zone and transmitted to adjacent zone. Though the small surface area of the divisions also meant that their influence was insignificant. In this section we determine the errors between simulation predictions for a cavity with a large horizontal fictitious division and for one without. In doing so, we assess the appropriateness of the control method.

6.8.1 The effect of large fictitious divisions

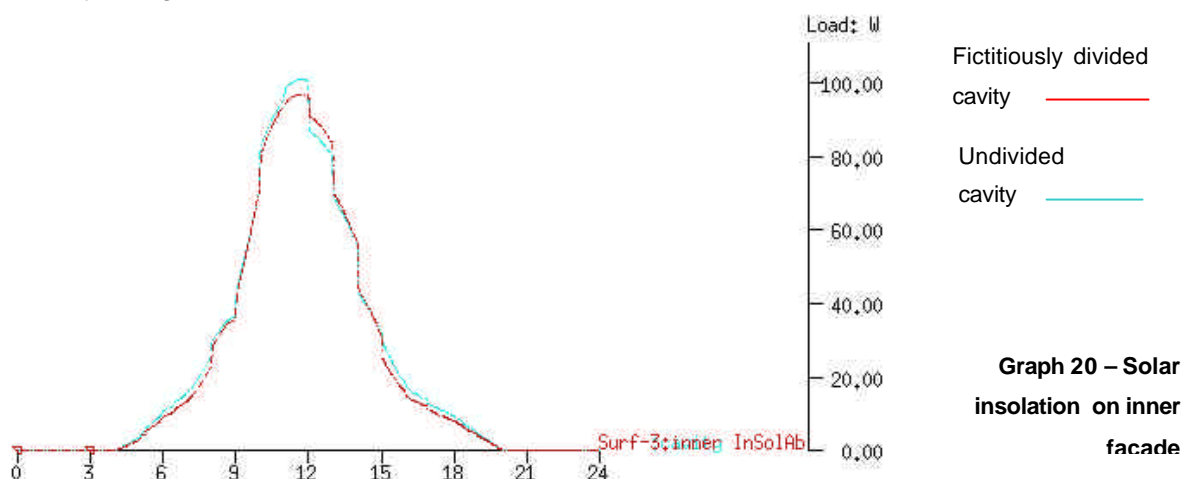
3 different operation regimes are considered in the use of fictitious surfaces when the shading is pulled up:

- Facade closed acting as a buffer space (operation mode 5 in Figure 1)
- Outer facade open – cavity airflow (operation mode 1 in Figure 1)
- Flow from outside to inside.

6 Double-Skin Facades with Roller-Blind Shading

The geometry and constructions of the models used in the investigation are based upon the pilot model as before.

- The solar tracing module within ESP-r is used to define insolation distribution in the external facing zones. Also this method is forced upon the inner division by assuming the dividing surface to be external. Good agreement with the insolation predicted in an undivided cavity is obtained by doing so (see below).



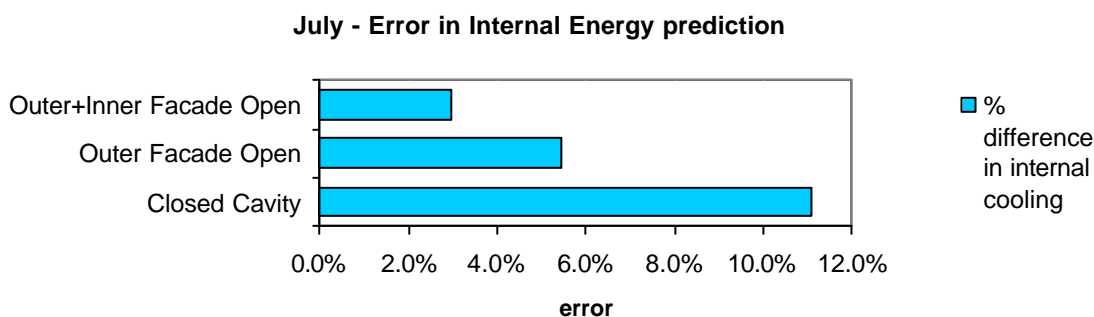
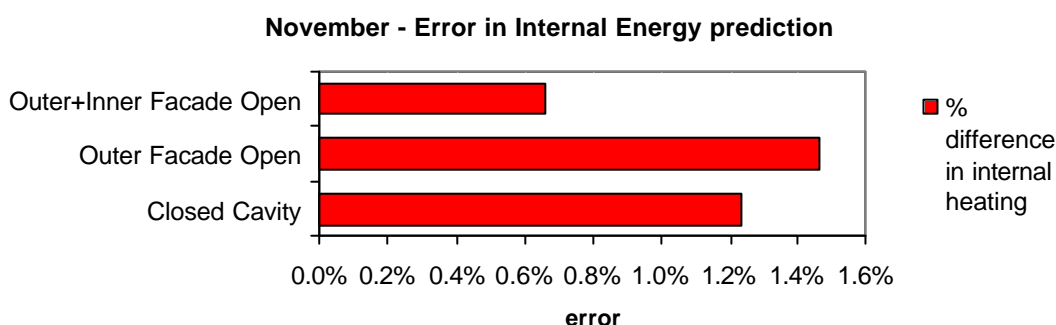
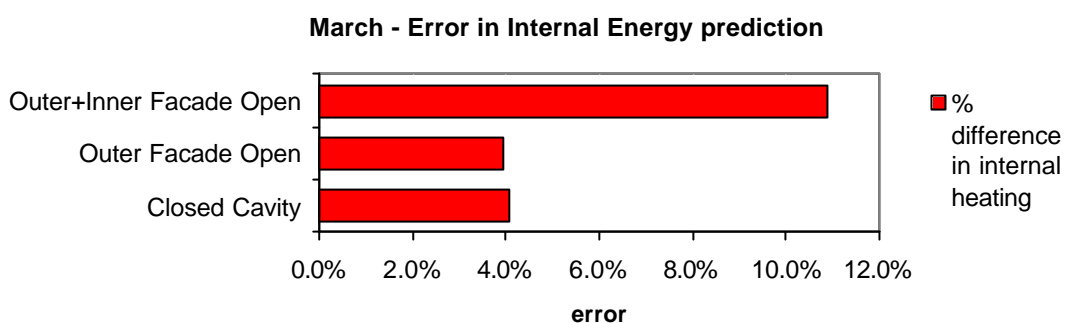
- The ray tracing method is used to calculate view factors.
- The air-flow network is different for each operation regime (also see Figure 17 in conclusions):

Facade closed (buffer space)	Outer facade open (cavity ventilation)	Flow from inside to outside
<ul style="list-style-type: none"> • Infiltration to cavity via crack components. • Cracks of 1mm (width) over perimeter of inlet & outlets (6.2m) • Inlet flush with bottom and outlet flush with top • Infiltration to internal zone via fixed flowrate controller (1Ac/h) 	<ul style="list-style-type: none"> • Natural ventilation to cavity via bottom inlet & top outlet.). • Inlet & outlet based on specific air flow opening: 0.3m² area, discharge co-efficient of 0.65. • Infiltration to internal zone via fixed flowrate controller (1Ac/h) 	<ul style="list-style-type: none"> • As opposite plus: • Bi-directional flow component [details as in the airflow-window model (section 5.5)] to represent one-sided window ventilation.
<ul style="list-style-type: none"> • NO connections across the divided cavity sections are required. This was found to make little difference to results. 		

6 Double-Skin Facades with Roller-Blind Shading

A comparison of the predicted energy consumption for each of the operations is undertaken. The internal zone is assigned ideal control for this purpose (cooling setpoint=23°C, heating setpoint=20°C), with a plant capacity of 1000W. No casual gains are assigned and infiltration is set to 1AC/h. The results of this investigation are shown in the following graphs.

Predicted energy comparison results (March, November, July):

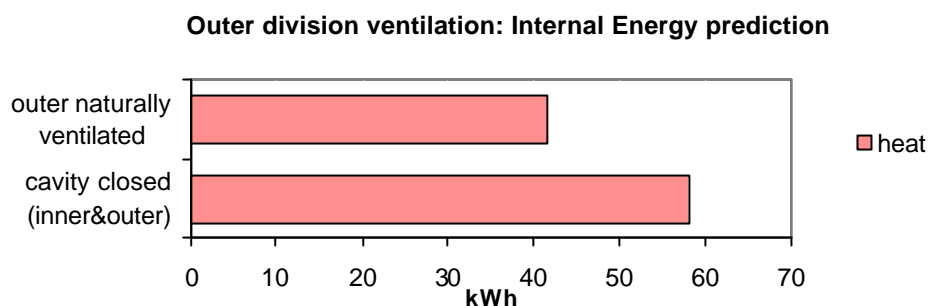


Nb. All of the above errors owe to underestimates in the energy predictions

6 Double-Skin Facades with Roller-Blind Shading

“Cavity closed” details:

The outer cavity formed by the fictitious division was naturally ventilated via the inlet opening. Otherwise if both cavities are closed, the internal heating energy is greatly underestimated - a further 20% difference over the March period is highlighted in the graph below:

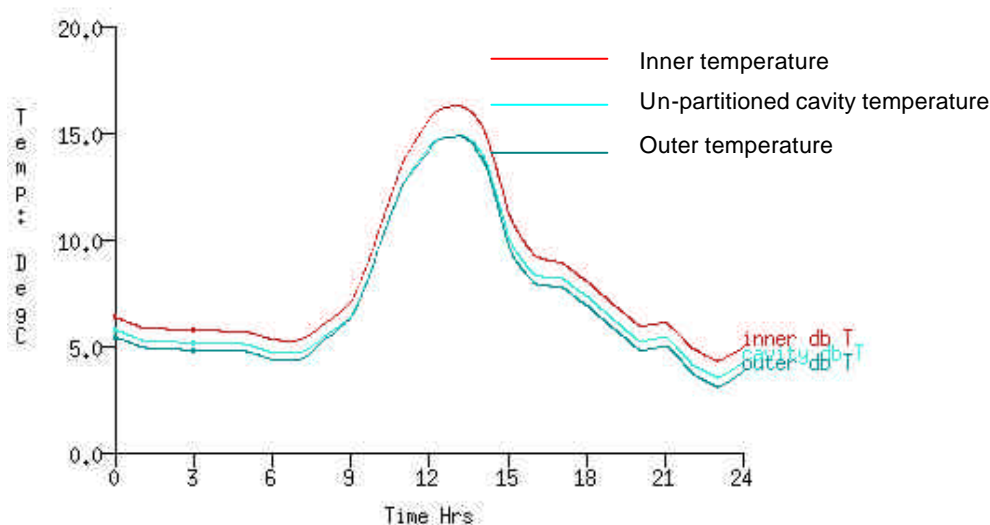


Graph 21 – energy prediction comparison of completely closed cavity with cavity having outer division ventilated

Even though the fictitious surface can readily transmit radiation without storage and time lag effects, its mere existence means that a temperature gradient will be formed across the closed cavity (due to fictitious surface convection values). Of course this then results in the surface temperature of the fictitious surface being greater than the outer facade and energy transfer to differ. Allowing ambient air to ventilate this cavity effectively removes this gradient.

“Outer facade open” details:

If we consider the temperatures throughout the partitioned cavity, it is clear that temperature prediction in the outer portion is closest to that in the un-partitioned cavity.



Graph 22 – Cavity temperature predictions in “outer facade open” operation

6 Double-Skin Facades with Roller-Blind Shading

In light of this, it is decided for the case where **flow to the internal zone** occurs, to connect the inside air node to the outer cavity node so as not to draw in excessive temperatures.

Other considerations:

The inner & outer divisions of the facade could be connected as would exist in reality. However, little benefit with regards to the energy prediction was achieved by doing so. Complicating the model with further air-flow connection was unwarranted therefore.

6.8.2 Conclusions on fictitious surface utilisation

The use of fictitious surfaces within double-skin facade cavities introduces errors in internal energy predictions. It is inevitable that introducing any dividing surface in the cavity will modify the temperature gradient from inner to outer facades. In terms of internal energy prediction, we have observed this effect can result in under-estimations from anywhere between 1 and 10% depending on the specific climatic conditions. It is found that the “closed facade” case is best represented by closing only the inner cavity division (maintaining ventilation in outer division). Also, when both inner and outer facades are opened, the airflow network connection should be made between the internal zone and outer cavity division. A summary of the airflow networks used is illustrated in Figure 17.

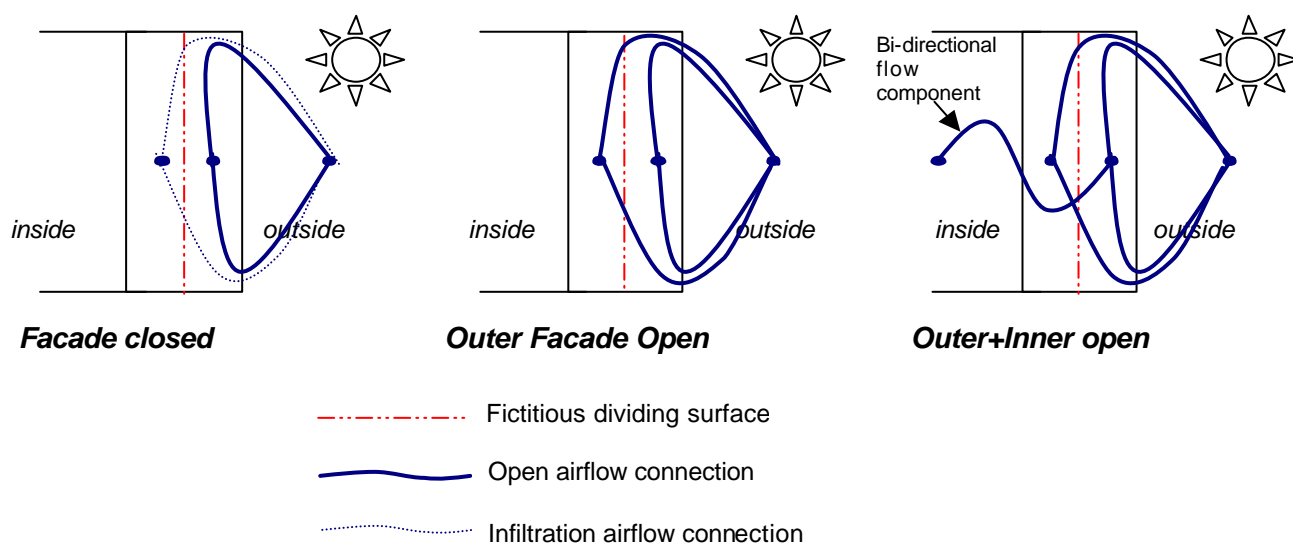


Figure 17 – Recommended set-up of airflow networks for a fictitiously divided cavity in 3 different operation modes

6 Double-Skin Facades with Roller-Blind Shading

It is important to take into account that this error range is based upon keeping the cavity mode & operation constant over an entire month. Of course this will not be the case with a controlled facade under normal circumstances and therefore this error range can be viewed as a worst-case estimate. Furthermore, it is less likely that the situations causing the worst errors will frequently occur (i.e. closed cavity in summer & open facade in winter).

The ability to model the control of a double-skin facade's operation is highly important though and will have a major impact on the energy predictions of the building. The low prediction error caused by the use of fictitious surfaces during part of the simulation is considered tolerable overall.

6.8.3 Example of shading control operation

The control concept highlighted in this section is for a naturally ventilated facade with shading being drawn and the cavity ventilated during high solar & cavity temperature conditions.

The pilot model is assigned the following control attributes:

- Fictitious division swapped for blind material based on direct normal solar radiation setpoint of 400W/m^2 . The blind material is as previous in Table 6 and is 0.2mm thick.
- Blind optical property swap is based upon the above setpoint The optical poroperties are for the fictitious and blind materials are shown below:

Angle of incidence (degrees)	0	40	55	70	80
<u>FICTITIOUS MATERIAL</u>					
transmissivity	0.998	0.987	0.986	0.985	0.984
refeectivity	0.001	0.012	0.013	0.014	0.015
absorptivity	0.001	0.001	0.001	0.001	0.001
<u>BLIND MATERIAL</u>					
transmissivity	0.998	0.987	0.986	0.985	0.984
refeectivity	0.001	0.012	0.013	0.014	0.015
absorptivity	0.001	0.001	0.001	0.001	0.001

Fictitious material visible transmittance = 0.99

Blind material visible transmittance = 0.1

Table 14 – Optical properties of dividing surfaces used in shading control

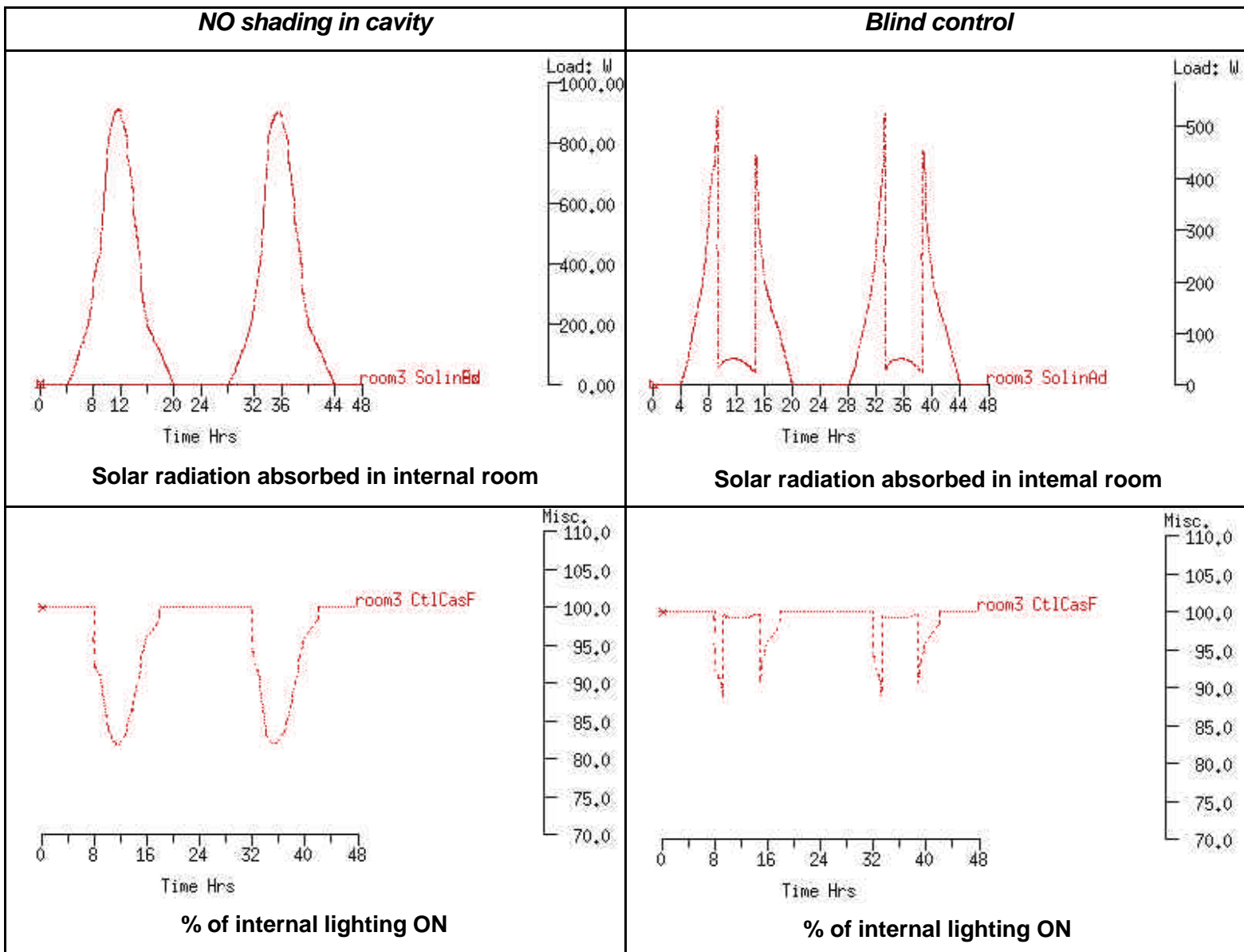
6 Double-Skin Facades with Roller-Blind Shading

- Cavity ventilation is as in pilot model, initiated when cavity air temperature is greater than 15°C.
- Convection control swap from Alamdari & Hammond correlations to Bar-Cohen & Rohsenow correlation, when cavity is opened.
- Internal lighting control (12W/m²) – ideal dimming, set-point 500lux, (daylight sensor at 5m room depth)

Infiltration in the cavity is accounted for by 1mm crack components at the inlet and outlets, as used in previous models. For the internal zone an infiltration rate of 1AC/h is specified via constant volume flow rate components. The internal zone is assigned 12 W/m² gains to represent lights and no other gains. The internal zone is assigned 1000W of cooling capacity, set to cool the zone to 20°C.

A graphical performance analysis, during the 10th-11th July, illustrates the shading control concept and is shown overleaf.

6 Double-Skin Facades with Roller-Blind Shading



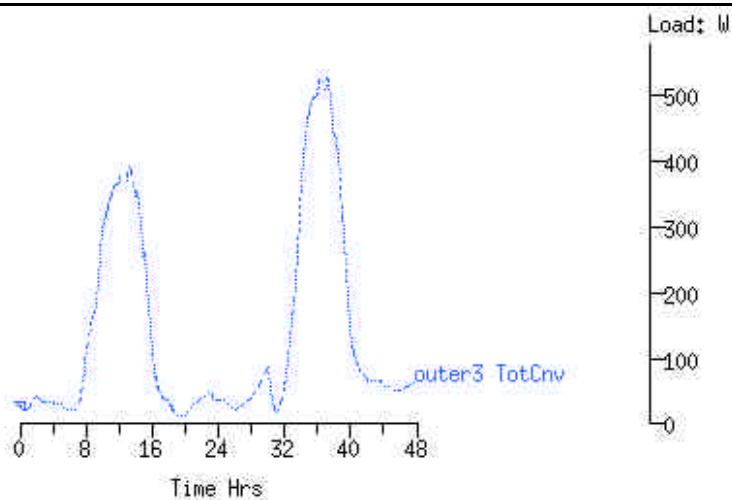
It is clear that the the blind switching considerably reduces the solar absorbed in the room in line with the blind low transmissivity. On the other hand, the internal lighting is load is increased when the blind is drawn. It is observed that the blind is open at the start and ends of the lighting day when the solar is low.

As well as blind switching control based on direct solar radiation, we may also control it via external air temperature or an internal temperature.

6 Double-Skin Facades with Roller-Blind Shading

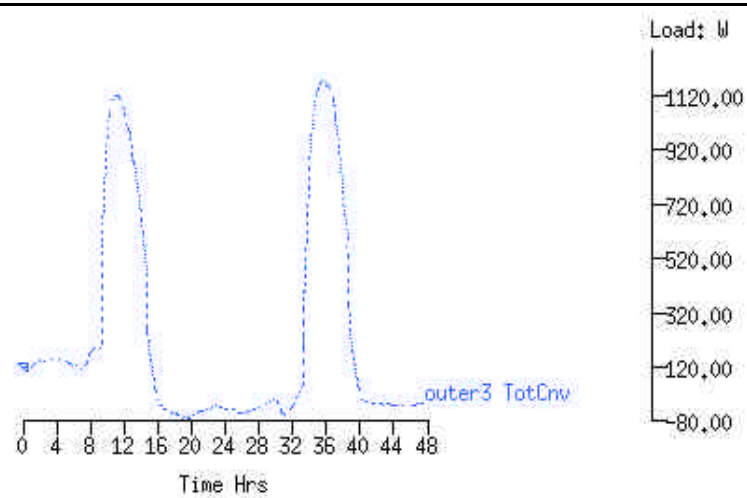
The blind switching also has a significant effect on internal cavity convection - since significant quantities of solar radiation are being absorbed by the blind and consequently liberated to the cavity air. Below it is clear that when the blind is down, surface convection is 2 to 3 times higher than when it is up. Also, the overall effect on internal cooling requirements is significant, with the cavity utilising shading control requiring no cooling in this case.

NO shading in cavity

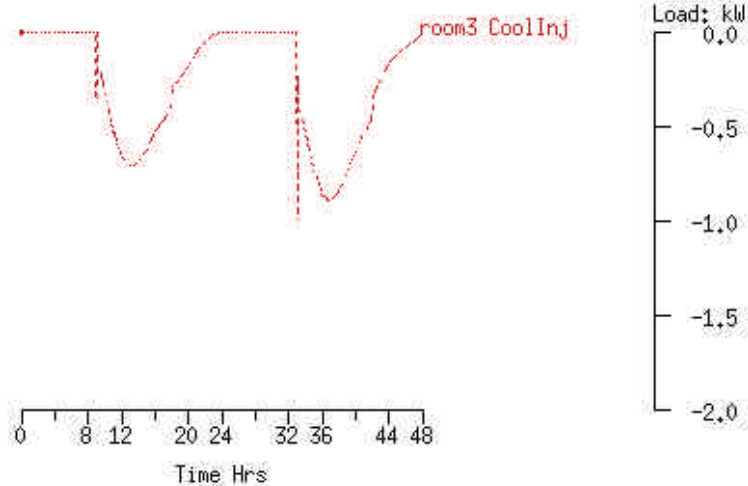


Total surface convection in outer cavity division

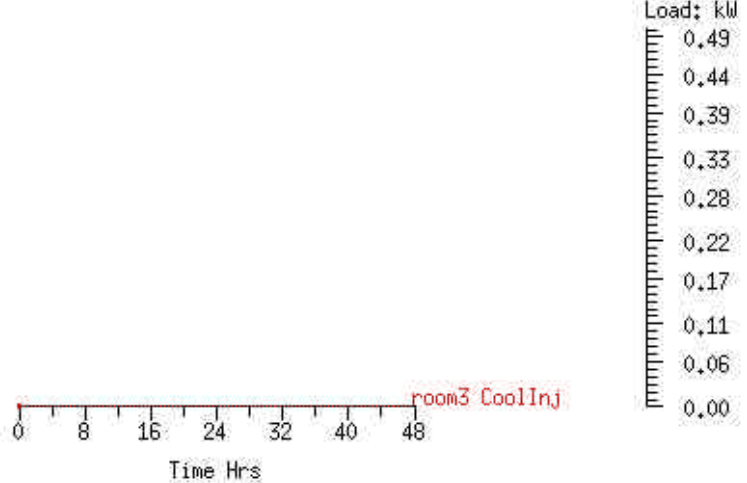
Blind control



Total surface convection in outer cavity division



Internal cooling energy



Internal cooling energy

7 Double-Skin Facades with Venetian Blinds

Modelling Venetian blinds within ESP-r pushes the program to its limits owing to the task of replicating blind geometry and thermo-physical processes with methods intended for large box like zones. Adjusting the software is no trivial task and will involve major re-coding & testing, particularly in the solar model area. To the best of the author's knowledge this is a problem faced by the other multi-zone building simulation programs.

7.1 Solar model issues

The ESP-r solar model as it was originally intended, presents a number of problems in the double-facade domain. Simplifications cause a significant alteration of solar-mechanisms. The treatment of solar radiation by ESP-r in a double facade with Venetian blinds and its divergence from reality is discussed below. How severe the effects of these flowpath distortions are is largely unknown and will be area investigated in the study.

To represent the proper progression of solar radiation throughout Venetian blinds, the International Standard ISO 15099 is consulted. It states that the following mechanisms need to be accounted for:

Diffuse - Diffuse transmission and reflection

The process by which external diffuse radiation, at various different angles of incidence, enters a glazed facade and is reflected or absorbed by the slats

Direct - Direct transmission (or unaffected direct radiation)

The portion of direct radiation which passes undisturbed between the slats.

7 Double-Skin Facades with Venetian Blinds

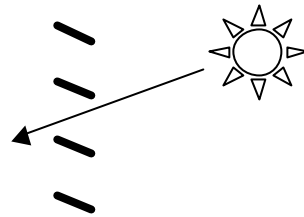


Figure 18 Direct - direct transmission through slats

ISO 15099 states that by geometric calculation from the angle and aspect ratio of the slats, the direct beam passing unhindered between the slats can be calculated for a given angle of incidence

Direct - Diffuse transmission and reflection

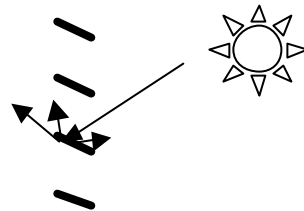


Figure 19 Direct –diffuse transmission and reflection

The portion of the direct radiation that is reflected by blind slats in a diffusive manner. ISO 15099 make the assumption that blinds are non-specular, such that all directly reflected radiation is non-directional.

7.1.1 ESP-r solar model

In ESP-r, diffuse transmission characteristics are based upon a 51° isotropic sky equivalent – that is a solar ray with an angle of incidence of 51° . The sum of all the incident rays in isotropic diffuse sky is found to be equivalent to that of a single ray of equal magnitude at this angle. In an actual sky this may differ though in terms of modelling a double-facade this is not a specific concern, rather it's an issue of boundary conditions being appropriate, which are ultimately stochastic anyway.

Within the zone, the diffuse radiation is shared among the zone's surfaces by area and absorptivity weighting. The reflected portion is shared in a similar manner, reflections repeated for 10 iterations to ensure the diffuse radiation is properly dissipated in the zone.

7 Double-Skin Facades with Venetian Blinds

With regards to external direct radiation, the incident direct beam is tracked throughout the first zone it enters till it hits an internal surface. At this point it is absorbed, reflected or transmitted.

Since direct and diffuse radiation transfer to adjacent zones are held separately the direct can be, for example, allocated to one or two surfaces in the adjacent zone. However, the directionality is lost so it is not possible to use ray-tracing to determine insulated surfaces (although this may be possible in future via, for example, a link to radiance routines). Also, because the incident angle for these internal glazing is unknown, the transmission/absorption/reflection properties in the glazing separating the zones is based on a 51 deg incidence angle.

7.2 Methods of modelling Venetian slats

In this section, different ways to model facades utilising Venetian blinds are discussed in order to ascertain the best method for further study.

Firstly, it should be recognised that a problem in relation to accurately modelling Venetian blinds pertains to the fact that the component's geometry is highly variable, from slats being horizontal to vertical. Different designs will also have differing slat widths and spaces. All in all this creates a multitude of design options and it must be stressed that no attempt is made to examine them all here; rather this is a specific design issue. In addition, some sort of automatic process to develop slat geometry would be necessary to analyse different options quickly, which this study doesn't lend itself too. Here, a generalised method and model is developed, which can be adopted for different blind designs. For the case where slats are pulled vertical, this can be simply represented with the roller blind model and issues associated with solar flowpaths will not be problematic.

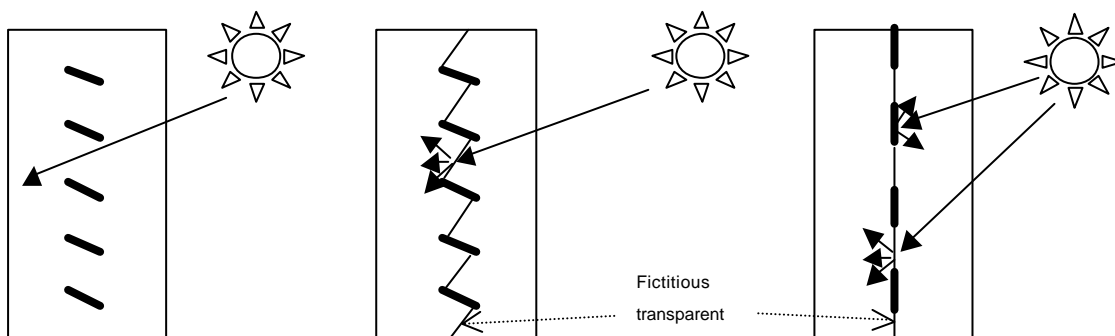


Figure 20 – Actual cavity geometry using floating surfaces, saw-tooth type model, simplified model

7 Double-Skin Facades with Venetian Blinds

Two ways of accurately representing the geometry of Venetian blinds (Figure 20 – left & middle models) would be to specify a series of floating surfaces in the cavity or by splitting the cavity into two zones, divided by a saw-tooth surface. In the floating surface model 4 vertices would be specified per slat and two surfaces assigned, one representing the front face of the slat and one for the back. These surfaces can then be connected adiabatically to form a properly bounded region. Ideally this type of model would allow the direct transmission of solar radiation to the inside facade, however the ESP-r insolation model has problems picking up these floating surfaces – this ability not being foreseen at the solar model's conception. Using such a model therefore would clearly cause major errors in solar absorbed by the blind and solar reaching the internal facade.

The saw-tooth modelling method avoids this problem by splitting the internal cavity into two, such that the saw-tooth surface representing the blinds forms an outer bounding surface of the zone and there are no floating surfaces. Additionally this design allows us to specify separate inner and outer air flow nodes in a network air flow model, and represent airflow through blind if desired. The saw-tooth consists of a series of blind slats separated by fictitious surfaces (100% transparent, very high conductivity with very low thermal mass). With this model, because of the ESP-r solar model mentioned previously, the solar passing through the transparent saw-tooth sections will become diffuse and apportioned on an area-absorptivity weighting. However ESP-r does allow a user-defined distribution of this radiation and it is likely that most of this radiation will fall evenly onto the internal facade, especially if the cavity is not too deep. A cautious approach would be to assign all of the diffuse to the internal facade in summer, producing a worst case scenario effect for internal cooling results.

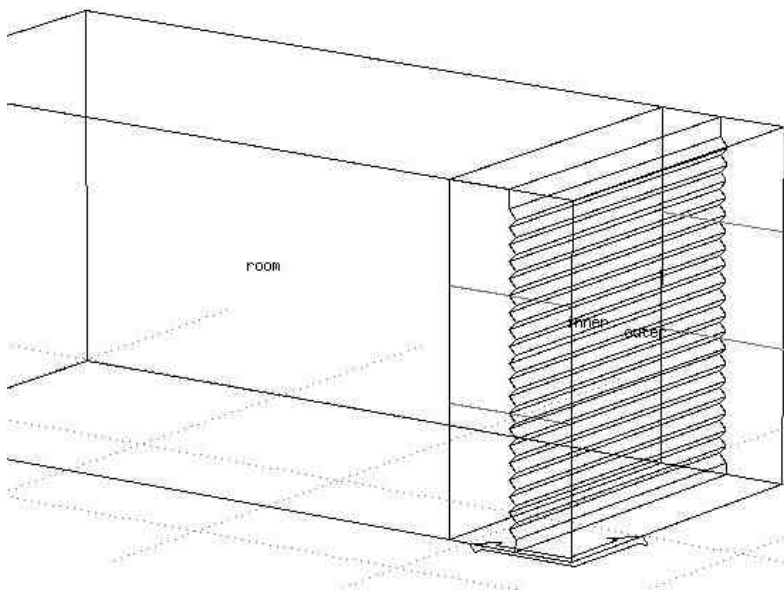
A simplified method to model Venetian blinds may be to specify a roller type blind but as in Figure 20 (simplified model) or to have one homogeneous roller blind material with different solar/optical properties that could let the right amount of solar through. Whether this is appropriate will be examined after the saw-tooth model is further investigated.

7.3 Saw-tooth Venetian model investigation

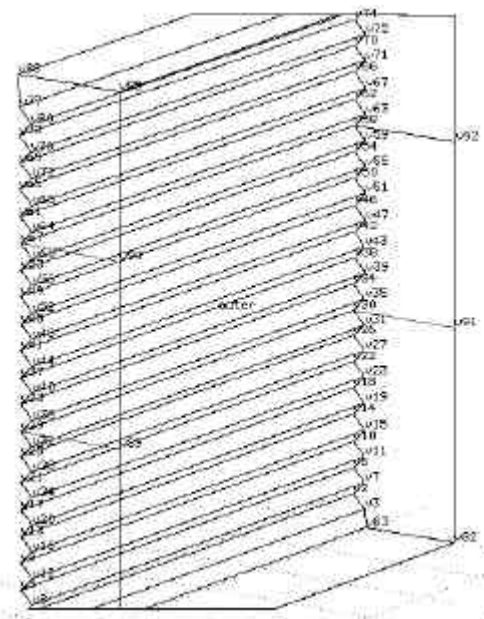
The saw-tooth model is based on the same single-storey dimensions of the previous pilot model (box-type window double facade with roller blind). It is important to restrict the model to the single-storey resolution for the following reasons:

7 Double-Skin Facades with Venetian Blinds

- the maximum number of surfaces is limited in ESP-r. The ESP-r code has been specially recompiled to allow for 62 surfaces per zone in this case (a number which has been tested).
- numerous vertices make up the saw-tooth surface and specifying them is a very time consuming process. Similarly, numerous surfaces also need to be specified and a second matching saw-tooth surface to mesh with in the adjacent zone is needed.



(1) Saw-tooth model consisting of inner/outer cavities & internal zone, based upon previous pilot model



(2) Outer zone highlighting saw -tooth surface

Figure 21 – Venetian blind saw-tooth model

In the saw-tooth model, Venetian blind slats are 7cm wide and angled at 45° with a spacing of 14cm between the slats axis of pivot, which ensures the blocking of direct radiation above at a solar altitude above 45°. Of course blind position can be very variable as mentioned, however blocking direct solar will be the desired goal of most blind systems and they will likely be positioned angularly at some point in the year to achieve this, hence the choice of this case. Even so, it is recognised that positioning of the blinds horizontally may be desirable in order to obtain a greater view outside and differences due to this set-up shall be consider. This will likely only happen outwith winter, when low solar altitudes and glare will necessitate some blind closure. Note that the sides of the cavity also require to be split into segments due to the large number of vertices associated with them.

7 Double-Skin Facades with Venetian Blinds

7.3.1 Testing the model (insolation)

Due to the many surfaces within the model, insolation prediction becomes problematic as ESP-r tracks a solar source to five internal surfaces and distributes the rest diffusively. In a traditional building simulation with rectangular, empty rooms this is not a great worry but in this situation it must be addressed.

To obtain a proper solar distribution within the double facade cavity, an investigation will be undertaken into:

- changing the source code slightly to track solar to more insolation surfaces
- splitting the outer facade into segments so that more solar sources exist

Changing source code significantly is not recommended due to the considerable knock-on effects it can have, so only moderate modifications will be examined in this study. Book-keeping of calculation results will increase in line with this change and computational burden may also be adversely affected. An outcome of this investigation is to determine the appropriate number of surface segments required to account for a complete insolation distribution and how changes to the source code affect it.

Firstly, by running an insolation analysis on the Venetian blind model without modification, we find that only a few slats are assigned a portion of the direct radiation. This is clearly not correct and so we split the outer facade in order to improve the results. Only in completely diffuse conditions would the insolation prediction be accurate. Table 15 below shows a sample of insolation distribution results when outer divisions are introduced (for particular slats on the 15th of January at 3pm):

Surface	Single outer transparent surface	6 divisions in outer surface
slat 15	0%	16.11%
slat 16	0%	16.11%
slat 17	0%	16.11%

Table 15 – Insolation distribution results for Venetian slats 15, 16 &17, [15th January at 15h00]

This table highlights an improvement in that we are now obtaining insolation on slats that were receiving none before. Whether the values are accurate or not is a different matter - the more divisions

7 Double-Skin Facades with Venetian Blinds

we make, up until some point, the more accurate it will become. Also by increasing the number of surfaces that can be insulated a similar effect will be reached. To do this, we need to edit a parameter, "misur" in the file "building.h" of the source code and recompile the program. Modifying this to account for 10 surfaces we may compare results with that of the standard case (6 surfaces). Table 16 below shows a sample of insolation results, using the previous case with 6 outer segments, for the change in "misur". This results sample is related to the insolation distribution from one particular segment of the outer facade ("outer 5" to be precise). To make these results samples clearer, Figure 22 illustrates the numbering procedure used in the model.

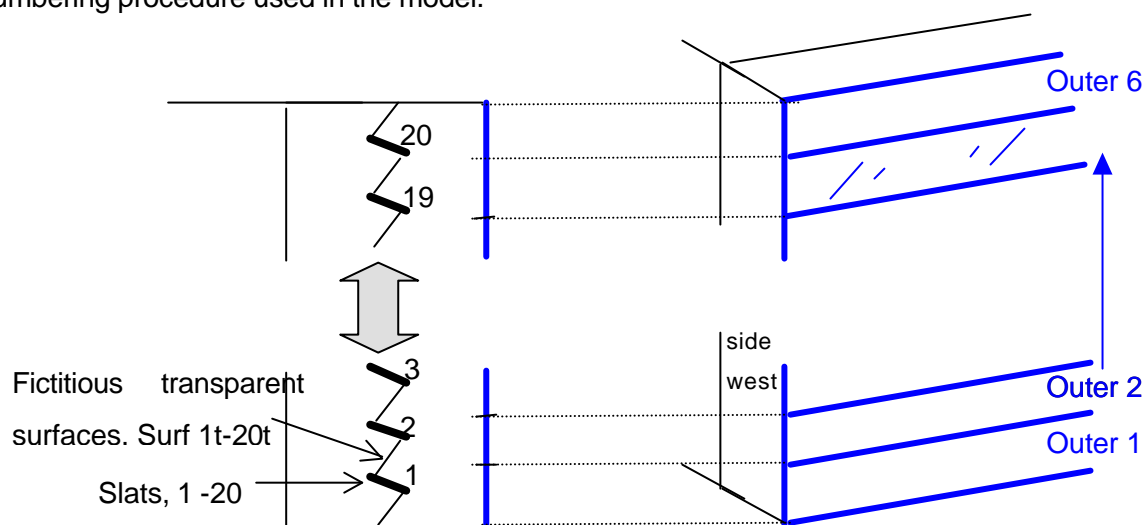


Figure 22 – Surface numbering procedure used in Venetian blind cavity

Surface	MISUR = 6	MISUR = 10
side_east3	19.46%	14.5%
slat 15	16.11%	12%
slat 16	16.11%	12%
slat 17	16.11%	12%
surf 15t	16.11%	12%

Table 16 – Insolation distribution result comparison for changing MISUR on model with 6 outer divisions, [15th January at 15h00]

Table 16 again shows differing results between MISUR=6 & 10 plus it is important to note that the individual percentages don't sum to 100%. It is therefore likely that more surfaces require to be accounted for. Also it is interesting to observe that only one transparent surface is included (surf 15t)

7 Double-Skin Facades with Venetian Blinds

in the insolation results– it would appear that the other transparent surfaces, which should receive solar from this particular segment, are not being reported.

This is confirmed when we consider the same situation in July, when the slats are designed to block direct radiation. Here we wouldn't expect the transparent surfaces to receive any direct radiation, only the slats, therefore insolation should have no problem summing to 100% this time. Table 17 below illustrates a sample of insolation distribution results for the 6 division model on July 10th. Note that because of the higher solar position, lower slats are seen by the segment (“outer5”) this time.

Surface	MISUR = 6	MISUR = 10
slat9	28.5%	28.5%
slat 10	28.5%	28.5%
slat 11	23.75%	23.75%
slat 12	14.25%	14.25%
side_west2	4.5%	4.5%

Table 17 - Insolation distribution results for model with 6 outer divisions, [10th July at 11h00]

This is indeed the case and furthermore all the percentages add up to 100% so we are confident that all insulated surfaces are being accounted for. Furthermore, when "misur" equals both 6 & 10 results are the same, so six outer divisions are entirely adequate to account for insolation in the high summer sun.

When the blinds are less angled and transparent sections of the saw-tooth are visible to the sun we need greater resolution though. Considering the geometry of the blinds in the model (20 slats with a further 20 transparent surfaces), 12 outer divisions are envisaged as adequate to account for the insulated surfaces in the zone at any time in the year. By considering the same blind geometry in a low winter sun we can show this. Table 18 below shows a sample of results from one segment of the 12 outer divisions (segment “outer11”), again comparing "misur" when equal to the standard six surfaces and when increased to ten.

7 Double-Skin Facades with Venetian Blinds

Surface	MISUR = 6	MISUR = 10
slat 18	24%	24%
slat 19	24%	24%
surf 18t	20%	20%
side_east3	20%	20%
surf 19t	12%	12%

Table 18 - Insolation distribution results (segment 11) for model with 12 outer divisions, [15th January at 15h00]

This table clearly shows that all insolation is being accounted for and the transparent surfaces are included in this account. The reason that transparent surface, "surf19t ", has a lower value than "surf18t" is because the segment providing the insolation source only partly sees it. If we look at the results for the segment above (segment "outer 12"), the transparent surface ("surf19t") is again included:

Surface	MISUR = 6	MISUR = 10
slat 18	24%	24%
slat 19	24%	24%
surf 18t	20%	20%
side_east3	20%	20%
surf 19t	12%	12%

Table 19 - Insolation distribution results for segment above (segment12), [15th January at 15h00]

Adding this percentage to the percentage from the previous segment we arrive at the same insolation result for surf18t – 20%. Also in these results we see that slat20, which is the top slat and is therefore not partially shaded by any slats above, receives slightly more solar than the other slats.

Considering the insolation results for segments below, they show the same insolation distribution pattern continuing as we should expect from the uniform blind geometry. Table 20 below captures the insolation results for the next segment down (segment 10).

7 Double-Skin Facades with Venetian Blinds

Surface	MISUR = 6	MISUR = 10
slat 18	24%	24%
slat 19	24%	24%
surf 18t	20%	20%
side_east3	20%	20%
surf 19t	12%	12%

Table 20 - Insolation distribution results for segment below (segment10), [15th January at 15h00]

Furthermore, the results are the same whether "misur" equals the standard 6 surfaces or the modified 10. In conclusion, 12 outer divisions are entirely adequate to account for insolation to all surfaces at any time in the year, high or low sun.

7.3.2 Further testing in complete simulations

To completely test these modelling adaptations it is wise to undertake complete simulations and analyse results for the absorbed solar radiation on surfaces. Also, we cannot continue simply to analyse percentage type results because these are measured relative to the insolation source – a source that will become lesser as more divisions are made. Rather we must run whole simulations and compare absolute surface solar absorptions.

If we check that when the sun is low in the sky:

- different results are given when "misur" equals 6 and 10, in the model with 6 outer divisions
- the same results are given using the model with 12 divisions,

we will confirm that the previous findings are being used correctly in the complete simulations. The 15th of March is used as the simulation period, having a high direct solar component (to highlight discrepancies) at low altitude sun.

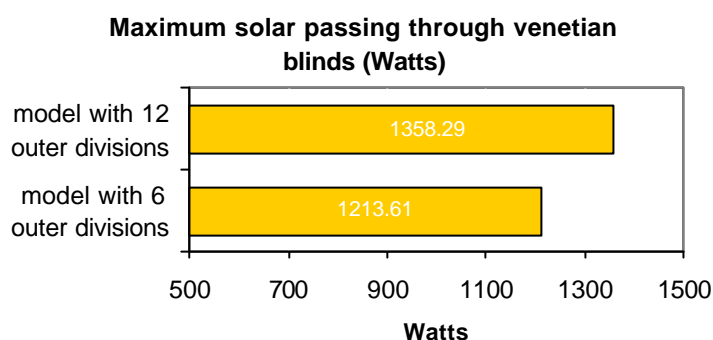
Analysis of results for 6 outer divisions with "misur" equal to 6 & 10 quickly show differences as anticipated. The results for 12 outer divisions are equal also as expected. Outputs of these simulations at five minute intervals between 11h00 & 13h00 on the 15th March can be viewed in Appendix C & Appendix D. In conclusion, 12 outer divisions allows for a proper insolation distribution.

7 Double-Skin Facades with Venetian Blinds

7.3.3 Significance of saw-tooth insolation results

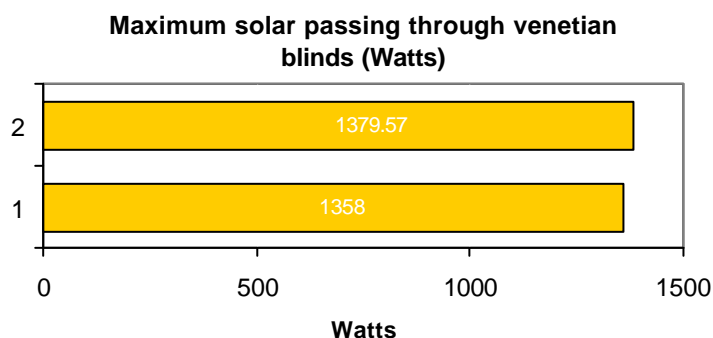
In terms of the increased modelling resolution obtained from splitting the outer cavity, solar flowpaths have been significantly affected within the domain. In particular the errors in solar transmitted to the internal zone between different resolutions can be great.

Graph 23 below illustrates the difference in the solar entering the inner cavity (i.e. that passing through the blind system) between models with 6 & 12 outer divisions.



Graph 23 – Difference in maximum solar passing through blind system for outer facade with 6 & 12 divisions

This difference would clearly have a direct impact on internal zone temperatures or plant requirements. The solar passing through the blinds is treated diffusely as previously discussed and shared equally among the inner cavities surfaces. Another interesting case to consider would be how the properly distributed insolation results compare with a single outer surface using the ESP-r default case. In actual fact results are very similar as Graph 24 shows:



Graph 24 –Difference in maximum solar passing through blind system with a single outer facade & one with 12 divisions

7 Double-Skin Facades with Venetian Blinds

The reason for this similarity is found to be due the specific properties of the blind system in this case, the solar absorptivity of the blinds in particular. Because the blinds used in the model are white painted steel they have a low absorptivity (0.3) and a high reflectivity (0.7). This means that the non-specular blinds will reflect the majority of incoming direct radiation diffusely – creating a situation that co-incidentally happens to be very much like that of the single surface case (which only tracks direct to five surfaces by default).

To highlight the errors that this assumption can really cause requires us to change the blind properties to a higher absorptivity (0.9) so that much less solar is reflected. We also need to simulate during a period when the solar altitude is high and only the blinds slats are in view (July 10th). At this solar position, very little of the sun's direct solar component should reach the inner side of the cavity via reflection. Table 21 shows the amount solar radiation passing through the blind system for both models and the associated errors from using the single outer surface.

	Max. solar passing through blind system (W)	
	Blind absorptivity= 0.3	Blind absorptivity =0.9
Model with outer surface with 12 divisions	1123.0	624.78
Model with single outer surface	1200.3	845.9
	Error = +7%	Error = +35%

Table 21 – Significance of absorptivity on solar results

Clearly an error of over one third illustrates that proper tracking of direct solar radiation is very necessary in a Venetian blind system and this simulation aspect should not be grossly simplified.

It can also be concluded from Table 21 that Venetian blinds made of highly absorbing materials are much more efficient at blocking solar getting to the inner facade. This will clearly effect the internal cooling requirements in summer.

Summary of insolation investigation

It is possible to conclude that by dividing the outer surface into 12 segments, this by itself will provide for a proper insolation distribution in the zone. We have observed that whether misur equal 6 or 10 the insolation distribution for 12 divisions is the same. Changing this parameter does make a difference when there are only 6 outer divisions. However, If we should want to increase “misur” to such an

7 Double-Skin Facades with Venetian Blinds

extent to allow an insulation account on all internal surfaces (misur=46), when we have just one single outer surface, erroneous results appear. A sample of the problematic insulation results for this case is presented in Appendix E.

7.3.4 Long-wave radiation exchange in Sawtooth model

Long-wave radiation exchange is another important thermodynamic flowpath which requires to be examined in the saw-tooth model, and in particular how the saw-tooth modelling abstraction effects view factors. Figure 23 below shows an exaggerated image of what the actual blinds would see in reality and what they would see in the saw-tooth model.

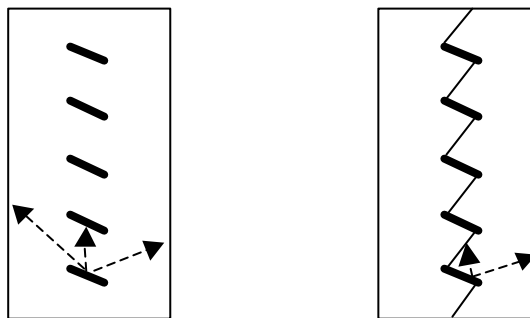


Figure 23 – Real view factors Vs saw-tooth model view factors

In reality, the top surface of a blind slat would see the bottom of the slat above, however in the saw-tooth model a fictitious transparent surface is in its line of view. Since in reality the slats are much closer together, the transparent surfaces connecting them really only block the view of adjacent slats and so view factors of the transparent surface should be similar. To confirm this, another model with floating slats (Figure 24), representing reality exactly, was constructed to compare view factors with that in the saw-tooth.

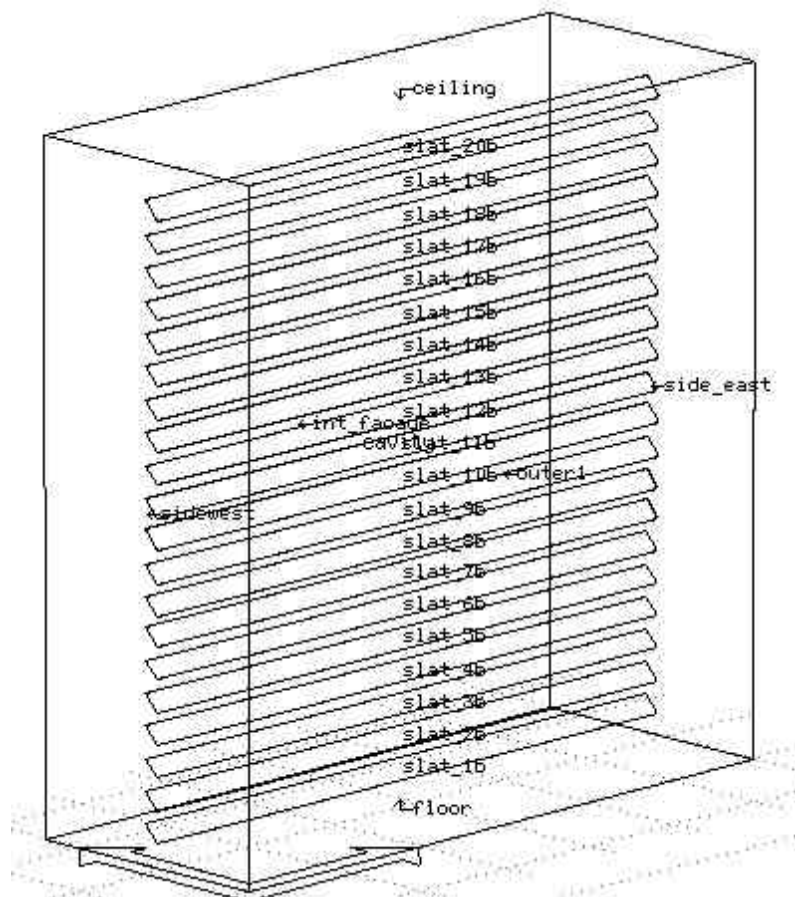


Figure 24 – Floating Venetian blinds made with back to back surfaces

When the results are compared, it is the case that view factors from the top-surface of a slat and the transparent surface are very similar to that between adjacent slats in reality. Table 22 below, illustrates this similarity for the 1st slat. In the case representing reality, “Slat2b” is the back of the slat above slat1. In the saw-tooth case this surface is blocked from view by the fictitious transparent surface, “Surf-1t”.

7 Double-Skin Facades with Venetian Blinds

Model representing reality (floating slats)		Model with saw-tooth surface	
View factor ref.	View factor (%)	View factor ref.	View factor (%)
Slat 1-> Slat 2b	20.13	Slat 1-> Surf-1t	29.31
Slat 1-> outer face	51.48	Slat 1-> outer face	51.46
Slat 1-> west	7.33	Slat 1-> west	5.7
Slat 1-> east	7.43	Slat 1-> east	5.8
Slat 1-> floor	7.129	Slat 1-> floor	7.122
Slat 1-> ceiling	1.287	Slat 1-> ceiling	0.597
Slat 1-> internal face	5.22	Slat 1-> internal face	0

Table 22 – Comparison of slat 1 view factors in reality to those in the saw-tooth surface

Note that in the saw-tooth case the internal face can no longer be seen and only one half of the floor & ceiling area are available in the split zone. A similar pattern is present throughout the blind system. Table 23 below shows the results for slat 15 in the blind system.

Model representing reality (floating slats)		Model with saw-tooth surface	
View factor ref.	View factor (%)	View factor ref.	View factor (%)
Slat 15-> Slat 16b	20.13	Slat 15-> Surf-15t	29.3
Slat 15-> outer face	51.49	Slat 15-> outer face	51.43
Slat 15-> west	6.35	Slat 15-> west	5.46
Slat 15-> east	6.37	Slat 15-> east	5.34
Slat 15-> floor	0	Slat 15-> floor	0
Slat 15-> ceiling	15	Slat 15-> ceiling	8.471
Slat 15-> internal face	0.68	Slat 15-> internal face	0

Table 23 - Comparison of slat 15 view factors in reality to those in the saw-tooth surface

In the case where the blinds are less angled, say horizontal, the view factors will be further distorted because a greater portion of the inner facade will be blocked. Significantly, the inner facade will have a much lower surface temperature than the blind slats when the sun is shining. Also if the cavity is deep, larger surface areas will be blocked, further intensifying errors. To achieve the correct set-up therefore, a manual specification of view factors between surfaces in different zones is required. The can be prior determined using the floating slat model.

7 Double-Skin Facades with Venetian Blinds

As well as blocking views, the fictitious surfaces also create new views that must be dealt with. They effectively present a system of blinds to the outside and inside facades having double the surface area they should have. For example each fictitious surface will see the outside and be able to transfer heat. To remedy this, the emissivity of the fictitious surfaces could be set to zero and then manual manipulation of view factors is necessary to ensure that a real slat's view of a fictitious surface is re-assigned to the adjacent slat (at a similar temperature).

In addition, the cavity surfaces not forming the blind system must also be adjusted so that they cannot see the fictitious surfaces. This is more problematic because the views being blocked are in another zone and specifying view factors between surfaces in different zones is not catered for presently unfortunately. Left alone, this error may result in a lower cooling estimate in summer because the hot outer facade cannot see the cooler inner facade. Whilst in winter a lower heating estimate would be obtained because the inner facade cannot see the cold outer facade. The true extent of this error is unknown however. It could also be argued that the long-wave radiation intercepted by the transparent surfaces will cause the blind system to heat up further, subsequently transferring more heat into the adjacent zone via the slat sections.

The inability to specify view factors between zones means that we must rely fully on standard fictitious surfaces to readily transmit radiation between the inner & outer facades. Hence we must set the emissivity of the fictitious surface close to unity. Also in this case therefore, the manual specification of view factors from the floating surface model doesn't apply.

7.3.5 Convection in Sawtooth model

Surface convection is another major thermodynamic flowpath which is distorted in the saw-tooth model. Due to the fictitious transparent surfaces in the saw-tooth division, double the area exists for heat transfer than does in reality. To remedy this, ESP-r allows us to specify convection correlations manually and those for the transparent surfaces should be set to zero. A change in the source code was required to allow for this (see Appendix F & Appendix G)

The surface convection correlation chosen for the cavity was the Bar-Cohen & Rohsenow general correlation for buoyancy driven flow in vertical channels. In the two cavities formed by the dividing

7 Double-Skin Facades with Venetian Blinds

Venetian blinds, both are assumed to have external air as their source. Of course with angled Venetian blinds, the cavities are now not purely vertically bounded.

CFD analysis in blind cavity

A CFD analysis of the Venetian blind system is unfortunately not fully possible with ESP-r presently because it only facilitates rectangular gridding in the zone. Restricting ourselves to a horizontal slat case neither helps because the maximum number of cells in a zone is limited and fine gridding required between every slat (20slats) would quickly cause this limit to be exceeded.

Alternatively, using a stand alone CFD application like FLUENT is an option. However assigning appropriate boundary conditions is difficult and would easily become erroneous. It would be possible to assign temperatures from the building simulation results, though assigning a velocity inlet corresponding to the stack effect ventilation would give the CFD model forced characteristics. Furthermore, assigning appropriate near wall functions around the Venetian blinds is difficult. Overall, the quality of the information gained would be ambiguous. Rather, experimental validation would be required to assess natural flow/convection around Venetian blinds in the cavity.

7.4 Conclusions from saw-tooth model

Modelling Venetian blind systems is very complex as the foregoing investigation illustrates and building simulation software doesn't naturally lend itself to the task.

Introducing modelling abstractions, necessary to represent the system, can have a significant effect on the result and care must be taken to ensure that major thermodynamic flowpaths are not severely affected. Due attention must be given to tracking direct solar radiation in the zone to ensure a correct insolation distribution over the blind system. This is critical to predicting the correct solar transmission of the system and thus predicting accurate plant requirements. Regarding surface convection, it would be desirable to ensure that the saw-tooth fictitious surfaces do not have access to this flowpath, by setting its convection co-efficients to zero. Careful consideration should also be shown to long-wave radiation exchange in the saw-tooth surface; associated view factors can be affected due to the fictitious surfaces present. These effects will be more serious for blinds at shallower angles and also those within deep cavity spaces. ESP-r does allow for a manual specification of view factors and

7 Double-Skin Facades with Venetian Blinds

appropriate adjustments can be made there. However, specifying view factors between surfaces in different zones is not possible and remains an area where errors exist. We must instead rely upon fictitious surfaces (emissivity close to unity) to readily transmit radiation between zones.

From a practical aspect, this method involves very complex geometry that is time consuming to input. An automatic blind creation/saw-tooth surface procedure would be recommended if this were to become practical to apply. Also having a separate model with floating surfaces to compare view factors with is time prohibitive. Furthermore it would be desirable to have the ESP-r code capable of distributing direct solar from a single source to many more internal surfaces. Though splitting the insolation source allow us to get around this.

Considering the question: "Can you represent Venetian blind geometry more simply - by a flat vertical surface?" the answer is likely to be yes, but only for a specific blind design and angle. This would have to be determined independently for each design. Furthermore if it was desired to study blind control via simulation, the code would need to be capable of modify geometry at each simulation time-step!

In terms of a generic simplification though, the answer is almost certainly no. More possible is the development of a set of common Venetian blind designs that can be simulated in different operational positions, say:

- Vertical (shut)
- 45 degree tilt
- Horizontal

From an analysis of these designs, an equivalently behaving vertical surface with appropriate solar/optical properties could be defined. It's entirely more feasible to substitute these physical properties at a certain time-step during the building simulation.

Alternatively a coarse saw-tooth having the same overall slat surface area could be utilised. This way, slat-to-slat view-factors could be maintained at appropriate angles easily and an insolation distribution would be appropriately predicted on the angled surfaces. Effectively, the actual blind slats would be lumped together into fewer, larger slats. This would be a very promising route to follow since it maintains all of the integrity of the saw-tooth model and with the ESP-r solar tracking ability increased

7 Double-Skin Facades with Venetian Blinds

to 10 surfaces, would easily accommodate accurate insolation predictions. Time to build the saw-tooth surface would also be greatly reduced.

7.5 Venetian modelling - The ideal simulation program

In essence the saw-tooth model attempts to address the complex thermodynamic processes in a double facade through the astute use of fictitious components and the forced manipulation of flowpath descriptions traditionally used in building simulation software. An alternative to this would be of course to completely re-code a vast section of the software to allow for a new greater resolution appropriate to the interactions present in these advanced facades. The criteria such software would need to meet are discussed here.

The ideal simulation program would perform a complete building solar analysis. It would provide an exact description of the way solar radiation travels through the system via a full-three dimensional calculation using the full matrix of the transmission, absorption and forward and backward reflection for each angle of incidence at each component. Significantly it would be able to keep track of the direct solar magnitude and angle relative to incident surfaces throughout the cavity space into the internal zone. For the evaluation of the spatial distribution of day-lighting, this would be the necessary procedure to adopt. Programs such as Radiance are capable of this level of resolution currently. A similar resolution for calculating the long wave view factors would be necessary. The capability is essentially catered for currently by the ESP-r ray tracing method, but cannot be properly integrated due the solar models inability to cope with floating surfaces.

Secondly the ideal program would have to be able to perform such calculations for an appropriate selection of blind slat angles, where a control strategy involved tilting slats. It would need to hold the results for each blind position for swapping at a particular time-step. Clearly of use would be an automatic blind generation procedure in this case. The down-side of such a program would be the vast increase in simulation time that it would incur.

A sufficient compromise in the author's opinion would be to address the solar models inability to recognise floating surfaces and track direct solar falling on them and going between them to fall on the surface behind. Limiting this to the facade cavity zone would be sufficient and allow for a very good representation of the insolation distribution and a proper description of long-wave radiation flowpaths.

7 Double-Skin Facades with Venetian Blinds

Regarding cavity airflow, for detailed studies it may also be desirable to include ESP-r's CFD domain in the cavity and to have airflow network connections between the internal zones and the outside. This is however hindered by the strict rectangular gridding available around slats, necessitating slat geometry to be built of a series of slender blocks that quickly increase the surface count to a prohibitive number. Equally, the number of slats subsequently requires excessive 3-D gridding.

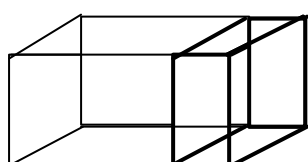
Overall, upgrading to the ideal state would be a huge coding task and involve necessary validation and testing. However the outcome would be a very versatile, representative and elegant solution for a double facade system.

8 Conclusions & Recommendations

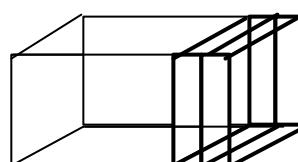
As observed throughout the study, the double facade is a highly dynamic system reacting to the climate through a co-ordinated use of shading, ventilation & construction components. It is a key zone that significantly impacts on the environment behind the internal skin and results are highly sensitive to the way it is modelled.

8.1 Initial geometrical considerations

Regarding a **single-storey** type double-skin facade, a model should consist of at least one repeating section of the double facade and adjoining internal perimeter zone:

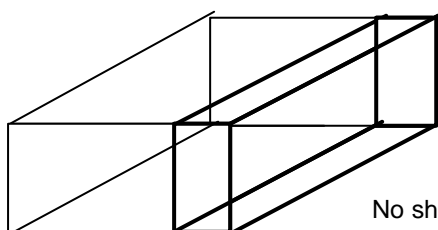


No shading

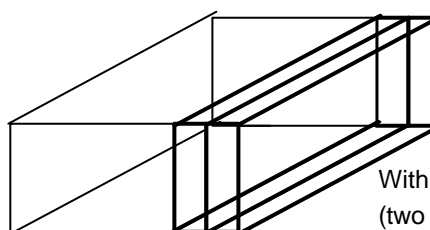


With shading
(two cavity zones required)

In a **corridor type** double-skin facade, the repeating section becomes either a floor of the building or part of it:

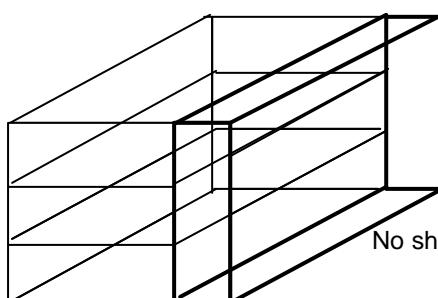


No shading

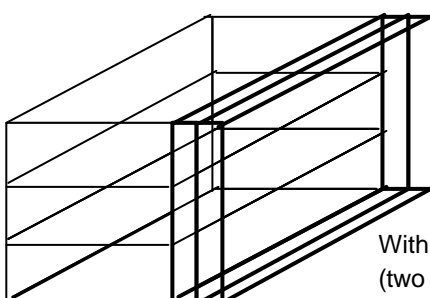


With shading
(two cavity zones required)

In a **multi-storey type** facade it is necessary to represent the full-height of the facade and perimeter storeys to account for the stack effect. Also wind effects become apparent over large heights.



No shading



With shading
(two cavity zones required)

8.2 Modelling Pre-requisites

8.2.1 Insolation distribution

Solar radiation is of course a key energy flowpath to consider in any fenestration design. Since the airflow-window is modelled as a separate zone due to cavity depth, it is strongly recommended that a pre-simulation insolation distribution be calculated via the ESP-r solar tracking facility. Otherwise solar radiation is assigned to all surfaces based on area weighting and an incorrect prediction of direct solar reaching the internal zone is obtained. This error becomes more significant as the cavity dimensions increase.

8.2.2 Longwave radiation

As a matter of course, the ray-tracing method within ESP-r is recommended to accurately determine the correct view factors within the cavity. Considerable temperature gradients can exist throughout the cavity and it is therefore important to ensure that surfaces have a correct view of one another. Especially in a cavity with a high aspect ratio, the errors from assuming a default area weighted distribution for view factors can be significant.

8.3 Airflow-window modelling (double-facades without shading)

For the typical cavity depths found within airflow-windows (0.2m), advection will occur and it is important therefore that the convection flowpath be represented appropriately. Consequently it is not suitable to represent the airflow-window as a single construction and requires a separate zone. The airflow window is effectively modelled as a separate zone positioned on the inner building skin. The window model used in the investigation was for a full-height case, though the geometry of the window zone can easily be modified to suit the specific design.

Operation modes

Convection regimes differ depending of the airflow-window's mode of operation. Three different modes of operation for the airflow-window were identified:

- Cavity closed
- External facade opened (internal cavity flow)
- Internal & external facade opened (full airflow)

8 Conclusions & Recommendations

Each of these is observed to have a significant effect on the internal zone environment and so requires to be properly represented. The concept behind the closed cavity is for the window to behave as a thermal buffer space in winter and as such very little cavity airflow occurs. An airflow network is necessary to represent the variability of natural ventilation and for the closed cavity case it can simply be represented as:

- One cavity and one external air node
- Two air-flow connections via cracks components: representing leakage at inlet and outlet, between the outside and the cavity

The flow & convection regime for the closed cavity case was predicted by CFD simulation in the cavity (utilising Yuan wall functions for natural convection). The results for the convection heat transfer were found to differ from those predicted by Alamdari & Hammond correlations commonly utilised in building simulation software. Of course these correlations were developed for large room-like zones where each surface is essentially isolated from one another. In the high aspect ratio cavity of the airflow-window, interaction between surface flows means that the results should not be expected to be the same. Over a range of different cavity aspect ratios, discrepancies of 5-15% in cavity convection were noted. In the 0.2m airflow-window an internal energy difference of 5% was affected by the differing convection predictions. Though the CFD simulation was felt robust, experimental validation was unfortunately unavailable. As a sensible measure, the Alamdari & Hammond correlations were utilised as a worst case scenario. Nevertheless, it is recommended that more suitable correlation be used when information becomes available however. CFD modelling does not lend itself to long-term modelling of double-skin facades due its intense computational requirements.

When the external facade is opened and cavity airflow occurs from the outside, it is appropriate to represent this as buoyancy induced flow. Static wind pressure differences over the height of an airflow-window will be small in any case. The airflow network can be represented by that used for infiltration in the closed cavity case, except that the inlet and outlet components are changed to represent the open conditions. The resistance caused by the cavity can in most cases be considered negligible compared to these openings. The convection transfer in a buoyancy induced flow regime is appropriately represented by the Bar-Cohen & Rohsenow correlation (Equation 3). This is confirmed by the Molina & Maestre correlation (Equation 7) specifically developed for an airflow-window. Using standard Alamdari & Hammond correlations impact severely on the internal energy requirements – overestimating by as much as 50%.

8 Conclusions & Recommendations

When the window is completely opened and air can flow to the internal zone, additional airflow connections are required to connect the external node to the inside. A bi-directional component can be selected to represent single sided ventilation in the model or two airflow connections, whatever is most suitable in the specific case.

Control of operation modes

All of the above operation modes and their characteristics can be completely controlled to enable a prediction of energy consumption over an entire range of conditions. Airflow connections to the cavity can be switched on and off based on the temperature of the internal zone. In addition, cavity convection regimes can be adapted depending on the operation mode (open or closed). Presently because convection control is based upon the switching of heat injection, a small (negligible) quantity of heat is required corresponding to when this switching is required. However, the software could be updated to allow switching of convection regimes based on temperatures if required.

8.4 Double-skin facades with roller blinds

It is very important to accurately depict the spatial sense of the roller blind in the double-skin facade cavity. It may be that the blinds are attached to the internal or external skins, and this can easily be accounted for with a single zone representing the cavity. Typically however, the blinds are located in the centre of the cavity. In that case it is necessary to split the cavity into two zones, with the vertical division forming the blind surface. Trying to represent mid-blinds otherwise will result in gross errors.

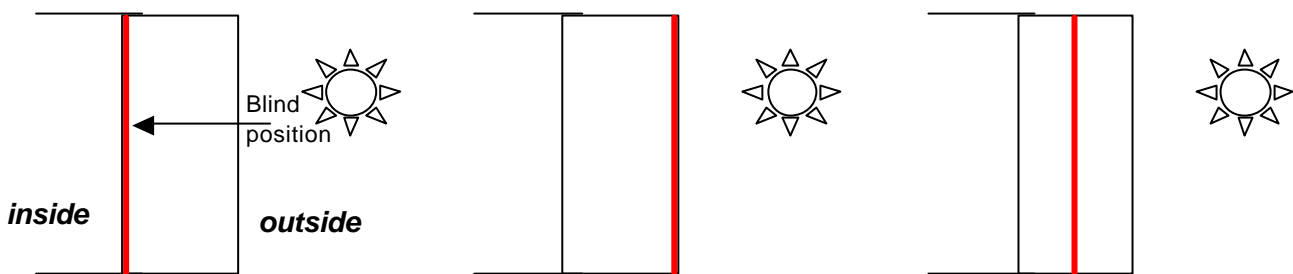


Figure 25 – One-storey elevation, showing different modelling methods for blind position within cavity space (placement: inner, outer, midway)

The blind properties also significantly effect the internal energy requirements. It is important to remember that surface properties on the inner and outer facing blind can be different and significantly impinge on the internal zone.

8.4.1 Ventilation

To represent natural ventilation and its variability, an airflow network is recommended for the cavity. At least two internal nodes are necessary to represent the air in front of and behind the blind. In the single storey facade configurations classified in Table 1, the single storey type facades can be suitably represented with one external node at single static wind-induced pressure:

- One-storey box type
- Corridor Facade

8 Conclusions & Recommendations

Where as in the multi-storey type facades, wind induced pressure differences across inlet & outlets will be significant:

- Multi-storey/envelope facade
- Shaft-box type facade

The airflow network can be represented in two ways, which give close agreement.

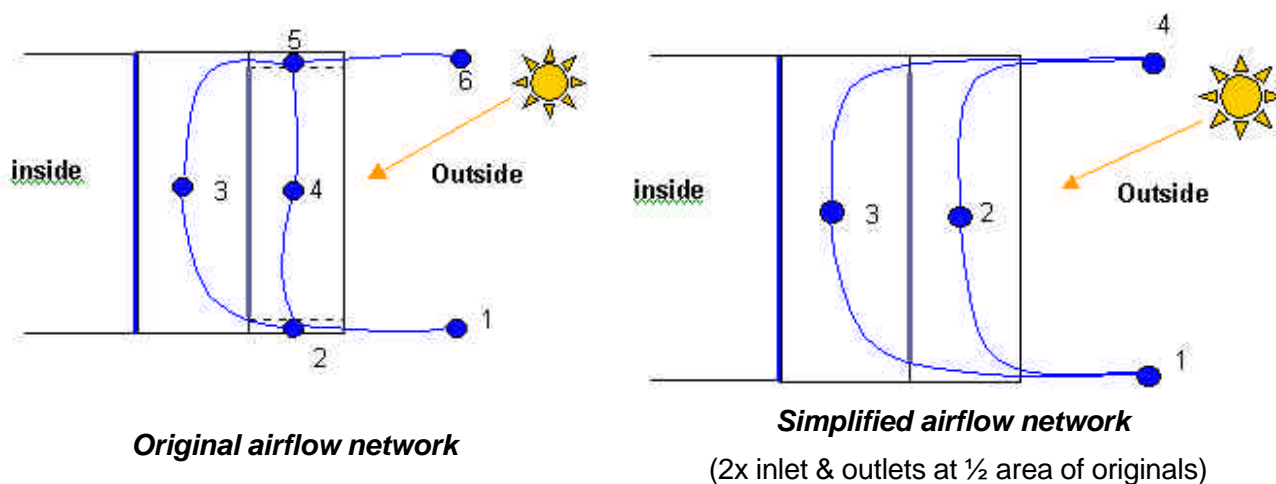


Figure 26 – Single Storey Facade Elevations: Airflow networks representations for cavity ventilation

The 1st network would be the desired representation but is prone to rapid fluctuations, linked to its ability to represent back-flow. Relaxation is commonly required to remove this problem. The simplified model however is a completely free of such fluctuations and still closely represents the airflow in the previous model though cannot account for back flow. This model can be used to good effect therefore.

In the cavity, the majority of the flow resistance will be caused by the inlet and outlet components. There is a significant lack of data concerning the necessary information describing mass-flow relationships through such components, particularly in a natural ventilation situation. An orifice type opening is used for inlet and outlet components in this investigation though specific data from manufacturers should be sought. Otherwise the orifice equation can be used and internal energy requirements and a sensitivity analysis is recommended. Positively, the sensitivity of the system to changes in the orifice characteristics was low to moderate in our case. A 25% variation in discharge co-efficient (initial $C_d=0.65$), resulted in a difference in predicted energy consumption of slightly more than a 5%.

8 Conclusions & Recommendations

When the cavity is mechanically vented, simple airflow schedules may be defined at the specified rate, or alternatively a constant volume flowrate component may be employed in a network.

8.4.2 Convection

When the cavity is naturally ventilated (as in modes 1-4 of Figure 1), the Bar-Cohen & Rohsenow correlation (Equation 3) is recommended to predict the convection heat transfer over the range of cavity aspect ratios. When the cavity is closed (as in mode 5 of Figure 1), the standard Alamdari & Hammond correlations are recommended as a worst case estimate until suitable correlations are made available. CFD simulations have predicted that the actual influence of cavity convection on the internal zone energy requirements is much lower. Experimental validation is the recommended course. When the cavity is mechanically ventilated, the convection regime will be better represented by Equation 5.

Switching between 2 convection regimes is only possible at present due to the control method which is based upon the binary condition of the heating/cooling operating. However the BBRI classification found that most frequently either natural ventilation or mechanical, but not both are employed in the double-skin facade. This means that convection will typically only require to switch between natural/closed or mechanical/closed regimes. In natural ventilation in multi-storey type facades, when wind effects become prominent a forced flow condition likened to that of mechanical ventilation will occur. Either a more appropriate correlation can be assigned based on wind speed (cavity Reynolds/Grashoff number) or the buoyancy induced flow model can be retained as a worst-case type scenario. The former method is not yet available, though there is no reason why it would not be possible.

8.4.3 Vertical division of cavity in multi-storey type facades

In the multi-story type facade it is recommended that fictitious surfaces (low thermal mass, low solar absorptivity, high-conductivity, high emissivity) be used to vertically divide the cavity on a floor-to-floor basis. Although not completely benign surfaces, their influence is small when used in this way. Such a division of a multi-storey exposes the facade vertical temperature gradient, which has a significant effect on floor-to-floor energy requirements. Particularly, energy requirements at the bottom storey's are over estimated if no vertical divisions are used. It is also apparent that a maximum vertical height of the cavity should be restricted in a natural ventilation scheme – 4 stories would appear to be a maximum limit as temperatures of 38°C were noted at the top of the cavity. For that reason, internal windows should therefore be kept shut to prevent warm air surges – instead the inside should be mechanically ventilated. Further vertical divisions (say per ½ storey height) are not recommended because the influence of fictitious surfaces becomes more prominent as they assume a bigger proportion of the overall area of the partition they occupy.

In the shaft-box type facade, the vertical division is important in terms of predicting the correct buoyancy driven flow in the cavity. If just one full-height zone is used to represent the shaft, an over estimated mass flow prediction would result. Again it is recommended to incorporate floor-by-floor fictitious divisions.

8.4.4 Control of operation mode

Due to the cavity division necessary to model the blind, in a control scheme it is necessary to replace the blind surface with a fictitious surface when the blind is not in use. Of course, and when compared to an empty cavity, placing any surface within the facade cavity will modify the temperature gradient through the cavity. Furthermore, because the dividing surface forms a large proportion of the cavity surface area it is difficult to force it to have a negligible influence. Fictitious surfaces will therefore have to be relied upon otherwise different operation modes will have to be modelled statically and this limited applicability. The use of these fictitious surfaces for this purpose is tolerable however and errors in energy predictions are likely to be much less than 10%. This applies to the cavity over a range of different operations and clearly the prediction error is only apparent when the shading is pulled up.

8 Conclusions & Recommendations

A number of crucial points are associated with the way the fictitiously divided cavity is modelled to ensure that these errors are indeed tolerable. Firstly it is recommended that the solar insolation calculation via the ray tracing be forced upon the internal cavity division - the source surface being that where the blind is positioned. This ensures that the solar radiation falling on the internal zone is almost identical to that predicted in an undivided cavity. Also this is applicable for the case where the blind is down and its material is not completely opaque. Secondly it is recommended that when the facade is closed (buffer space mode), the outer portion be left open to ensure an appropriate temperature gradient within the space and good prediction estimate.

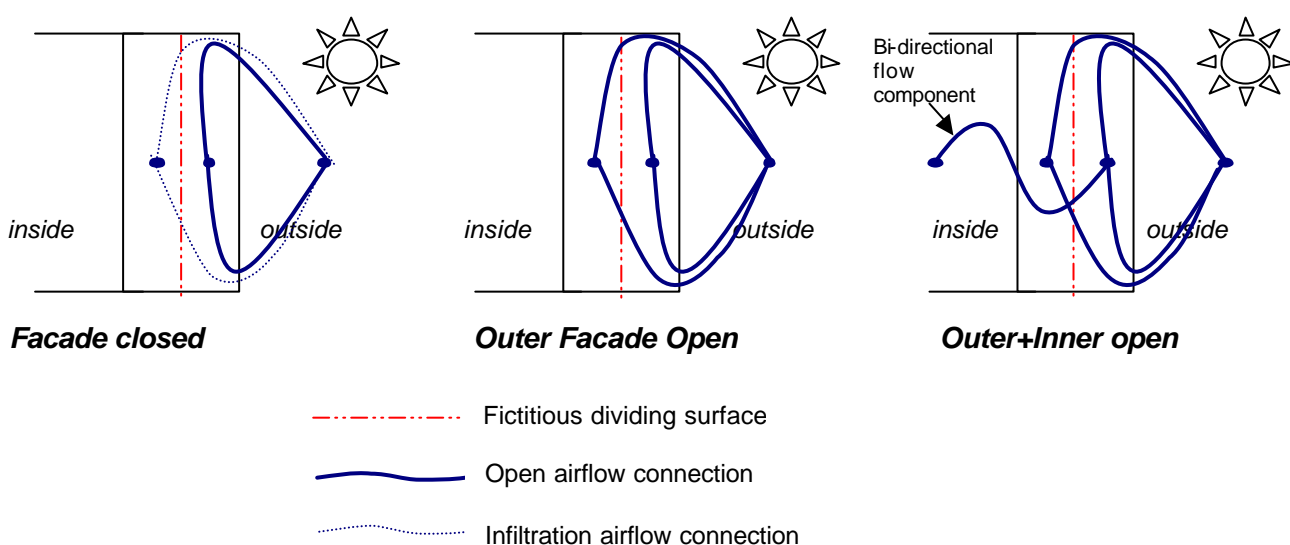


Figure 27 - Single Storey Facade elevations: recommendations for air-flow network in fictitiously divided cavity

Finally it is recommended for the case when the inner facade is opened (via internal windows) that the airflow connection to the inside be connected to the outer cavity division. The temperature prediction in the outer division is closer to that predicted in an empty cavity (i.e. that without a fictitious division).

8 Conclusions & Recommendations

8.5 Double-skin facades with Venetian blinds

Modelling Venetian blind systems is difficult owing to the task of replicating blind geometry and thermo-physical processes with methods intended for large room like zones. ESP-r's capability to model floating slat surfaces is very limited. Predicting solar insolation distribution & long-wave view-factors around such floating surfaces is not possible presently.

To obtain the best representation of a double-skin facade with Venetian blinds it is recommended that the cavity zone be split into two by a saw-tooth surface. The saw-tooth surface being made up of the blind slats, with fictitious surface in between. The way that the ESP-r solar model is presently composed means that only non-specular slats can be modelled.

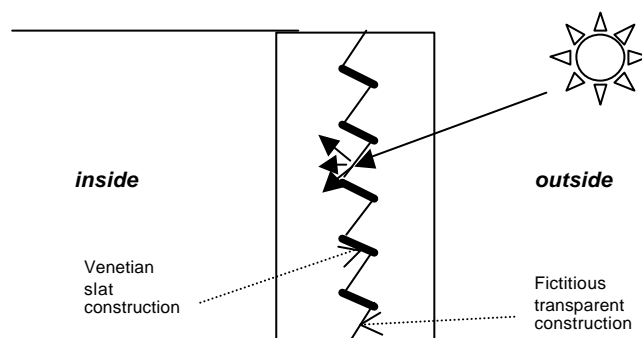


Figure 28 – Single Storey Facade Elevation: Saw-tooth Venetian blind representation

With such a representation, an accurate insolation distribution can be predicted in the outer cavity section at least. To account for direct solar tracking to all saw-tooth surfaces, it is recommended that the outer facade be split into between an appropriate number of segments – between $\frac{1}{2}$ & $\frac{3}{4}$ times the number of blind slats is recommended. At least until the code is updated to account for tracking to more than five surfaces. An increase to 10 surfaces was tested and found to cause no problems in this investigation.

With the saw-tooth surface, the total amount of solar radiation reaching the inner cavity is also accurately accounted for. However, when the solar radiation enters the internal cavity it loses its directional attributes and so requires that the insolation distribution be assigned manually or by default

8 Conclusions & Recommendations

area weighting. In a cavity which is not that deep, the overall errors will be small by assuming an area weighting. The most significant factor is to accurately predict the insolation distribution upon & through the slats.

Regarding longwave radiation transfer appropriate view factors between adjacent slats can be accounted for. This is very important since these slats will essentially exist at a very different temperature from the other cavity surfaces. For radiative heat transfer between inner & outer zones the model relies upon fictitious surfaces.

The extra surfaces in the cavity augment the surface convection but as in the previous models, the low solar absorptivity means that they don't heat up as much as the slats and the resulting convection is small in comparison. Ideally the convection co-efficients of these surface would be set to zero. In terms of the convection regime however, specific correlations for Venetian blinds in a channel are not available. CFD analysis would be an option to help improve the estimation in this domain, but ESP-r requires further work to increase its CFD resources before such geometry can be modelled.

It is recommended that the Bar-Cohen and Rohsenow correlation for buoyancy induced flow in vertical channels be used – this limit being approached as the slats tend towards a fully closed position.

Overall building simulation software doesn't naturally lend itself to the task of modelling Venetian systems and the saw-tooth representation is required to manoeuvre around this fact. However, this modelling method is very time consuming and is of course a static depiction of a Venetian blind system. Having said that, the generation of the saw-tooth surface could feasibly be made automatic.

Alternatively the model could be greatly simplified by creating a coarser saw-tooth, while still maintaining the essential characteristics that make the model representative. An acceptable coarseness has not yet been determined though and further study is required to exactly define this. Another approach in the future would be to represent the Venetian blind simply as in the roller blind model, as an equivalent flat surface. This surface would have equivalent optical properties, which would mimic transmission/absorption of a specific Venetian blind design over a range of angles. Fortunately the overall surface area of a Venetian blind system will typically be similar to that of a flat roller blind surface and so solar absorption & convection shall not be compromised. However so as to specify appropriate view factors between slats, the roller blind surface will require to be split into at least two segments. Developing such a lumped parameter to represent Venetian blinds as vertical

8 Conclusions & Recommendations

surfaces is not a trivial task - much experimental work to build up a database of suitable equivalent surfaces would be required. As and when such information is made available, the roller blind method can however be used to completely model the control & operation of a double-skin facade with Venetian blinds.

9 References

Alamdari F and Hammond G P (1983), "Improved Data Correlations for Buoyancy-Driven Convection in Rooms". Building Services Engineering Research Technology, 4(3) 106-12.

Abrisa (2004).

Web address: www.abrisa.com/downloads/borofloat.complete.7.04.pdf

Bar-Cohen, A & Rohsenow W.M. "Thermally optimum spacing of vertical natural convection cooled parallel plates". J. Heat Transfer, 106, 1984.

Beausoleil-Morrison, I. (2000) "The Adaptive Coupling of Heat and Air Flow Modelling within Dynamic Whole-Building Simulation". PhD Thesis, University of Strathclyde, Glasgow, UK.

Belgian Building Research Institute (BBRI) (2002). Source book for a better understanding of conceptual and operational aspects of active facades. Department of Building Physics, Indoor Climate and Building Services, Belgian Building Research Institute. Version no 1.

Web address: <http://www.bbri.be/activefacades/index2.htm>

Bejan, A (1984). "Convection heat transfer", New York. Wiley.

Bejan, A (1993). "Heat transfer", New York. Wiley.

Catton, I (1978). "Natural convection in Enclosures" Proceedings 6th Int. Heat Transfer Conference. Toronto, Canada, 1978, Vol6, pp.13-31.

Clarke, J.A. (1977). "Environmental Systems Performance", PhD Thesis, University of Strathclyde, Glasgow UK.

Clarke & Tang. "A Co-operating Solver Approach To Building Simulation". Energy Systems Research Unit, Department of Mechanical Engineering, University of Strathclyde, Glasgow, UK.

ESRU Publications. University of Strathclyde, Energy Systems Research Unit, Department of Mechanical Engineering, University of Strathclyde, Glasgow, UK.

Web address: <http://www.esru.strath.ac.uk/publications>

Heiselberg (1999). "Characteristics of Air Flow through Windows". IEA Annex35, Hybrid Ventilation in New and Retrofitted Office Buildings. Presented at the First International One day Forum on Natural and Hybrid Ventilation, HybVent Forum'99, 09/1999, Sydney, Australia.

Incropera F.P. and DeWitt D.P. (1996). "Fundamentals of Heat and Mass Transfer". John-Wiley and Sons.

Molina J.L., Maestre I.R (2002). "Modeling the effect of ventilated air cavities in the SOLVENT prototype: A reversible solar-screen glazing system. Proceedings of the 3rd European Conference on Energy Performance & Indoor Climate in Buildings and The 23rd Conference of the Air Infiltration & Ventilation Centre, Lyon, France, pp. 425-430.

Oesterle. (2001). Double Skin Facades – Integrated Planning. Prestel Verlag: Munich, Germany

Ostrach, S. "Natural convection in enclosures" in **Incropera F.P. and DeWitt D.P. (1996)**. "Fundamentals of Heat and Mass Transfer". John-Wiley and Sons.

Poirazis, Harris. (2004). Double Skin Facades for Office Buildings, Literature Review, Lund Institute of Technology

Web

address:

<http://www.ebd.lth.se/avd%20ebd/main/personal/Project%20home%20page/main/publications/LITERATURE.pdf>

Rogers, G.F.C. & Mayhew Y.R (1999). "Thermodynamic and Transport Properties of Fluids". Blackwell.

Saelens, D. (2002). Energy Performance Assessments of Single Storey Multiple-Skin Facades. PhD thesis, Laboratory for Building Physics, Department of Civil Engineering, Catholic University of Leuven, Belgium.

Web

address:

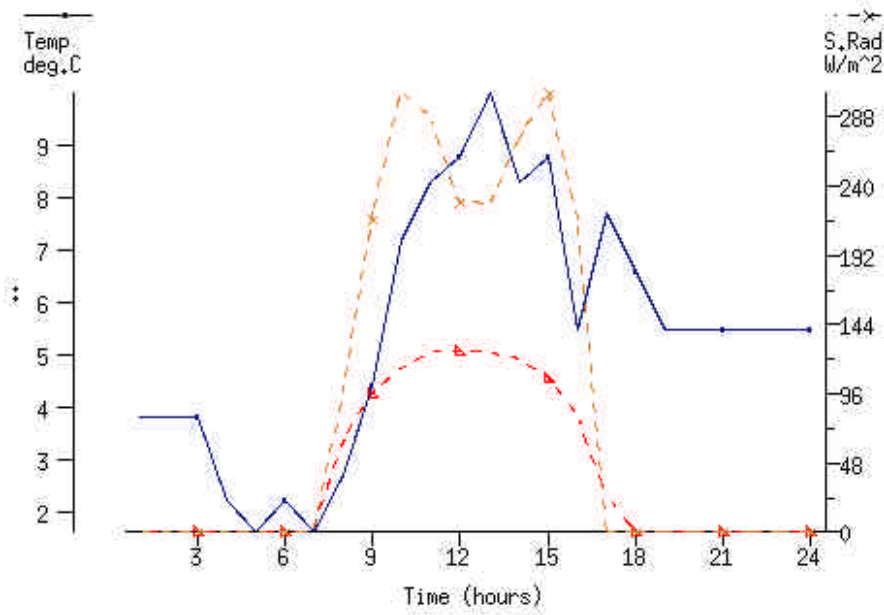
http://envelopes.cdi.harvard.edu/envelopes/content/resources/pdf/case_studies/PhD_Dirk_Saelens.pdf

Yuan X, Moser A, and Suter P. (1993). "Wall Functions for Numerical Simulation of Turbulent Natural Convection Along Vertical Plates", *Int. J. Heat Mass Transfer*, 36 (18) 4477-4485.

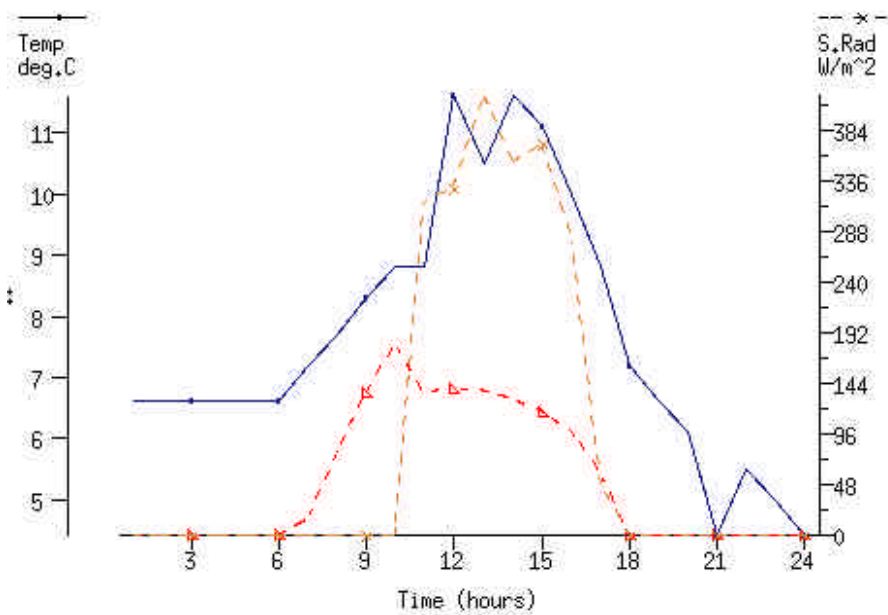
Appendix A – Climatic analysis of periods used in simulations

The climate used in all simulations is the Default ESP-r UK climate (Kew67). A graphical presentation of the climatic periods used in the simulations can be found below:

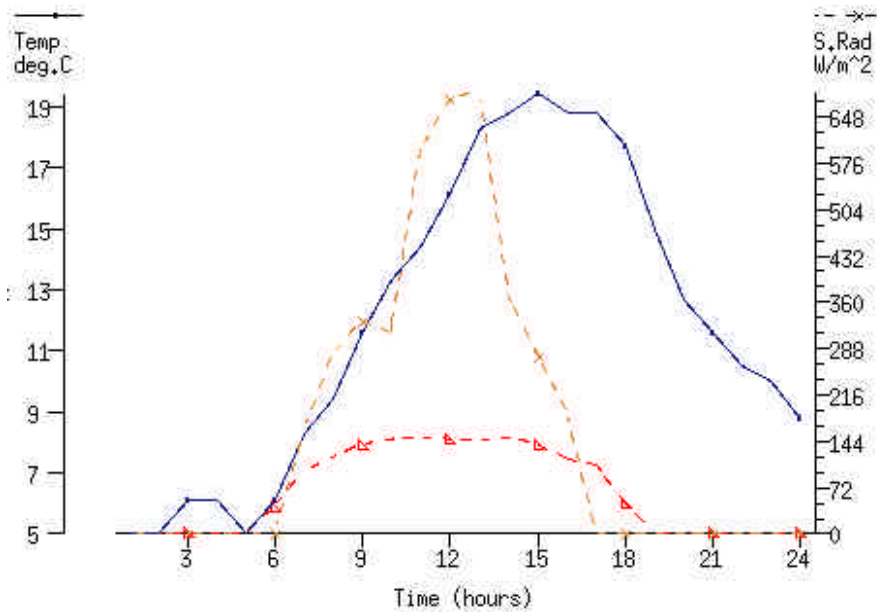
1 March



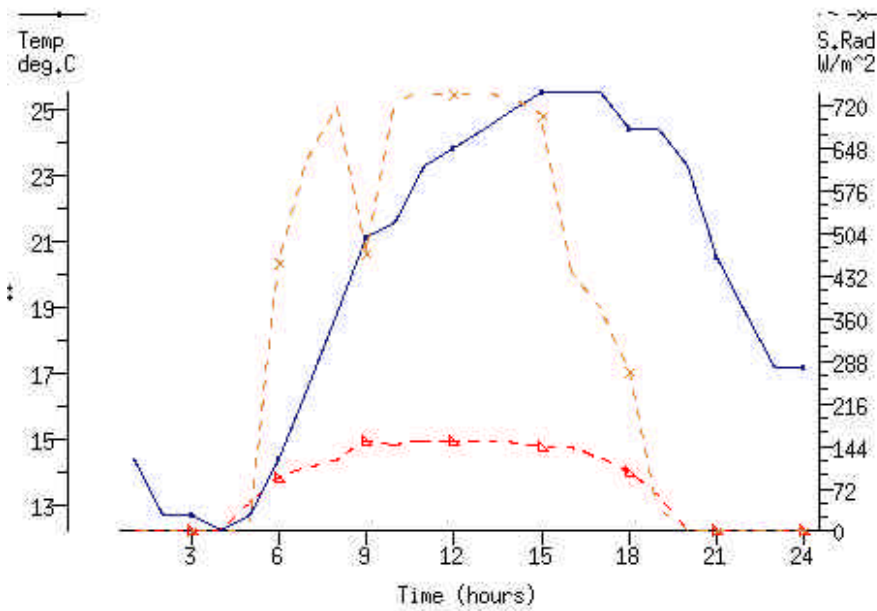
15 March



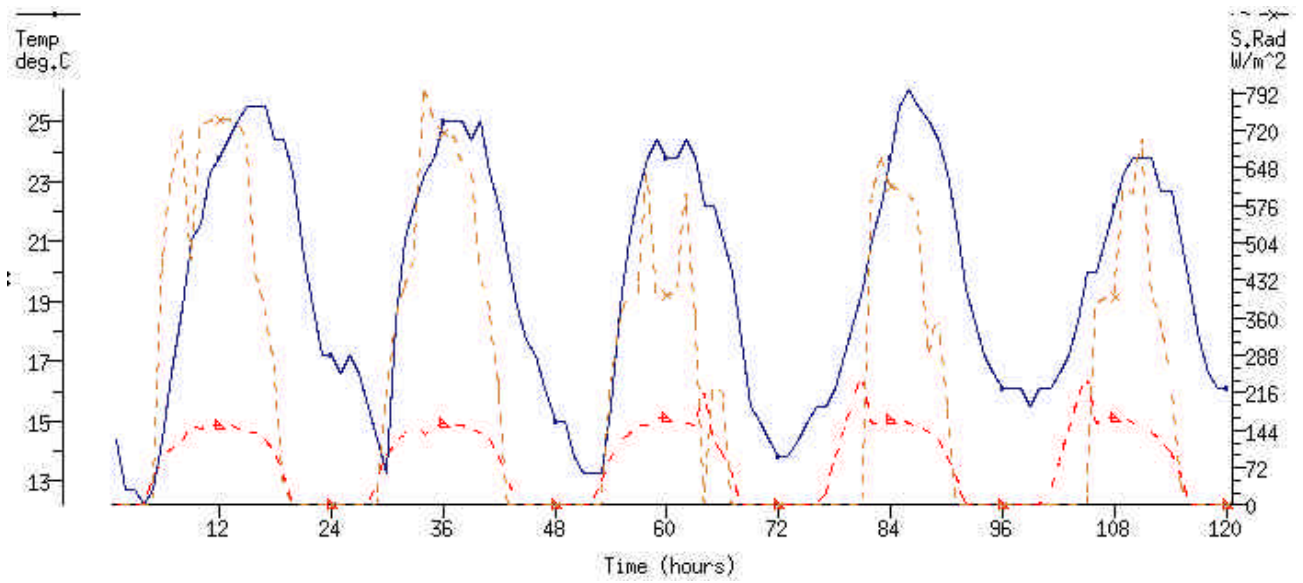
17 April



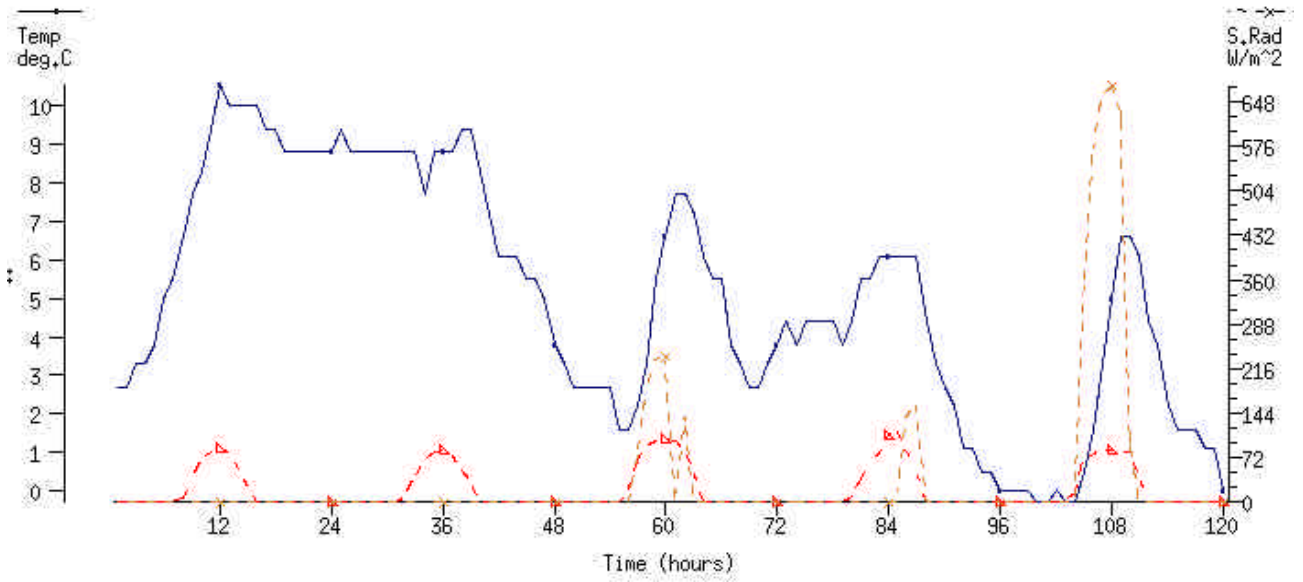
10 July



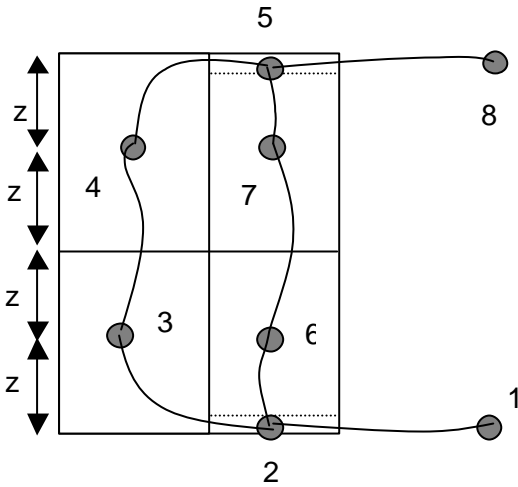
10-14Jul (Summer Week)



13-17November (Winter week)



Appendix B – Nodal network air-flow calculation check



Applying steady flow energy equation to above network assuming hydrostatic pressure law (i.e control volume air velocity is negligible):

For internal connections:

$$P_2 - P_3 = dP_{23} + r_3gz \quad -[1]$$

$$P_3 - P_4 = dP_{34} = (r_3+r_4)gz \quad -[2]$$

$$P_4 - P_5 = dP_{45} = r_4gz \quad -[3]$$

$$[1]+[2]+[3] \Rightarrow P_2 - P_5 = dP_{23} + dP_{34} + dP_{45} + 2gz(r_3+r_4) \quad -[4]$$

$$\text{Similarly, } P_2 - P_5 = dP_{26} + dP_{67} + dP_{75} + 2gz(r_6+r_7) \quad -[5]$$

For external connections:

$$P_1 - P_2 = dP_{12} \quad -[6]$$

$$P_5 - P_8 = dP_{58} \quad -[7]$$

$$[7]+[6]+[4] \Rightarrow P_1 - P_8 = dP_{12} + dP_{23} + dP_{34} + dP_{45} + dP_{58} + 2gz(r_3+r_4)$$

Substituting, $P_1 - P_8 = r_0g(4z)$:

$$r_0g4z - (r_3+r_4)g2z = dP_{12} + dP_{23} + dP_{34} + dP_{45} + dP_{58} \quad -[8]$$

Similarly from $[7]+[6]+[5]$:

$$r_0g4z - (r_6+r_7)g2z = dP_{12} + dP_{26} + dP_{67} + dP_{75} + dP_{58} \quad -[9]$$

Equations [8] & [9] are the analytical solutions which will be used to compare the numerical results. The validation process will involve substituting mass flows from the numerical results to find the pressure drops (dP) on the RHS of the equations. These will then be checked to balance with the LHS via substitution of the densities derived from the numerical simulation temperature results. The ideal gas law is used to determine densities with an atmospheric pressure of 101.325kPa.

Assumptions

*Ideal gas law applies.

*Atmospheric Pressure (P_{atm}) = 101.325kPa

*Density at each node calculated assuming $P_{\text{node}}=P_{\text{atm}}$ since changes in P due to height and flow resistance are of the order of 0.01kPa or less. Effect on density very small.

Calculation Check @ 9July, 12h23 (peak mass flow)

Flow1->2 (inlet)

ESP-r results:		Analytical:
$T_1 = 18.3 \text{ C}$ $m_{12} = 0.1772 \text{ kg/s}$ $Cd = 0.65$ $A = 0.3\text{m}^2$	From ideal gas law: $r_1 = P_1/RT_1 = \mathbf{1.212 \text{ kg/m}^3}$ where $P_1 = P_{\text{atm}}$	Connection Pressure drop: $dP_{12} = m_{12}^2 / 2r_1.Cd^2.A^2$ $\mathbf{dP_{12} = 0.34067 \text{ Pa}}$

Flow2->3 (bottom shading gap)

ESP-r results:		Analytical:
$T_2 = 18.3 \text{ C}$ $m_{23} = 0.034 \text{ kg/s}$ $Cd = 0.65$ $A = 0.3\text{m}^2$	From ideal gas law: $r_2 = P_2/RT_2 = \mathbf{1.212 \text{ kg/m}^3}$ where $P_2 = P_{\text{atm}}$ <small>negligible change in P with height & flow.</small>	Connection Pressure drop: $dP_{23} = m_{12}^2 / 2r_1.Cd^2.A^2$ $\mathbf{dP_{23} = 0.01254 \text{ Pa}}$

Flow3->4 (cavity resistance)

ESP-r results:		Analytical:
$T_3 = 22.806 \text{ C}$ $m_{34} = 0.0304 \text{ kg/s}$ $Cd = 0.65$ $A = 0.3\text{m}^2$	From ideal gas law: $r_3 = P_3/RT_3 = \mathbf{1.1935\text{kg/m}^3}$ where $P_3 = P_{\text{atm}}$ <small>negligible change in P with height & flow.</small>	Connection Pressure drop: $dP_{34} = m_{34}^2 / 2r_3.Cd^2.A^2$ $\mathbf{dP_{34} = 0.00015 \text{ Pa}}$

Flow4->5 (top shading gap)

ESP-r results:		Analytical:
$T_4 = 25.962 \text{ C}$ $m_{45} = 1.181 \text{ kg/s}$ $Cd = 0.65$ $A = 0.3\text{m}^2$	From ideal gas law: $r_4 = P_4/RT_4 = \mathbf{1.1809\text{kg/m}^3}$ where $P_4 = P_{\text{atm}}$ <small>negligible change in P with height & flow.</small>	Connection Pressure drop: $dP_{45} = m_{45}^2 / 2r_4.Cd^2.A^2$ $\mathbf{dP_{45} = 0.01287 \text{ Pa}}$

Flow5->8 (outlet)

ESP-r results:		Analytical:
$T_5 = 18.3 \text{ C}$ $m_{58} = 0.1772 \text{ kg/s}$ $Cd = 0.65$ $A = 0.3\text{m}^2$	From ideal gas law: $r_5 = P_5/RT_5 = \mathbf{1.212 \text{ kg/m}^3}$ where $P_5 = P_{\text{atm}}$ <small>negligible change in P with height & flow.</small>	Connection Pressure drop: $dP_{58} = m_{58}^2 / 2r_5.Cd^2.A^2$ $\mathbf{dP_{58} = 0.34067 \text{ Pa}}$

$\mathbf{dP_{12} + dP_{23} + dP_{34} + dP_{45} + dP_{58} = 0.707 \text{ Pa}}$

From LHS of eqn [8]:

$\mathbf{r_0g4z - (r_3+r_4)g2z = 0.730 \text{ Pa}}$

Appendix C– Insolation results when “misur” =6&10 for Venetian saw-tooth model with 6 divisions in outer façade

Lib: venetian6ish.res **MISUR =6**

Period: Wed 15 Mar @11h59 to: Wed 15 Mar @12h59 Year:2000 : sim@ 1m, output@ 5m (averaged)

Time	Slat 1	Slat 5	Slat 10	Slat 15	Slat 20	Slat 1t	Slat 5t	Slat 10t	Slat 15t
	InSolAb	InSolAb							
	W	W	W	W	W	W	W	W	W
11h03	31.85	37.21	33.12	33.12	13.51	0.02	0.02	0.02	0.02
11h08	32.11	37.74	33.35	33.35	13.59	0.02	0.02	0.02	0.02
11h12	32.30	37.98	33.56	33.56	13.65	0.02	0.02	0.02	0.02
11h18	32.49	38.21	33.76	33.76	13.71	0.02	0.02	0.02	0.02
11h23	32.66	38.42	33.94	33.94	13.77	0.02	0.02	0.02	0.02
11h27	32.82	38.61	34.11	34.11	13.82	0.02	0.02	0.02	0.02
11h33	32.97	38.78	34.26	34.26	13.87	0.02	0.02	0.02	0.02
11h38	33.11	38.95	34.40	34.40	13.91	0.02	0.02	0.02	0.02
11h42	33.23	39.09	34.52	34.52	13.95	0.02	0.02	0.02	0.02
11h48	33.33	39.22	34.63	34.63	13.99	0.02	0.02	0.02	0.02
11h53	33.42	39.33	34.73	34.73	14.02	0.02	0.02	0.02	0.02
11h57	33.42	39.13	34.75	34.79	14.05	0.02	0.02	0.02	0.02
12h03	32.18	34.01	33.78	34.55	14.07	0.02	0.01	0.02	0.02
12h08	32.57	34.22	34.22	35.04	14.17	0.02	0.01	0.02	0.02
12h12	33.05	34.73	34.73	35.57	14.30	0.02	0.01	0.02	0.02
12h18	33.52	35.23	35.23	36.08	14.42	0.02	0.01	0.02	0.02
12h23	33.96	35.70	35.70	36.57	14.54	0.02	0.01	0.02	0.02
12h27	34.39	36.16	36.16	37.04	14.65	0.03	0.01	0.02	0.02
12h33	34.80	36.60	36.60	37.49	14.76	0.03	0.02	0.02	0.02
12h38	35.19	37.01	37.01	37.92	14.86	0.03	0.02	0.02	0.02
12h42	35.57	37.41	37.41	38.33	14.95	0.03	0.02	0.02	0.02
12h48	35.91	37.78	37.78	38.71	15.04	0.03	0.02	0.03	0.02
12h53	36.24	38.13	38.13	39.07	15.12	0.03	0.02	0.03	0.02
12h57	36.46	38.37	38.37	39.36	15.19	0.03	0.02	0.02	0.02

Lib: venetian10ish.res: **MISUR =10**

Period: Wed 15 Mar @11h59 to: Wed 15 Mar @12h59 Year:2000 : sim@ 1m, output@ 5m (averaged)

Time	Slat 1	Slat 5	Slat 10	Slat 15	Slat 20	Slat 1t	Slat 5t	Slat 10t	Slat 15t
	InSolAb	InSolAb							
	W	W	W	W	W	W	W	W	W
11h03	30.76	35.37	30.76	30.76	13.23	0.02	0.02	0.02	0.02
11h08	31.02	35.68	31.02	31.02	13.30	0.02	0.02	0.02	0.02
11h12	31.21	35.90	31.21	31.21	13.37	0.02	0.02	0.02	0.02
11h18	31.39	36.11	31.39	31.39	13.43	0.02	0.02	0.02	0.02
11h23	31.56	36.31	31.56	31.56	13.48	0.02	0.02	0.02	0.02
11h27	31.71	36.49	31.71	31.71	13.53	0.02	0.02	0.02	0.02
11h33	31.85	36.66	31.85	31.85	13.58	0.02	0.02	0.02	0.02
11h38	31.98	36.81	31.98	31.98	13.62	0.02	0.02	0.02	0.02
11h42	32.10	36.94	32.10	32.10	13.66	0.02	0.02	0.02	0.02
11h48	32.20	37.06	32.20	32.20	13.69	0.02	0.02	0.02	0.02
11h53	32.29	37.16	32.29	32.29	13.72	0.02	0.02	0.02	0.02
11h57	32.27	37.15	32.26	32.26	13.75	0.02	0.02	0.02	0.02
12h03	30.80	35.52	30.66	30.66	13.67	0.02	0.02	0.02	0.02
12h08	31.16	35.96	31.01	31.01	13.77	0.02	0.02	0.02	0.02
12h12	31.62	36.51	31.46	31.46	13.90	0.02	0.02	0.02	0.02
12h18	32.06	37.03	31.90	31.90	14.01	0.02	0.02	0.02	0.02
12h23	32.48	37.54	32.32	32.32	14.12	0.02	0.02	0.02	0.02
12h27	32.89	38.03	32.72	32.72	14.23	0.02	0.02	0.02	0.02
12h33	33.27	38.49	33.11	33.11	14.33	0.02	0.02	0.02	0.02
12h38	33.64	38.94	33.48	33.48	14.42	0.02	0.02	0.02	0.02
12h42	33.99	39.36	33.83	33.83	14.51	0.02	0.02	0.02	0.02
12h48	34.32	39.75	34.15	34.15	14.59	0.02	0.02	0.02	0.02
12h53	34.63	40.13	34.46	34.46	14.66	0.02	0.02	0.02	0.02
12h57	34.85	40.37	34.68	34.68	14.73	0.02	0.02	0.02	0.02

Appendix D- Insolation results when “misur” =6&10 for Venetian saw-tooth model with 12 divisions in outer facade

Lib: venetian6ish.res: **MISUR =6**

Period: Wed 15 Mar @11h59 to: Wed 15 Mar @12h59 Year:2000 : sim@ 1m, output@ 5m (averaged)

Time	Slat 1	Slat 5	Slat 10	Slat 15	Slat 20	Slat 1t	Slat 5t	Slat 10t	Slat 15t
	InSolAb	InSolAb	InSolAb	InSolAb	InSolAb	InSolAb	InSolAb	InSolAb	InSolAb
	W	W	W	W	W	W	W	W	W
11h03	33.03	33.03	33.03	33.03	13.19	0.02	0.02	0.02	0.02
11h08	33.31	33.31	33.31	33.31	13.27	0.02	0.02	0.02	0.02
11h12	33.52	33.52	33.52	33.52	13.33	0.02	0.02	0.02	0.02
11h18	33.72	33.72	33.72	33.72	13.39	0.02	0.02	0.02	0.02
11h23	33.90	33.90	33.90	33.90	13.44	0.02	0.02	0.02	0.02
11h27	34.07	34.07	34.07	34.07	13.49	0.02	0.02	0.02	0.02
11h33	34.22	34.22	34.22	34.22	13.54	0.02	0.02	0.02	0.02
11h38	34.36	34.36	34.36	34.36	13.58	0.02	0.02	0.02	0.02
11h42	34.48	34.48	34.48	34.48	13.62	0.02	0.02	0.02	0.02
11h48	34.60	34.60	34.60	34.60	13.66	0.02	0.02	0.02	0.02
11h53	34.69	34.69	34.69	34.69	13.69	0.02	0.02	0.02	0.02
11h57	34.67	34.68	34.66	34.66	13.71	0.02	0.02	0.02	0.02
12h03	33.09	33.15	32.88	32.86	13.63	0.02	0.02	0.02	0.02
12h08	33.49	33.56	33.26	33.25	13.74	0.02	0.02	0.02	0.02
12h12	33.99	34.06	33.76	33.74	13.86	0.02	0.02	0.02	0.02
12h18	34.48	34.55	34.24	34.23	13.98	0.02	0.02	0.02	0.02
12h23	34.94	35.02	34.71	34.69	14.09	0.02	0.02	0.02	0.02
12h27	35.39	35.47	35.15	35.13	14.20	0.02	0.02	0.02	0.02
12h33	35.82	35.89	35.57	35.56	14.30	0.02	0.02	0.02	0.02
12h38	36.23	36.30	35.98	35.96	14.39	0.02	0.02	0.02	0.02
12h42	36.61	36.69	36.36	36.34	14.48	0.02	0.02	0.02	0.02
12h48	36.98	37.06	36.72	36.70	14.57	0.02	0.02	0.02	0.02
12h53	37.32	37.40	37.06	37.04	14.64	0.02	0.02	0.02	0.02
12h57	37.55	37.62	37.30	37.28	14.71	0.02	0.02	0.02	0.02

Lib: venetian10ish.res: **MISUR =10**

Period: Wed 15 Mar @11h59 to: Wed 15 Mar @12h59 Year:2000 : sim@ 1m, output@ 5m (averaged)

Time	Slat 1	Slat 5	Slat 10	Slat 15	Slat 20	Slat 1t	Slat 5t	Slat 10t	Slat 15t
	InSolAb	InSolAb	InSolAb	InSolAb	InSolAb	InSolAb	InSolAb	InSolAb	InSolAb
	W	W	W	W	W	W	W	W	W
11h03	33.03	33.03	33.03	33.03	13.19	0.02	0.02	0.02	0.02
11h08	33.31	33.31	33.31	33.31	13.27	0.02	0.02	0.02	0.02
11h12	33.52	33.52	33.52	33.52	13.33	0.02	0.02	0.02	0.02
11h18	33.72	33.72	33.72	33.72	13.39	0.02	0.02	0.02	0.02
11h23	33.90	33.90	33.90	33.90	13.44	0.02	0.02	0.02	0.02
11h27	34.07	34.07	34.07	34.07	13.49	0.02	0.02	0.02	0.02
11h33	34.22	34.22	34.22	34.22	13.54	0.02	0.02	0.02	0.02
11h38	34.36	34.36	34.36	34.36	13.58	0.02	0.02	0.02	0.02
11h42	34.48	34.48	34.48	34.48	13.62	0.02	0.02	0.02	0.02
11h48	34.60	34.60	34.60	34.60	13.66	0.02	0.02	0.02	0.02
11h53	34.69	34.69	34.69	34.69	13.69	0.02	0.02	0.02	0.02
11h57	34.67	34.68	34.66	34.66	13.71	0.02	0.02	0.02	0.02
12h03	33.09	33.15	32.88	32.86	13.63	0.02	0.02	0.02	0.02
12h08	33.49	33.56	33.26	33.25	13.74	0.02	0.02	0.02	0.02
12h12	33.99	34.06	33.76	33.74	13.86	0.02	0.02	0.02	0.02
12h18	34.48	34.55	34.24	34.22	13.98	0.02	0.02	0.02	0.02
12h23	34.94	35.02	34.71	34.69	14.09	0.02	0.02	0.02	0.02
12h27	35.39	35.46	35.15	35.13	14.20	0.02	0.02	0.02	0.02
12h33	35.82	35.89	35.57	35.55	14.30	0.02	0.02	0.02	0.02
12h38	36.23	36.30	35.98	35.96	14.39	0.02	0.02	0.02	0.02
12h42	36.61	36.69	36.36	36.34	14.48	0.02	0.02	0.02	0.02
12h48	36.98	37.06	36.72	36.70	14.57	0.02	0.02	0.02	0.02
12h53	37.32	37.40	37.06	37.04	14.64	0.02	0.02	0.02	0.02
12h57	37.55	37.62	37.30	37.28	14.71	0.02	0.02	0.02	0.02

Appendix E - Erroneous insolation results sample (for 15th March) when MISUR=46

Error type - surfaces that should clearly receive insolation are missing, also insolation adds to 100.8% i.e. in the results at 13h00, the slats above slat 1 (slats 2,3,4,5) receiving no insolation but slats 6,7,8,9 and so on do. The surface numbering system is illustrated in Figure 22

13h00 hours			15h00 hours		
surface		insolation	surface		insolation
surface	floor	9.85	surface	side_east1	9.5
surface	0t	4.8	surface	floor	9
surface	1	4.55	surface	side_east2	8
surface	6	4.55	surface	side_east3	6
surface	7	4.55	surface	5	3.75
surface	8	4.55	surface	6	3.75
surface	9	4.55	surface	7	3.75
surface	10	4.55	surface	8	3.75
surface	11	4.55	surface	9	3.75
surface	12	4.55	surface	10	3.75
surface	13	4.55	surface	11	3.75
surface	14	4.55	surface	12	3.75
surface	15	4.55	surface	13	3.75
surface	2t	4.55	surface	14	3.75
surface	3t	4.55	surface	19	3.75
surface	4t	4.55	surface	1t	3.75
surface	16t	4.55	surface	2t	3.75
surface	17t	4.55	surface	3t	3.75
surface	18t	4.55	surface	15t	3.75
surface	side_east2	3.28	surface	16t	3.75
surface	side_east1	2.53	surface	17t	3.75
surface	side_east3	2.27	surface	0t	3.75
	TOTAL	100.08 %		TOTAL	100

Appendix F – Source code fix in “Convect2.F”, convection correlations

The Bar-Cohen & Rohsenow correlation is shown inserted into the code below (**bold**). The convective control that allows for different surfaces to have different convection correlations (Type 2), was lacking the ability to account for fictitious surfaces with zero convection. The lines below, in **bold italic** were added to “Convect2.F” to facilitate this.

```
C Bar-Cohen and Rosenhow general correlation for buoyancy driven flow in
vertical channels.
```

```
C Air entering from outdoors.
```

```
C CWIDTH is the Channel width and CHEIGHT the channel height
```

```
C RAS is the Raleigh number and CNUSS the Nussel number
```

```
C Air properties fixed at 300 K values.
```

```
      RAS=9.8*1/ABS(TF)*ABS(TFS(ICOMP,ISUR)-TF)*
&      CWIDTH**3*1/(1.932E-5*1.343E-5)

      CNUS=(576*(RAS*CWIDTH/CHEIGHT)**(-2)+
&      (2.87*RAS*CWIDTH/CHEIGHT)**(-0.5))**(-0.5)

      HC=CNUS*0.0249/CWIDTH

      write(outs,'(A,E10.2,E10.2,F4.1)')'RAS,CNUS,HC ',RAS,CNUS,HC
      if(dotrace)call edisp(itu,outs)
      ELSEIF((ICOR.EQ.16).AND.(IAORZ.GT.0))THEN
```

```
C Bar-Cohen and Rosenhow general correlation for buoyancy driven flow in
vertical channels.
```

```
C Air entering from another building zone
```

```
      RAS=9.8*1/TFA(IAORZ)*ABS(TFS(ICOMP,ISUR)-TFA(IAORZ))*
&      CWIDTH**3*0.707/(1.59E-5)**2
```

```
      CNUS=(576*(RAS*CWIDTH/CHEIGHT)**(-2)+
&      (2.87*RAS*CWIDTH/CHEIGHT)**(-0.5))**(-0.5)
```

```
      HC=CNUS*0.0263/CWIDTH
```

```
      write(outs,'(A,E10.2,E10.2,F4.1)')'RAS,CNUS,HC ',RAS,CNUS,HC
      if(dotrace)call edisp(itu,outs)
      ELSEIF(ICOR.EQ.17)THEN
```

```
C Zero-convection co-efficient for a fictitious surface
```

```
      HC=0.001
```

```
      write(6,'(A,F9.3)')' Fictitious surface (vert): HC',HC
      ELSEIF(ICOR.EQ.30)THEN
```

```
C##### WINDOWS #####
C Khalifa & Marshall correlation for windows when a radiator is located
C under the window (Table 2, eq.9 of K&M paper).
```

Appendix G – Source code fix to display multi-page Surface Convection menu

It was found that the menu for specifying surface convection co-efficients wouldn't appear. Due to the many surface present in the saw-tooth model, the single page menu couldn't cope. A multi-page menu similar to that in the vertex operations was included. The new code (**in bold**) in the "hcfmk.F" file in "esurprj" is shown below, starting from the "EPHCF" routine:

```
C ***** EPHCF *****
C EPHCF edits one period of convection-calculation control data.

      SUBROUTINE EPHCF(IZ,IN,NS,IER)
#include "epara.h"
#include "building.h"
      common/pophelp/h(60)
      COMMON/G6/SSNAME(MCON),SSOTF(MCON),SSMLCN(MCON),SSVFC(MCON),
&          SSOTHER(MCON),SSPARENT(MCON)
      COMMON/HCFP/IHCFP,ST(MP),EN(MP),HCI(MP,MS),HCE(MP,MS),
&          ICTL(MP),IHCI(MP,MS),IHCE(MP,MS),CVdata(MP,MS,8)
      common/HCFPHI/hcfpdescr(MP)
      COMMON/C20/NZSUR(MCOM),NZTV(MCOM)
      COMMON/C24/IZSTOCN(MCOM,MS)
      COMMON/PMENU/MHEAD,MCTL,MIFULL,MFULL,IST,ILEN,IPM,MPM,IPFLG
      character H*72,outs*124,SN*12,ITEM(MS+5)*30,KEY*1,SSPARENT*12
      CHARACTER SSMLCN*12,SSVFC*4,SSOTF*4,SSOTHER*15,SSNAME*12
      CHARACTER stuff*10
      character hcfpdescr*72
      logical close

      NS=NZSUR(IZ)

C Get time period for control interval.
      V1=ST(IN)
      H(1)='Time must be between 0. and 24. '
      CALL EASKR(V1,' ',' Start time ? ',
&          0.,'F',24.,'F',0.,'start',IER,1)
      ST(IN)=V1
      V2=EN(IN)
      call eclose(V2,0.0,0.001,close)
      if(close) V2=24.
      H(1)='Time must be between 0. and 24. '
      CALL EASKR(V2,' ',' End time ? ',
&          V1,'F',24.,'F',0.,'start',IER,1)
      EN(IN)=V2

C Determine type of control over calculations.
      h(1)='Three `convection-calculation control` methods are'
      h(2)='supported: '
      h(3)=' '
      h(4)='Type 1 allows fixed coefficients to be specified for each'
      h(5)='surface (interior and exterior to the building).'
      h(6)=' '
      h(7)='Type 2 allows you to specify the correlation to use for'
      h(8)='each surface (only applicable for surfaces interior to'
      h(9)='the building). This could allow, for example, the use of'
      h(10)='the Alamdari & Hammond correlations for a wall, while '
      h(11)='using one of the Khalifa & Marshall correlations for a '
      h(12)='window. '
      h(13)=' '
      h(14)='Type 3 allows adaptive control of the calculations (only'
      h(15)='applicable for surfaces interior to the building). '
```

```

h(16)=' '
h(17)='Note that the `outside` surface of a mlc may be interior'
h(18)='to the building, ie. it may face the air-point of an '
h(19)='adjacent zone. '
CALL EASKABCD('calculation control:', ' ', 'type 1',
&          'type 2', 'type 3', 'cancel', IW, 19)
IF(iw.eq.4) RETURN
ICTL(IN) = iw

C Type 1 control: fixed coefficients.
IF(iw.eq.1) THEN
  hcfpdescr(IN) = 'User supplied hc values'

C Initialise zone vertex menu size variables based on window size.
C IVERT is the menu position, MVERT the current number of menu lines.
  MHEAD=1
  MCTL=3
  ILEN=NS
  IPACT=CREATE
  CALL EKPAGE(IPACT)

C Initial menu entry setup.
20 IER=0
  ILEN=NS
  INO=-2

C Loop through the items until the page to be displayed. M is the
C current menu line index. Build up text strings for the menu.
  ITEM(1) = ' Surface orien. hci hce'
3 M=MHEAD
DO 10 L=1,ILEN
  IF(L.GE.IST.AND.(L.LE.(IST+MIFULL)))THEN
    M=M+1
    icc=izstocn(iz,1)
    CALL EMKEY(L,KEY,IER)
    WRITE(ITEM(M), '(a,1x,3a,2f5.1)') KEY,SSNAME(icc), ' ',
&      SSVFC(icc),HCI(IN,L),HCE(IN,L)
  ENDIF
10 CONTINUE

C Number of actual items displayed.
  NITEMS=M+MCTL

C If a long list include page facility text.
IF(IPFLG.EQ.0)THEN
  ITEM(M+1)=' _____ '
ELSE
  WRITE(ITEM(M+1),15)IPM,MPM
15 FORMAT ('0 page: ',I2,' of ',I2,' -----')
ENDIF
  ITEM(M+2) = '? Help '
  ITEM(M+3) = '- Exit '

  CALL EMENU('Conv coefficients',ITEM,NITEMS,INO)

C Edit data or display help.
if (INO.eq.NITEMS) then
  goto 99
elseif (INO.eq.NITEMS-1) then
  H(1)='This data is usually from measurements. '
  H(2)='A -1 signals use of calculated values. '
  CALL PHELPD('conv coef data',2,'-',0,0,IER)

```

```

elseif (INO.eq.NITEMS-2) then
C If there are enough items allow paging control via EKPAGE.
  IF(IPFLG.EQ.1)THEN
    IPACT=EDIT
    CALL EKPAGE(IPACT)
  ENDIF
elseif(INO.gt.1) then
C Edit vertex identified by KEYIND.
  CALL KEYIND(NITEMS,INO,IS,IO)
  icc=izstocn(iz,is)
  write(outs,'(a,i3,1x,a)')'Hc values for surface',J,
&   SSNAME(ICC)(1:lnblnk(SSNAME(ICC)))
  H(1)='This data is usually from measurements. '
  H(2)='A -1 signals use of calculated values. '
  write (SN,'(2f5.1,1x)') HCI(IN,IS),HCE(IN,IS)
  CALL EASKS(SN,outs,'inside, outside?',12,' -1.0 -1.0',
&   'hc values',IER,2)
  K=0
  CALL EGETWR(SN,K,HCI(IN,IS),-1.5,1000.,'F','hci value',IER)
  CALL EGETWR(SN,K,HCE(IN,IS),-1.5,1000.,'F','hce value',IER)
endif
goto 20
99 continue
ENDIF

```